Natural Resources Canada
Ressources naturelles Canada

ᓄᓇᖅᐊᓕᕆᓂᖅᓯᒪᔪᓂ ᖃᐅᔨᓴᖃᖅᑐᑦ ᑲᓇᑕ

ᑲᓇᑕ ᓄᓇᓕᒃ ᖃᐅᔨᓴᓂᖅᓯᒪᔪᓂ ᓄᓇᖅᐊᖃᖅ 255S

ᓄᓇᕗᑦᓗ ᐅᓴᖃᐅᓂᒃ ᖃᐅᔨᓴᖃᖅᑐᑦ ᑎᑎᕋᕐᓇᖅᓱᒃ

ᒪᑐᐃᖅᓱᖃᖅ ᓄᓇᖅᐊᖃᖅ 2016-12S

ᓄᓇᓕ ᖃᐅᔨᓴᕋᓂᖅ

AMITTOK LAKE (NORTH)

ᖁᑭᖃᖅᑕᓗᒃ, ᓄᓇᕗᑦ

ᓄᓇᓵᖅᐊᓕᒃ
ᑭᓯᓕᕆᓂᕐᒥᒃ
ᑎᑎᖃᕐᓂᖅ

ᐱᒋᐊᕋᓂᖅ

ᓄᓇᖅᐊᓕᕆᓂᖅᓯᒪᔪᓂ ᖃᐅᔨᓴᖃᖅᑐᑦ ᑲᓇᑕ
ᑲᓇᑕ ᐅᓴᖃᐅᓂᒃ ᖃᐅᔨᓴᖃᓂᖅᓯᒪᔪᓂ ᓄᓇᖅᐊᓕᒃ

2016

Canada

ᓴᖅᑭᖅᑎᑕᐅᔪᑦ

CANADA-NUNAVUT GEOSCIENCE OFFICE
ᑲᓇᑕᐅᓪ-ᓄᓇᕗᑦ ᑭᒃᑯᑐᓂᒃ ᓴᖅᑭᖅᑎᑕᐅᔪᑦ

BUREAU GÉOSCIENTIFIQUE CANADA-NUNAVUT
KANATAMI-NUNAVUMI GEOSCIENCE TITIGAKVIIT

ᓄᓇᕗᒻᒥᐅ ᐊᓴᐅᑎᖓ

ᓄᓇᒥᐅᑕᓕᕆᔨᖅᑯᑦ ᑲᓇᑕᒥ, ᓄᓇᖏᕗᒻᒥᓕᕆᓂᖏᓐᓂᑦ ᖃᐅᔨᓴᖅᑎᑦ ᑲᓇᑕᒥ ᑲᓇᑕᒥ ᓄᓇᓕᖅ ᖃᐅᔨᓴᓂᖏᓐᓂᑦ ᓄᓇᖏᕗᖅ 253S (ᐱᒋᐊᖏᖓ), ᑲᓇᑕ ᓄᓇᕕᒃᓗ ᐅᓴᖅᑲᓂᑦ ᖃᐅᔨᓴᖅᑎᑦ ᑎᑎᕋᖏᖓ ᒪᑐᐊᖏᖅ ᓄᓇᖏᕗᖅ 2016-12S

ᐊᑎᖓ

ᓄᓇᓂ ᖃᐅᔨᓴᕋᓂᖅ, Amittok Lake (north), ᖁᑭᖅᑕᒃᓗᒃ, ᓄᓇᕗᑦ

ᐊᖏᑕᓂᖓ

1:100 000

ᑎᑎᕋᖅᓯᒪᔪᑦ ᑐᑭᓯᑕᐊᕈᑎᖏᑦ

ᑎᑎᕋᖅᓯᒪᔪᑦ ᐅᓴᐅᑎᖓ. M183-1/255-2016S-PDF
ISBN 978-0-660-05092-8
doi:10.4095/298758

ᐊᔪᓚᑦᑕᐅᔭᓚᐊᕋᖅᖏᑦᑐᑦ

ᑐᓴᒃᖴᐅᑎᑕᐅᔪᑦ ᐅᕐᓂ ᐅᓴᒃᑕᒪᒐᕋᒥ ᐅᕙᓪᓕᐊᓂᓕᑦ ᐱᔪᑯᑎᑦᑐᖅ ᓴᖅᑭᑎᑕᐅᖅᑲᓐᓂᕋᓂᖅᑐᖅ, ᐃᑕᐃᓐᓇᖑᔪᑦ ᑕᒪᐃᑎᔪᓪᓗᓂᓕᕆᓂᓕᕆᓂᖅ, ᐊᓚᒪᓗ ᖃᓄᐃᑐᐃᓐᓇᖅ, ᐃᒥᒧᑦ ᐅᕙᓪᓕᐊᓂᓕᕆᓂᓕᕆᓂᖅ ᑭᖅᑯᑕᒪᓄᓕᓂ ᑮᓇᐅᔭᑕᐅᔪᓂᕆᓂᖅᑯᖅᑎᑐᖅ, ᐊᑭᖅᖃᕐᓗᓂ ᐅᕙᓪᓕᐊᓂᓕᕆᓂᓕᕆᓂᖅ ᐊᓐᓂᖅᑕᐅᔭᓂᖅᖃᓕᕆᔨᐸᑭ

ᐃᒪᓐᓇᐃᑕᐅᔪᓐᓇᕐᓂᐊᕐᓂᓗᑎᒃ ᑕᒪᓐᓇᖅᑐᒥᓂᓗᑎᒃ ᑕᒪᖅᑯᓇᖏᓐᓂᑕᒃ ᑲᑎᒪᔨᖅᑎᑦ ᐃᓕᓴᕐᓂᖅᑐᑦ;

- ᓇᓗᓇᐃᔭᓗᒍ ᑲᑎᑎᖅᑯᓂᖅᑕᕐᕕᖏᓂ ᑕᐃᒍᓱᖓᓐ, ᐊᒻᒪᓗ ᑎᑎᕋᖅᑕᐃᓂ ᐊᑎᖓᓂ; ᐊᒻᒪᓗ
- ᓇᓗᓇᐃᔭᓗᑎᒃ ᑲᑎᑎᖅᑯᓂᖅᑕᕐᕕᐃᓂ ᑕᕐᕋᑐᐃᓐᓇᐅᑎᓄᑦ ᐱᓕᕆᔨᐅᑎᓄᑦ ᐅᑯᐊᖓᓐ ᐊᑐᖅᑲᓐᓂᑕᕆᓚᐅᖏᓐᓂᑦ ᓄᓇᖏᕗᖅ (NRCan) ᐊᒻᒪᓗ ᒎᓐᓇ ᑲᑎᑕᐅᔪᖅ ᑲᑎᑎᖅᑯᓂᖅᑕᕐᕕᖏᓐᓂᒍᓱᖓᓐ ᐅᑯᐊᖓᓐ ᐅᕙᓪᓕᐊᓂᓕᕆᓂᓕᕆᓂᖅ ᐊᑐᖅᑲᓐᓂᑕᕆᔨᒪᓂᖏᓐᓂᑦ ᐅᑯᐊᖓᓐᓂᑦ NRCan-ᑯᓐᓂᑦ.

ᐊᑐᓕᖅᑯᐅᔾᔨᑦ ᐅᖅᑲᖅᑕᐅᓯᒪᔾᔨᑦ ᖃᐅᔨᓕᐊᖅᐲᓗᓐᓂᑦ

St-Onge, M.R., Weller, O.M., Dyck, B.J., Rayner, N.M., Chadwick T., ᐊ ᓚᒪ Liikane, D., 2016. ᓄᓇᓂ ᖃᐅᔨᓴᖅᓂᖅ, Amittok Lake (north), ᖃᑭᖅᑕᓗᒃ, ᓄᓇᕗᑦ; ᓄᓇᖕᒪᐊᓕᕆᓂᖅᓯᒪᑦ ᖃᐅᔨᓴᖅᑎᑦ ᑲᓇᑕᒥ, ᑲᓇᑕᒥ ᓄᓇᓂᑦ ᖃᐅᔨᓴᓂᖅᓯᒪᑦ ᓄᓇᖕᒪᐊᖅ 255S (ᐱᒋᐊᖅᓂᖓ); ᓄᓇᕗᑦᓗ ᐅᓴᖅᑲᓂᑦ ᖃᐅᔨᓴᖅᑎᑦ ᑎᑎᕋᖅᓐᖓ, ᒪᑐᐃᖓᒐᔪᖅ ᓄᓇᖕᒪᐊᖅ 2016-12S, ᐊᖏᕐᓂᖓ 1:100 000. doi:10.4095/298758

ABSTRACT

This map summarizes the field observations for the Amittok Lake (north) map area following eight weeks of regional and targeted bedrock mapping on western Hall Peninsula. The 2015 field campaign completes a two-decade mission to update map coverage for the whole of Baffin Island south of latitude 70°N. The bedrock is dominated by a Paleoproterozoic metaplutonic suite, ranging in composition from gabbro to syenogranite, with crosscutting relations indicating a progression from mafic to silicic magmatism. Prevailing upper amphibolite to lower granulite facies metamorphic conditions overlap the stability limits of magnetite and orthopyroxene, which is consistent with equilibrium phase diagrams and regional aeromagnetic data. Metasedimentary rocks, including quartzite, pelite, marble, and metagreywacke, are present as screens and enclaves between and within plutonic bodies. An examination of the ‘ghost’ stratigraphy suggests that the metasedimentary rocks can be correlated with the middle Paleoproterozoic Lake Harbour Group in the south and Piling Group in the north. Two basaltic dyke swarms and shallowly dipping Ordovician limestone respectively crosscut and overly the Paleoproterozoic units.

ᐃᓕᒋᕆᐅᔾᔨᑦ

ᑕᓐᓇ ᓄᓇᖕᒪᐊᖅ ᓇᓗᓇᐃᕆᐃᔾᔨᖅ ᖃᐅᔨᓴᖅᑎᓪᓗᑎᑦ ᖃᐅᔨᓴᕆᐅᔾᔨᑦ Amittok Lake (north) ᓄᓇᖕᒪᐊᖅ 8-ᓂᑦ ᐱᓇᓱᐊᕈᓴᓂᑦ ᐊᕐᕌᒍᖅᓯᒪᔾᔪᑎᑦ ᐊᒻᒪ ᖃᐅᔨᓴᖅᓂᖃᖅᓯᓗᓪᓗᐊᓕᐅᖅᑐᑦ ᖁᓕᖕᒪᐊᖅᑐᓂᓕᕆᓂᖅᓯᒪᔪᓂ ᓄᓇᖕᒪᐊᓕᐅᕈᑎᒋᔭᐃᓐᓇᕐᓂᖅᓯᒪᔪᓂ ᐱᕐᓂᖅᓯᒪᔪᓂ 70°N. ᖁᓕᖕᒪᐊᓕᐅᖅᑐᑦ ᐃᓗᓕᖅᑎᓂᕆᔨᖏᓐᓄ Paleoproterozoic metaplutonic suite, ᐊᔨᔪᐊᓕᐅᓂᖅᑐᑦ ᐃᓗᓕᖏᓂ ᐱᑎᐊᖅᑐᑦ gabbro ᑎᑭᑐᒍ syenogranite, ᖁᓕᑕᔭᓴᖅᑎᑕᐅᑎᓪᓗᑎ ᖃᓄᐃᓗᓐᖃᖅᑎᑕᐅᑎᓂᕐᓂᔅᓗᓗᐃᓴᖅᓯᔪᖅ ᐱᖓᓕᒻᒥᐊᓂᖓ mafic ᑎᑭᑐᒍ silicic magmatism. ᒪᓕᐅᕈᑎᑦ ᑕᓯᐊᕆᔨᖅ ᖁᓕᑎᓂᖅᐊᖏᓐᓄᒍ amphibolite ᐊᑎᓕᓂᖏᓐᓄᑦ granulite facies metamorphic ᖃᓄᐃᓕᓂᐅᓴᖏᓐᓂᑦ ᖁᓕᓴᖅᑎᑕᐅᑎᔪᑦ ᒪᑭᑕᑎᐊᑭᓕᕆᓂᖏᓐᓄ ᑭᓕᓕᖅᖃᑎᑕᑎᔪᖅ magnetite ᐊᒻᒪ orthopyroxene, ᒪᓕᓕᓂᖅᖃᖅᑐᖅ ᓇᓕᒧᑎᑕᑎᓂᕐᒥᑦᑕᑐᓂᑦ ᐊᔨᔪᕕᒃᓯᐊᑦ ᐊᒻᒪ ᐊᐃᕐᑐᖅᓯᒪᔾᔪᑎᑕᖅᖏᓐᖏᑦᓴᓕᖅᓂᕕᓂᑦ ᑐᑭᓯᐊᓂᑎᑦ. Metasedimentary ᐅᓴᖅᖃᐃᑦ, ᐱᖅᓯᐅᑎᓪᓗᑎ quartzite, pelite, ᑐᓴᓄᓴᖅ, ᐊᒻᒪ ᐊᐃᕐᑐᖅ metagreywacke, ᑕᓯᐊᕆᐅᑎᑕᐅᔾᔨᑦ ᐊᒻᒪ ᐊᐃᕐᑐᖅᓯᒪᔾᔪᓂᑦ ᐊᑯᓂᕕᖏᓂᕕᓂ ᐃᓗᐊᓂᓗ plutonic

ᐃᓗᓕᓴᐅ. ᖃᐅᔨᓴᖅᑕᐅᓂᒪᖏᖅ ‘ᑕᕿᐃᑕᑐᖅ’ ᓄᓇᕋᓂᒃᓴᒻᒥᑦ ᓇᓗᐃᓚᖅᓯᐊᖅ metasedimentary ᐅᖃᖅᑲᐃᑦ ᑲᑎᵒᖏᓂᖃᕈᵒᓇᖅᑐᑦ ᖃᑎᖏᑦᑐᑕᑐᓂ Paleoproterozoic ᑭᒡᒋᑭᒡ ᐱᕕᓂᒃ ᓂᑎᖏᓂ ᐊᒡᒪ >ᑐᓕᔨᑦᐅᐊᵒᓇᖏᓂ. ᒪᕐᑐᖅ basaltic ᐅᖃᖅᑲᐃᑦ ᐊᒋᓯᐊᑦ ᐊᒡᒪᐃᓚᖅᑕᑐᒍᖏᐊᑦ Ordovician limestone ᖃᑯᕕᖏᑦᑕᐅᑎᐊᑦ ᐊᒡᒪ ᖃᑯᓪᒥᑦ Paleoproterozoic ᑲᑎᵒᖏᓚᐊᓂᑦ.

ᓄᓇᖕᖏᐊᑦ ᒥᔪᓴᓂᑦ

ᑐᑭᓯᐊᕈᑎᑦᓗᐊᑕᐃᑦ

ᑎᑎᕿᖅᑐᑦ: M.R. St-Onge, O.M. Weller, B.J. Dyck, N.M. Rayner, T. Chadwick, ᐊ ᒪᒪ D. Liikane

ᓄᓇᓂ ᖃᐅᔨᓴᖅᑎ M.R. St-Onge, O.M. Weller, B.J. Dyck, N.M. Rayner, T. Chadwick, ᐊᒡᒪ D. Liikane, ᓄᓇᕐᓯᐊᒋᑕᒪᓂᒻᒥᑦ ᖃᐅᔨᓴᖅᑭᑦ ᑲᓇᑕᒥ; S. Noble-Nowdluk, T. Milton, ᐊᒡᒪ T. Rowe, ᓄᓇᕗᑦ ᒪᕐᒪᒃᑯᑦ, 2015

ᓄᓇᒥ ᖃᐅᔨᓴᕐᓂᒻᒧ ᓇᓗᓇᐃᔪᐃᔪᖅ M.R. St-Onge ᐊᒡᒪ ᑎᑎᕿᖅᑕᐅᖅᑲᓐᓂᖅᑐᑦ ᐅᒧᐊᓪ M.R. St-Onge ᐊᒡᒪ O.M. Weller, 2015

ᓄᓇᒥ ᖃᐅᔨᓴᓂᒻᒥᑦ ᒪᑕᵒᓂᐊᖅᑐᖅ ᐱᑕᕆᐊᒧᑦ ᖃᑯᐊᐅᖓᑕᒫᖅᑐᑦ ᑐᑭᓯᐊᕈᑎᓂᑦ, ᕿᔪᓪᓚ 2.6

ᓄᓇᓪᓯᐊᑕᐊᖅᑭᑦ A. Morin, A. Ford, C. Gilbert, L. Robertson, G. Buller, ᐊ ᒪᒪ R. Buenviaje

ᓄᓇᕐᓯᐊᒋᑕᐊᔪᖅ N. Côté

ᑐᑭᑕᐅᓚᐅᐅᔪᖅ ᖃᐅᓪᓗᓀᑎᑐ ᐃᓄᐅᑎᑐᒻᒥᑦ Wintranslation; ᑐᑭᑕᐅᓚᓯᒪᔪᖅ ᓯᑕ ᓱᒪᒪᐅᓗᐊᓚᐊᕐᓴᖅ ᐅᖃᐅᔨᓯᐅᓯᒪᕐᕕᑐᑐᖅ.

ᐅᓇ ᓄᓇᕐᓯᐊᖅ ᐃᓕᑎᔨᓪᓚ ᓄᓇᐅᑦ ᖃᐅᓄᐃᑕᕐᓚᕐᓂᑕ ᓄᓇᕐᓯᐊᒋᑕᐅᖓᓂᒻᒥᑦ ᐅᑯᓄᓪᓚ ᐅᒪᒻᖁᑎᑎᒋᑕᓚᐅᖅᑯᑦ ᐊᒡᒪ ᐅᖃᖅᐅᔨᒋᑕᓚᐅᖅᑯᓄᑦ (GEM) ᐱᑕᓚᐊᖏᔪᒋᑦ ᖃᑭᖅᑦᑕᒻᒪᖅ ᑐᑭᓯᐊᒋᑕᓚᐅᖅᑯᑦ ᖃᐅᔨᓴᖅᑭᑦ ᑲᓇᑕᒥ (GSC) ᐱᑕᓚᖃᑎᖃᖅᓴᓗᑎᑦ ᑲᓇᑕᒥ ᓄᓇᕗᑦᓗ ᓄᓇᐅᑦ ᖃᐅᔨᓴᖅᑭᑦ ᑎᑎᕿᖅᓴᕕᓂ (CNGO), ᓄᓇᕗᒻᒥ ᓱᓕᓕᖅᓴᓴᒃ, ᑲᐅᕐᒥᐅᑉ ᓱᓕᓕᖅᓴᓴᒃᔪᐊᖅ, ᓱᓕᓕᖅᓴᓴᒃᔪᐊᖅᓂᒃ ᐋᒃᑲᑦ, ᐊᒡᒪᓗ ᓄᓇᕗᑦ ᒪᕐᒪᒃᑯᑦ.

ᐃᖅᑲᓇᐃᔨᖅᑕᕈᑕᓂᒻᒥᑦ ᐃᑲᔪᖅᑕᑦ ᓱᓕᔪᐊᒥ ᐅᑭᐅᕙᖅᑐᖓᓂᑕ ᐱᓕᕐᓂᖅ ᐃᓕᑎᓂᖅᑐᑦ ᑐᑭᖁᓪᓕᖏᓐᓂᒃᑯᓂᒃᓴᓂᑦ ᖃᐅᔨᓴᖅᑭᑦ ᖃᐅᔨᓴᖅᑎᓄᑦ ᐅᑭᐅᙵᖅᑐᑦ. PCSP 05615

ᓄᓇᕐᓯᐊᖅ ᖃᓄᐃᑕᕐᓚᕐᓂᖓᓄᑦ Universal Transverse Mercator, ᐊᐃᒃᑐᖅᓱᒪᓕᒃᑯᑦ 19. North American Datum 1983

ᓄᓇᖅᓯᐊᕐᓂ ᐅᑦᑐᕐᖁᑕᐅᓯᒪᔪᓕᕐᓂᑐᑦ 1:250 000 ᓄᓇᒥᐅᑕᓪᓗᓂᑦᓴᓂᐅᓂᒃ ᑲᓇᑕᒥ, ᐊᑦᖁᑎᐊᖅᑕᐅᓯᒪᓪᓗᑎᑦ.
ᖃᓄᐊᓕᓴᐅᓂᖓ ᒫᑕᓂᒃ ᖃᓄᓕᒍᑦ ᑐᑭᖁᕐᑐᖅ ᐃᒪᐅᕐ ᓇᐅᑦᑎᐊᓂᖓᓪᓕᑕ ᖃᓄᐊᓕᓴᐅᓂᖓ

ᑐᑭᖁᕐᑐᖅ ᓂᐱᐅᓇᖅᑐᖁᕐᓂᖓᓪᓕᑕ ᒥᑭᓪᓕᐊᓪᓕᐊᓂᖓ 2016, 31°36'W, ᒥᖁᔨᐊᓪᓕᐊᓪᓚᑐ 29.5' ᐊᕐᕋᒍᒧᑦ.
ᓇᓱᐅᓂᖓᑭᓚᓄᑦ ᖁᐅᐅᓇᓴᐅᓂᖓᓪᓕᖅ ᐊᔪᒋᐊᖓᑕᑦᑐᑦ ᐅᐸᖓ 31°04'W ᐱᖓᓂᓇᖅ ᐅᐸᓂ ᓂᒥᐊᑕ ᐱᖓᓂᓇᖅᕕᓴᐊᓂ ᑎᓇᖅᑯᐊᓂᑦ ᐅᑉᖓᓂ 32°05'W ᐱᖓᓂᓇᖅ ᐅᐸᓂ ᐅᐊᖏᓇᖓᓪᓕᑕ ᑲᓇᖏᓇᖅᕕᓴᐊᑕ ᑎᓇᖅᑯᐊᓂ ᓄᓇᒥᐊᕐᒥᑦ.

ᐅᓇ ᓄᓇᒥᐊᖅ ᐊᑐᖅᑕᐅᔭᓇᐊᖅᖏᑦᑑᑦᖅ ᑕᓴᒪᖏᑎᐅᓗᓂᓂ ᓄᓇᑯᖅᑐᓗᓂᑦ.

ᐊᔪᓐᖓᓕᐊᖅ ᐊᑎᖓᒐ: Lᓂᑦᑐᓴᒪᓗᑦ, potassium feldspar megacrystic, garnet-biotite monzogranite, ᐊᒥᑦᑐᖅ ᑕᓯᖅ, ᖁᑭᖁᖅᑕᓗᑦ, ᓄᓇᑐᖅ. ᐊᔪᓕᐅᑎᓴᖅ M.R. St-Onge. 2015-127

ᓄᓇᒥᐊᓕᓪᓚᓂᒋᑦ ᖁᐅᐅᓴᖁᖅᑏᑦ ᑲᓇᑕᒥ ᑐᒃᓯᓯᓄᑎᑦᓴᓂ ᐃᖁᑭᐅᐊᑭᑎᓂᑦ ᐃᓕᑭᐊᑭᑎᓂᖓᔪᓂᓐᓂᑦ ᑐᑭᓯᑎᐊᖅᑕᓂᓂᑦᑐᐊᓂ ᐊᐅᓚᑦᑐᖅᑐᓂᑦ.

ᑐᑭᓯᐊᖅᑕᓂᑦ ᐱᖁᑭᓯᐅᓴᓂᓇᖅᑐᑦ ᑕᑯᔪᐅᑲᓂᑦ ᐊᐃᑭᑭᑦᑐᑦ ᑕᑯᓴᐊᑎᑕᐅᖓᓂᑦ ᓄᓇᒥᐊᖅᑎᒋᑦ.
ᑕᑯᑐᔪ ᑎᑎᕆᖁᓪᓚᑦ ᐃᓕᓴᐅᔨᐅᓪᓚᓂᑦ ᑕᐅᔨᐅᓂᒃ ᑲᑎᕆᖁᓪᓚᑦ.
ᓇᑐᓇᐃᔨᖁᓪᓚᑲᑲᓂᖓᓂᑦ ᑎᑎᕆᖁᓪᓚᑦ, ᖁᑲᐅᑦᑎᖁᕐᐃᑦ, ᐊᓪᒪ ᐊᔪᓐᖓᓕᐊᑦ ᓄᓇᒥᐊᒋᑦᑐᑐᖅ ᑐᑭᓯᑎᐊᖅᑕᓂᖓᓐᓂᑦ ᑎᑎᕆᖁᓪᓚᑦᓴᑦ.

ᑕᐅᓇ ᓴᖁᑭᖅᑎᑕᐅᔨᖅ ᐊᑭᖁᖏᑦᑐᑦ ᖁᑎᕆᐊᑦᓴᑲᑦ ᐊᑐᐃᓐᓇᐅᔨᑦ ᐅᑯᑎᒍᓇ
GEOSCAN (http://geoscan.nrcan.gc.ca/)
ᑲᓇᑕ ᓄᓇᖅᓴᒋᒥᓗ ᐅᔨᖁᑲᑲᓂᑦ ᖁᑎᕆᐊᖅᑕᓂᑦ ᑎᑎᕆᖁᐃᖏᓐᓂ (http://cngo.ca/).

ᓴᖁᑭᑎᑕᐅᑭᐅᖁᓕᖅᑭᓚᕐᓂᑦ ᑕᑯᑯᓂᖓᓂ ᖁᑎᕆᐊᑦᓴᑲᑦ ᐊᐃᑭᑭᑦᑐᑦᑕᐅᔨᓚᖏᑦᑐᑦ.

ᓄᓇᖅᓯᐊᓂᑦ ᖁᑎᖁᔭᓂᒋᑦ ᑎᑎᕆᖁᓪᓚᑦ

ᓴᖁᑭᖁᖅᑎᑕᐅᓪᓚᑦᖅ ᓄᓇᖅᓯᐊᖅᖏᑦ ᑐᓂᐅᖁᖅᑲᖁᖅᑕᐅᔨᑦ ᖁᑎᕆᐊᐅᕐᒪᔪᑦ ᖁᑎᕆᔭᕐᓴᓴᐅᓕᓗᑐᓂ Portable Document File (PDF)–ᖅᓕᓗᑐᓂ, ᐊᓪᒪ ᐃᓗᑕᖁᔭᓇᖅᑐᑦ ᓄᓇᒥᑦ ᖁᑎᕆᐊᖅᑕᓂᖓᓪᓕᒋᑦ ᐅᖁᑕᒪᒐᕐᓴᐊᑎᐊᖁᓂᖅᑎᑐᓄᓇᓕᒫᑦ ᐱᔨᔪᑎᑕᓕᓗᓐᓂᑦ ᐊᖏᑎᑐᓂᖓᓄᑦ ᐊᖏᑎᑐᓂᓄᑦ.

ᓄᓇᖅᓯᐊᕐᐅᓂᓪᓕᑦ ᑕᑯᓴᐊᑎᑕᐅᔨᑦ ᐊᑐᖁᑕᐅᔨᑦ ᓄᓇᖅᓯᐊᒥᑦ

ᐅᓇ ᓄᓇᖅᓯᐊᖅᖏᑦ ᐊᑐᖁᖅᑕᑦᑐᖁᖅᑐᖅ ESRI ᓄᓇᖅᓯᐊᓂᑦ ᑕᑯᓴᐊᑎᑕᐅᑎᑐᓂᖓᓂᑦ ᐊᖅᑲᓗᒥᓄᑦ ᐃᓕᖅᑭᔪᓄᓇᓂᐊᓕᓚᒍ ᑕᑯᓴᐊᓂᖓᓪᓕᖅ ᐊᑐᖁᑕᐅᑕᓚᑦᑕᑐᓂᑦ GSC ᓄᓇᓗᐃᓄᖅᑯᑕᐃᑦ ᑕᑯᓴᐊᓂᖓᓪᓕᖅᑕᓚᒍ ᓄᓇᓗᐃᓄᖅᑯᑕᐃᑦ PDF–ᒥᑦ ᓄᓇᖅᓯᐊᑐᐊᒥᑦ. ᖁᑎᕆᐊᖅᑕᓂᖓᑦ ᑐᑭᓯᑎᐊᖅᑎᑦ ᐃᓗᑕᖁᔭᓇᖅᑐᑦᑕᐅᓂᖓᓂᑦᑐᑦ ᓄᓇᓗᐃᓄᖅᑯᑕᐃᑦᓂᑦ ᓄᓇᓗᐃᓄᖅᑯᑕᐃᑦ ᓄᓇᖅᓯᐊᒥᑦ ᐊᑐᖁᑕᐅᑕᓚᑦᑕᑐᓂᑦ GSC ᓄᓇᓗᐃᓄᖅᑯᑕᐃᑦ ᐃᓕᖅᑭᔪᓄᓇᓂᑦ. ᐅᑯᐊ ᓄᓇᓗᐃᓄᖅᑯᑕᐅᔨᑦ ᑕᑯᓴᐊᑎᑕᐅᓂᓪᓚᖅᑐᑦ ᓄᓇᖅᓯᐊᕐᐅᓂᓪᓕᑦ ᑕᑯᓴᐊᑎᑕᐅᔨᑦ ᐊᑐᖁᑕᐅᓂᖓᓪᓕᖅ:

Normal fault; solid circle indicates downthrown side
Oblique-slip fault, normal, inferred
Antiform, defined
Antiform, overturned, defined
Synform, defined
Synform, overturned, defined

ᐅᓴᖅᑲᓂᕐ ᖃᐅᔨᓴᓂᖏᓐᓂ

ᖃᓄᖅ ᐅᖅᑲᒥᒃᓴᓴᐅᓪᓚᖅᑎᓐᓂ ᓄᓇᖓᐊᖅ

ᑐᖅᓴᓚᖕᖏᓐ ᓄᓇᖓᐊᒥᐅᑎᓂᖏᓐ ᓂᑎᖕᓴᓂ ᖃᑎᐊᓂ ᖃᑭᖅᑲᒃᓗᓄ 2015 ᐱᐅᓯᑎᑎᐊᖅᑕᐅᓗᓂ ᐅᓴᖅᑲᓂ ᖃᑲᐅᔨᓴᓂᖏᓐ ᖃᑲᐅᔨᒪᓴᐅᓪᓕ ᑎᑎᕆᖅᑕᐅᓯᒪᔪᓪᓗ ᑭᓇᐅᓴᒥᐅᕆᓯᐊᑭᑎᓴᓴᐅᔨᓪᓇᖅᑐᓂᓂ ᐃᖅᑲᓗᐃᓐ ᖃᑲᓂᑭᖕᖏᓐᓂᓂ. ᓄᓇᖓᐊᓐ ᑕᑯᓴᐅᑎᑕᑦᓂ ᓇᒧᓐᓂᑎᓂ ᓄᓇᖕᓂ ᖃᑲᓇᐃᒥᖓᓂᖕᖏᓐᓂᓂ, ᐱᖃᑯᐅᑎᓪᓗᑎ ᐊᔨᔪᐃᖕᓂᑦᑐᓂ ᐅᓴᖅᑲᐃᐃᓐ ᐊᒪᒪ ᓄᓇᐃᓐ ᑲᑎᓂᖏᓐᓂ. ᓄᓇᒥᓂ ᖃᑲᐅᔨᓴᓂᖏᓐᖅ ᐊᔨᔪᐃᖕᓂᑐᖓᓂᖕᓇᐅᑲᓗᖅᑎᓪᓗᓗᒥᓂ, ᓄᓇᖓᐊᒥᓪᓚᑦᓂ ᐊᖏᓪᓕᐊᓂᑦᑎᓪᓗᓂ: ᐊᒥᐊᓪᓂ ᐊᒪᒪ ᑎᑎᖅᑲᖏᓐᓂ ᓇᓗᓇᐃᖅᑲᓪᓗᑎ ᖃᑲᓇᐃᔪᓐᓇᖏᓐᓂ ᐅᓴᖅᑲᐃᐃᓐ ᓄᓇᐅᑦ ᖁᓪᖏᓐᓂᔪᑦ, ᑎᑎᑯᒋᔨᓕᓪᓗᑎ ᑲᑎᖅᑲᐅᑎᓂᖏᓐᓂᓂ ᓇᓗᓇᐃᖅᑲᓪᓗᑎ ᖃᑲᓇᐃᔪᓐᓇᖏᓐᓂ ᐊᒪᒪ ᓄᓇᐃᓐ ᐳᓪᓕᓐᓂ, ᑎᑎᑲᒋᔨᓕᓪᓗᑎ ᑲᑎᖅᑲᐅᑎᓂᖏᓐᓂᓂ ᓇᓗᓇᐃᖅᑲᓪᓗᑎ ᖃᑲᓇᐃᔪᓐᓇᖏᓐᓂ ᐊᒪᒪ

ᐅᔭᖏᕆᐅᓪᓗᒃ ᑕᐃᔨᐅᓪᓗᒃ "ᑭᒪᒥᑭᒪᒥ ᐱᓕᕆᓪᓗᒃ". ᑕᐃᒪᐃᓐᓂᖅᓱᓄᑦ PLHq ᓄᓇᖓᐊᒥᑦ ᐊᓗᐊᐃᓐᓂᐊᕐᑐᕐᓯᖏᓐᓄᖏᓐᓄᖏ ᑭᒪᒥᑭᒪᒍᑦ ᐱᓕᕆᓪᓗᓄᑦ ᐅᔭᖏᕆᖏ quartzite (ᓄᓇᒧᖏᓪᓗᒃ Paleoproterozoic–ᒥᑦ). ᐊᔪᐸᓗᐊᓂᑦ, Nd ᐊᓗᐊᐃᓐᓂᐊᕐᑐᕐᓯᖏᓐᓄᖏᓐᓄᖏ ᐊᑎᖏᖏᑎᑕᐅᓐᕕᑭᑦᓄᓂᑦ ᐊᐃᖏᑐᖏᓪᓗᔪᓄᑦᐅᔭᖏᖏᐃᓐᑦ diabase ᐃᓕᓴᓪᓗᑦ Neoproterozoic–ᖃᐅᑎᒃᓗᒍ.

ᒪᖏᖅᑲᒃ ᐊᔪᐱᕐᕈᑐᑦ ᐅᔭᖏᖏᑉᒃ ᓴᓂᓕᕆᑐᑎᑦ ᑕᐃᔨᐃᔨᓪᓗᑦ ᖃᑎᐅᓂᖓᖅ, ᐊᓪᒪ ᑉᐅᓇ ᐅᓗᐊᐃᖏᑕᐅᔨᖏᖏᖅ ᐊᔪᐱᕐᕈᑕᕐᕈᓂᓂᓂ ᑎᑎᖏᑕᐅᓪᓗᔪᓂᓂᓇᖓᐊᒥᑦ. ᐊᔪᐱᕐᕈᓂᓕᕆᖏᕐᓄᓂᑉᑲᕐᑕᐅᓪᓗᔪᓂᓂ ᓴᓂᕐᑎᐊᕐᓴᓂᓂ ᐃᓪᒥᓂᖅ ᑕᐃᒪᐃᓕᐅᐅᖏᑎᑦᓗᑎᓂᑦ ᖃᑎᐅᓂᖓᖅ ᐊᐃᖏᓪᓗᖏᖏᖅᑐᖏᖅ. ᐅᔭᖏᖏᐅᔨᖏᖏᖅ ᐊᔪᓂᑕᐅᖏᖏᖅ (ᓱᓕᓗ ᐅᔭᖏᖏᐃᓐᓂ granite ᐊᑐᖏᖏᑕᐅᑎᑦᓗᓂᐅᐅᖅ sedimentary strata) ᐊᑐᖏᓂᓕᕆᖏᕐᓂᑦ ᐊᐅᓪᓚᐃᐃᓂᓂᖏᖏᖅᑐᓂᑦ ᐊᑐᖏᓂᖓᖅ. ᐊᔪᐸᑕᐅᖏᖅ ᑕᑯᓴᐅᑎᑕᐅᔨᑦ ᑐᐸᓪᐊᖏᖅᑐᓂᑦ ᓄᓇᓄᑦ ᓄᓇᖓᐊᑦ ᐱᓚᔭᓇᖏᖅᑐᖏᖅ. ᐃᓪᒥᐸᐊᖏᓗᑐᓄ ᑲᑎᑕᐅᓂᖓᔪᓄᑦ, ᑲᑎᑕᐅᓂᖓᔪᓄᑦ, ᓄᓇᓪᓚᓂᖏᓗᑦ ᐊᐃᓓᑐᖏᖏᖅᑐᖏᖅ ᓂᐅᖓᓂᖏᖏᖅᑐᓂᑦ ᐃᖓᓚᓂᖏᓂᖏᖏᖅᑐᓂᑦ. ᑐᐸᓪᐊᖏᖅᑐᓂᑦ ᑎᑎᖏᑕᐅᑎᑕᐅᔨᖏᖏᖅᑐᓂᑦ ᖁᑲᖓᑕᐅᔨᖏᖏᖅᑐᓂᑦ ᑐᐸᓪᐊᖏᖅᑐᓂᑦ. ᑎᑎᓇᑦᓯᓂᑦ ᓄᓇᖓᐊᑦ ᐊᐃᖏᓪᓗᖏᖏᖅᑐᓂᑦ ᐊᔪᐱᕐᕈᑕᐅᔨᖏᖏᖅᑐᓂᑦ ᐊᔪᐱᕐᕈᑕᐅᔨᖏᖏᖅᑐᓂᑦ ᑎᑎᓇᑦᓯᓂᑦ ᐊᔪᐱᕐᕈᑕᐅᔨᖏᖏᖅᑐᓂᑦ (ᐱᖓᓚᔪᓂᑦ ᓴᓂᕐᑎᓂᑦ, ᒥᑭᔨᓂᑦ ᑎᑎᖏᖅᑐᓂᑦ, ᖁᑲᓂᖓᓪᓚᐃᓂᑦ, ᖁᔪᖏᑦᓗ) ᑐᑭᔪᓂᐊᑭᑎᖏᖏᖅᑐᖏᖅᑐᓂᑎᓂᓂᖏᖏᖅᑐᓂᑦ ᑎᑎᓇᑦᓯᓚᔨᒧᑦ. ᐅᑦᑐᑎᓂᓗᑐᓄ, ᖃᑎᐅᓂᖓᔪᓄᑦ ᐱᖓᓚᔪᓄᑦ ᓄᓇᓪᓚᓄᑦ ᐱᖓᓚᔪᓄᑦ ᓴᓂᕐᑎᓂᑦ ᐱᖓᓚᔪᓄᑦ ᓴᓂᕐᑎᓂᑦ ᓴᓇᕐᓂᐊᕐᑐᖏᖏᖅᑐᓂᑦ ᓴᓂᕐᑎᓂᑦ ᐱᖓᓚᔪᓄᑦ ᓴᓂᕐᑎᓂᑦ ᐱᖓᓚᔪᓄᑦ ᐃᓚᖓᑎᓪᓚᖅᑐᓂᑦ ᑎᑎᓇᑦᓯᓂᑦ ᓄᓇᖓᐊᑦ ᐅᓗᐊᐃᓐᓂᐊᕐᑐᖏᖏᖅᑐᓂᑦ ᓄᓇᖓᐊᑦ ᐅᓗᐊᐃᓐᓂᐊᕐᑐᖏᖏᖅᑐᓂᑦ ᐊᔪᐱᕐᕈᑕᐅᔨᖏᖏᖅᑐᓂᑦ ᓄᓇᖓᐊᑦ ᐅᓗᐊᐃᓐᓂᐊᕐᑐ

ᓇᓗᓇᐃᔨᖏᓪᓗᓂ ᓇᓗᓇᐃᔨᐃᓱᒪᓂᐊᕐᓕᕐᓂ ᖃᓄᐃᑦᑐᐃᓐᓇᖅᑎᓂ ᐊᓱᖅᑎᓂ ᓄᓇᒧᑦ ᓇᓗᓇᐃᒃᑕᐃᑦ ᐊᑐᖅᑕᐅᔪᓂ ᓄᓇᖓᐊᒥᑦ (ᐅᑦᑐᑎᑕᓗᒍ ᓇᒋᓐᓂᖅᓂ ᐅᖃᖅᓄᐃᑦ ᓇᓂᖏᐅᑦ, ᓇᒋᓐᓂᖅᓂ ᓴᓇᕆᑦᑎᐊᕐᕈᐃᑦ, ᐊᓪᓚ ᐊᓱᖅᓂ ᓄᓇᖓᓂ ᑕᔪᓴᐅᑎᑦᑎᔪᑦ ᐱᓪᓚᓇᐅᔪᓐᓇᖅᑐᑦ ᐊᐃᑦᑐᖅᓱᓚᔪᒧᑦ ᑎᑎᕆᖅᑕᐅᓱᓚᔪᑦ ᓄᓇᖓᐊᒥᑦ). ᐱᓕᔪᑎᑦᓗᒍ ᓄᓇᑕᓇᓂᐅᔪᖅ ᐊᐃᑦᑐᖅᓱᓚᔪᑕᒻᒥᓂ ᐊᔨᔾᕆᖓᑕᐅᓐᓇᐃᑦ, ᓄᓇᖓᐊᒧᑦ ᐃᓗᓇᐃᒃᔪᑕᐃᑦᐱᓪᓚᓇᐅᔪᖅ ᑐᑭᓯᑎᐊᑦᓗᒍ ᓄᓇᖓᐊᖅ.

ᖃᐅᔨᓚᑦᓂᐅᔪᖅ ᐊᓪᓚ ᓄᓇᖓᐊᑕᐅᑦᓂᖅ ᓂᑎᖏᓂᓕᖅᑐᓂ ᖃᑭᖅᑦᑕᓗᒃ ᓴᖅᑭᑎᑦᑎᓕᐅᖅᑐᑦ ᐃᑦᑐᓂᖏᑐᓂ metasedimentary ᐅᓴᖅᑲᐃᑦ (ᑭᓪᒥᑭᓪᒥ ᐱᓕᕆᔨᑦ; ᑭᓴᖖᐊᑦ ᐃᓕᓴᐹᖏᓪᓕᔪᑦ PᓪHq, PᓪHc, PᓪHs, PᓪHp; >ᑐᓵᔨᑦ; ᐊᖏᔪᖅᓯᓚᔪᓂᑦ Pᑭᓪ) ᐊᓱᐊᓄᑦ ᐊᑦᑐᐊᓂᖅᑭᑭᓇᖅᑐᖅ ᐅᕐᐊᑉᑐᓂᓂ ᐅᓴᖅᑲᖅᑲᖅᑲᐅᖓᓕᓂᒪᓂ Meta Incognita Peninsula-ᒥᑦ. ᐊᒥᓱᖏᓕᐃᑦ ᑲᑎᕐᓂᐅᖅᑐᑦ magmatic (sills) ᑎᑎᕆᖅᑕᐅᓕᐅᖅᑐᑦ ᐊᓪᓚ ᖃᑲᐅᔨᖅᑕᒻᓕᑐᐊᓵᔪᐅᓂᐊᖅᑐᑦ (ᓄᓇᖓᐊᑦ ᐊᖏᔪᖅᓯᓚᔪᑦ PᓪHu, PᓪHm, PᓪHd). Ċᖃᑯᐊ ᑭᓇᐅᔪᓕᐅᕆᓯᐊᕈᑎᔨᑲᐅᔪᓐᓇᕆᓂᖓᓂᒪᓂᑦ ᐱᓪᓚᓇᐅᔪᑦ ᐃᑐᓕᖅᑲᐅᓕᒪᑕ ᔨᓇᕆᔨᔨᓕᓂᑦ ᐅᓴᕆᓂᐅᑦᑎᕆᔨᐅᔪᓐᓇᖅᑐᑦ (sulphides), ᐅᓪᓚ ᔨᖅᑭᖅᑕᕆᓂᖅᓂᒪᓂᑦ ᓇᑐᐃᓇᖅᓯᓚᔪᓐᓇᖅᑐᑦ ᐱᑕᖅᖃᓂᐅᑦᑐᓂ ᑭᑭᑭᑦᑐᓂᑦ ᑭᑭᑭᑦᑐᓂᑦ ᑭᑭᑭᑦᑐᓂᑦ

ᑎᑎᕎᕐᓇᖅ (CNGO), ᐃᓕᐅᖅᑲᑕᐅᔪᓐᓇ ᓄᓇᕗᒻᒥ ᓯᓚᑕᑐᕎᕐᓴᖅ, ᑲᐅᑭᑕᖅ ᓯᓚᑕᑐᕎᕐᓴᖅᔪᐊᖅ, ᓯᓚᑕᑐᕎᕐᓴᖅᔪᐊᓇᖅ ᐊᑲᓴᑦ, ᐊᒻᒪ ᓄᓇᕗᑦ ᓴᖅᒪᖅᑯᑦ.

ᖃᐅᔨᓴᖃᑦᑕᕐᓂᐅᔪᖅ ᓄᓇᓕᓚᓂᕐᒥ ᖁᑭᖅᑕᒋᔭᑦ ᓂᑎᐊᓂ ᓴᓂᒧᑦ 66°N ᐱᓕᓚᐊᖓᓕᐅᖅᓯᒪᕗᖅ 1949-ᒥᑦ 1965-ᒧᑦ, ᑕᒪᖅᑯᐊ ᖃᐅᔨᓴᐅᕙᓪᓕᐊᔪᑦ ᑲᑎᑕᐅᕙᓪᓕᐊᑦᑐᑎᑲ ᐊᒻᒪ ᐊᑦᑭᖅᑕᐅᓕᕐᖅᑐᓂ ᐅᓴᕐᐃᑦ ᓇᑐᓇᐃᓴᖅᑕᐅᓯᒪᓪᑐᑎᑲ 18-ᓂ 1:250 000 NTS ᓄᓇᖕᖓᐊᓕᐊᓂ ᐊᑐᖅᑐᑎᑲ (ᕿᓂᑲᑐᐊ, 1967 (Blackadar, 1967)). Ċᖅᑯᐊ ᑭᖓᓂᐊᒧᑦ ᖃᑯᒥᔪᑦᓕᑯᑦ ᐱᓕᓚᖃᑕᖅᑐᑎᑲ ᖁᑭᖅᑕᒋᔭᑦ ᖁᑎᐊᓂᑦ (ᓯᐢᑐᓗ, Henderson, 1985). ᖃᑲᓂᓂᕐᓄᑯᓪᓕ, ᒪᓂᓇᓕᕐᓴᐅᑐᓂᑦ ᓄᓇᒥ ᖃᐅᔨᓴᖅᑐᑕᓚᓂᕐᓗᑦ ᖃᐅᔨᓴᒪᔭᐅᓯᒪᔪᓂ ᑐᓴᖅᑎᑕᐅᓯᒪᔪᑦ ᓄᓇᒥ ᖃᐅᔨᓴᕿᑎᐅᔪᓗᑦ ᖃᑯᒥᔪᑦᓕᑯᑦ ᐊᑐᖅᑕᖅᑐᑎᑲ ᓄᓇᒥ ᐱᓯᒪᑕᖅᑕᖅᑐᑎᑲ ᒪᑐ: ᓂᕈᖅᑕᕐᓯᐊᓂᑦ ᖁᑭᖅᑕᒋᔭᑦ (1995-1997; ᐅᔨᐅᔨᐅᓪᓗᓂᑐ, ᐊᔨᓴᖓᐊᖅ 1), ᖁᑭᖅᑕᒋᔭᑦ ᓂᑎᐊᓂ ᐱᓴᖓᓇᖅᑕᕐᓯᐊᓂᑦ (2006; ᖃᐊᖅᓯᖅᑎᕐᓯᒪᔪᖅ, ᐊᔨᓴᖓᐊᖅ 1), ᑎᓄᔨᕎᓇᔭ (Cumberland Peninsula) (2009–2011; ᑲᔪᒪᓕᐅᓪᓗᑎᑲ, ᐊᔨᓴᖓᐊᖅ 1), Hᐊᓪᑦ ᕿᓂᐅᓯᓕ (2012-2013; ᑐᖓᔪᖅᑐᖅ, ᐊᔨᓴᖓᐊᖅ 1), ᐊᒻᒪ ᒥᑕ ᐃᓄᑲᓱᑕ ᕿᓂᐅᓯᓕ (2014 ᓴᓴᓪᓗᓂᑐ, ᐊᔨᓴᖓᐊᖅ 1). 2015 ᐊᐅᔨᖓᒪᑕ ᓯᕐᓂᐊᓂᑦ, ᐊᑕᐅᓯᑐᐊᖅ ᐱᐊᓂᑲᑕᐅᔨᕿᑎᐊᖅᑕᓚᐅᖅᑐᖅ ᓄᑲᖓᓚᐊᖅᓯᒪᔪᖅ ᑕᒪᖏᒥ ᖁᑭᖅᑕᒋᔭᑦ ᓂᕈᖅ 70°N: ᓂᕈᖏᑦ-ᖁᑎᖅᕿᓯᐊᓂᑦ ᖁᑭᖅᑕᒋᔭ ᐅᕐᓂ ᓯᐅᕕᐊ ᔫᓚᓄᑦ ᓴᓂᒧᑦᑕᒪᓂᑦ ᑭᖅᑎᖅᑕᒋᔭᑦ ᓴᓐᓂᖅᓱᒍᑐᑐᖅ ᑲᖏᖅᓱᒍᑐᑐᖅ ᑭᒃᑯᓂᑦ (ᐊᐅᕿᖅᑐᑦ, ᐊᔨᓴᖓᐊᖅ 1).

ᓂᕐᕈᖏᑦ-ᖁᑎᖅᕿᓯᐊᓂᑦ ᖁᑭᖅᑕᒋᔭ ᓄᓇᕐᓗ ᐃᓕᖏᖅᓴᖅ ᐅᐊᕐᓇᖅᕿᓯᕐᒥᑦ (ᑯᕿᐃᒃ-ᖁᑭᖅᑕᒋᔭᒃᑯ) ᓄᓇᐅᑦ ᐃᓕᑭᓪᓗᓂᐅᒃ ᑕᐅᔨᐅᔪᖅ Trans-Hudson Orogen (THO), ᑕᒪᓇᓕᓕ ᐃᒪᐅᑦ ᐊᑕᔪᐃᓴᖅ ᐊᕐᑎᕈᐊᓗᓪᓕᓗᓂ ᓴᖅᓴᕐᓂᕆᑦᑐᖅᑕᖅᑐᓂ ᐅᐊᕐᓇᖅᕿᓯᕐᒥᑦ ᑲᓇᕐᓇᖏᑦ ᒪᐅᕐᓂ ᓂᕈᖅᕿᓯᐊᓇᓄᑦ ᖁᑎᕐᓂᓂᓂ ᓄᓇᑦ ᐊᒥᐊᓕᕐᓂᐊᖅ (Hoffman, 1988). ᐅᓇ THO ᐊᑭᑭᕐᓂᑯᐃᓂᖅ ᑭᖅᑯᓕᕐᓂᕿᒥ ᐅᓇ ᐱᐅᖅᕿᓕᓕᐊᑎᓕᓗᔪ Nuna supercontinent, ᐊᒻᒪᓗ *sensu lato* ᑎᑎᕎᐅᔪᓴᖅᑭᖅᓯᒪᔪᖅ ᒪᑐᓂᐃᓂᕐᓂᓕᕐᒥᑦ ᐅᓇ Manikewan Ocean ᖁᑎᐊᓚᑦᑐᖅ ᐃᓂ ᐊᑎᑕᕐᓂᕐᓂᒥ ᓴᐱᐅᓇᔨᒥᑦ ᐊᒻᒪ ᖃᑯᑕᕐᓂᕐᓂᒥ ᓴᐱᐅᓇᔨᒥᑦ ᐊᒻᒪ ᖃᑯᑕᕐᓂᕐᓂᒥ 1.92-ᒥᑦ 1.80-ᒧᑦ Ga. ᐅᓪᓗᐅᐃᕐᐃᓯᒪᔪᓐᓇᑦ, THO ᓄᓇᐅᑦᑐᖅ ᑐᓪᓕᖅᑭᓯᐅᑯᓪᓗᓂᑦ ᐊᔨᔭᕆᕐᑎᑦᑐᑎᑲᑯᑦ ᐅᐃᓵᔪᓯᒪᔪᓐᓇᐅ ᖃᐅᔨᓴᐅᓕᕐᖅᑐᓂᑦ ᐊᕐᑎᕈᐊᓕᕐᓂᐊᖅ 120 Myr ᑕᒪᐅ ᐃᒪᐅᑦ ᐃᓂᕐᓂ ᒪᑐᓕᕐᓂᐊᓂᕐᓂᓂᑦ ᐃᒪᐅ ca 1920 ᐅᓇᕐᓂ 1800 Ma (Corrigan et al., 2009; St-Onge et al., 2009). ᖁᑭᖅᑕᒋᔭᑦ ᓂᕈᖅᑐᐊᓂ ᐅᓇᕐᓇᖅᕿᓯᐊᓂᑦ, ᑎᐊᒪᑦ ᓄᓇᓚᓂᑦ ᖃᑯᓂᓪᓕᔪᑦ ᐅᑐᓇᐃᓴᖅᑕᐅᓯᒪᔪᑦ (ᐊᔨᓴᖓᐊᖅ 2). ᐊᑎᕈᐃᖅᑕᕐᓂᐊᓂᑦ ᖃᑯᑎᕐᓂᖅᑕᒧ ᐊᑭᑭᖅᑕᕐᓂᐊᓂᓄ, ᐃᒪᐃᓕᕐᓂᕐᓯᒪᔪᖅ:

1) ᓄᓇᓚᓂᑐᖅᑲᐃᑦ ᐱᑎᐊᖃᓚᕐᑎ, ᑐᑭᓕᐅᓪᓚᕆᐅᓯᒪᔪᑦ ᐅᑭᐅᖅᑕᖅᑐᖃᑎᑦ ᑲᔪᓯᖏᓕᓕᐊᓂᕐᓂᓂᓂ ᐅᓇ Superior ᐱᑎᐊᖃᓚᕐᓯᒪᔪᕐᓂᓂᑦ, ᐊᒻᒪᓗ ᖁᑎᐊᓚᑦᑐᖅ ᐃᒪᐃᑐᑐᖅᑲᖅᑐᓂ Paleoproterozoic supracrustal ᖁᑲᓂᒧᑦ (Povungnituk Group; St-Onge et al., 1996;

2) ᖁᑎᐊᓚᑦᑐᑦ ᐅᔨᖃᐃᑦ Paleoproterozoic ᐃᒪᐃᑐᑐᓂᖃᐅᔨᓪᓗᑎᑲ monzogranitic ᐊᒻᒪ granodioritic orthogneiss, ᑐᑭᓕᐅᓚᕆᐅᓯᒪᔪᖅ ᐊᑭᑭᑕᑎᐊᖅᓯᒪᑕᑎᐊᖅᑭᕐᓄᓂᓂᑦ arc-magmatic terrane (Narsajuaq arc; Scott, 1997; St-Onge et al., 2009), ᐅᕐᓀᑐᕐᓄᑦ ᐃᒪᓄᐅ ᓇᖃᖅᓴᐊᖅᑐᑦ-ᐊᑯᓂᐅᑎᑎᓪᓕᖅᑕᖅ ᐱᓴᓴᕈᓕᖅᑕᕐᓴᓂᓂᑦ ᖃᑯᓚᑲᑐᑎᓂᑦ (Corrigan et al., 2009);

3) ᓄᓇᕕᓂᑐᖅᐃᓕ ᐱᑎᐊᖏᖅᓯᒪ ᓴᓂᒋᖕᓴᓪᓚᕆᓪ ᐊᒻᒪ ᖃᑎᐊᑉᓂᑐᖅ Paleoproterozoic supracrustal ᖃᑲᖕᓴᔪᓂ (Lake Harbour Group), ᑲᑎᓂᒪᑦᓗᑎ ᑕᐃᓴᐅᓂᒪᕗᓪᓚᓂ ‘Meta Incognita microcontinent’ ᐅᒪᖏᖕᓂ St-Onge et al. (2000a), ᑕᒪᑲᑯᐊᓗ ᓇᓗᓇᐃᖅᓂᓂᒪᕗᓪᓚᓂ ᒪᑯᓂᖕᓴ crust rifted ᐅᕐᖏᖕᓴ the Rae ᐅᖅᕐᒋᔭᖅᑉᓂ Superior craton, ᐅᖅᕐᒋᔭᖅᑉᓂ ᑕᒪᐃᖅᓄᑦ ᐊᑐᖅᑕᐅᓂᒪᖕᖏᖅᓂᖅᑐᓂᑯᐅᑦ: ᐊᒻᒪ

4) ᓄᓇᕕᓂᑐᖅᐃᓕ ᐱᑎᐊᖏᖅᓯᒪ ᓴᓂᒋᖕᓴᓪᓚᕆᓪ, ᑐᑭᓕᐅᕆᓴᐅᓂᒪᕗᓪᓚᕆᖅ ᓂᑎᕆ ᑲᔪᓂᒪᓂᖕᓴᓂᓄᑦ ᐅᓇ Rae craton, ᐊᒻᒪ ᐅᓇ ᖃᑎᐊᑉᓂᑐᖅ Paleoproterozoic supracrustal ᖃᑲᖕᓴᓄᑦ (Piling Group; Wodicka et al., 2014), ᐅᓴᕋᐃ ᐱᑭᕋᐊᐅᕐᓕᒫᓇᖅᓂᑐᖅᓂ ᐊᔪᕐᓴᖕᖏᓂᖅ ᐅᑯᓇᓄᑦ Hoare Bay Group ᐅᕐᓄᑦ Cumberland Peninsula.

ᖁᑯᕐᓂᒪᓂᖕᖏᓂᑦ 3 ᐊᒻᒪ 4 ᐃᓚᒪᒍᓂᖅᑎᑎᓂᒪᓕᓗᐊᒧᑦ ᐅᒧᖕᓴ Cumberland batholith, ᑭᓇᓗ ᐊᔪᕆᖕᖏᑦᑐᑎᓄ ᐅᓴᕋᐅᓴᐅᖁᑯᑯᓂᒪᓂᒪᓕᕆᓄ ᓴᖅᑭᕐᕿᓕᓂᒪᓂᒪᓕᕆᓄ ᐱᑕᖅᑲᖅᓴᑦ ca. 1865–1845 Ma (Whalen et al., 2010). ᐅᓗ Cumberland batholith ᑐᑭᓕᐅᕆᓴᐅᓂᒪᓕᕆᖅ ᐃᒪᒍᓗ Andean-type batholith (St-Onge et al., 2009), ᐅᕐᖏᓕᓂᒍᓄ ᐱᔪᐊᑎᖅᑲᖅᓴᓄ ᑲᑎᖅᑲᑎᕆᓂᖅᓄᑯᒍᓂᒪᓂᑦ ᐅᑯᐊ lithospheric delamination ᐊᒻᒪ ᓄᓇᐅᕐᓴ ᖃᑎᐊᑉᓂᑐᖅ (Whalen et al., 2010). ᑕᒪᐃᒍᓄ ᖁᑯᓱᒃᑲᓕᓕᒫᓂᑦ ᐅᖓᓗ ca. 720 Ma basaltic ‘Franklin’ ᓴᓐᓕᑎᐅᔪᓄ, ᑭᓯᐊᓂᓕ ᐊᑭᓕᓱᔭᑎᑲᐊᖏᓂᑐᓂᑦ ᐅᖓᓗ Ordovician limestone strata (Blackadar, 1967).

ᑎᑦᓱᒪᑦ ᓄᓇᐅᕐᓴ ᖁᑲᖕᓴᑦ ᐱᑎᐊᖕᖏᓪᓕᖅ ᓂᑎᕆ ᐅᐊᖁᓕᔭᖏᐅᖅᓯᓕᕆᔨᓂᑦ ᐋᖁᑭᕐᕿᓕᓕᒫᐋᑦᓗᑎ ᐅᔭᓕᐊᑦ THO. ᓄᑕᐅᖏᓪᓂᖕᖏᖅᕐᕿᖅ ᓄᓇᕕᓂᖅᓂᒥᑦ, ᖁᑯᓱᓴᑐᓂᒥᑦ 3–4 'ᖁᑭᖕᖏᖅᑕᓗᓴ ᐅᑦᖁᑲᒪ', ᐃᓱᒪᒃᑯᐅᓪᓚᕐᖓᖅ ᐱᑎᐊᑭᑎᖅᑲᖁᓱᓴᕆᐊᓴᖕᖏᖅᓯᒪᓂᒥᑦ ᐋᖁᑭᓴᕐᕿᓕᓕᒫᓂᖓᔪᑦ ᐅᓗ Meta Incognita microcontinent ᐅᕐᖏᓄ Rae craton ᐊᖁᕐᔪᐃᑦ ᐊᑯᓂᖕᖏᓂᒥ ᐅᑯᐊ ca. 1880-ᒥᑦ 1865-ᒧᑦ Ma (St-Onge et al., 2006). ᐅᓗ ᓄᓇ ᐋᖁᑭᓴᕐᕿᓕᒫᖕᖏᓄ ᐅᓴᖁᓇᓕᐊᖅᑲᓚᕐᑐᓂᖅ ᐱᔪᐊᑎᖅᑲᖅᓴᓄ ᓴᖁᑭᓴᕐᕿᓕᒫᖕᖏᓂᒡᒐ ᓂᐱᖁᓪᓗᖅᑐᓂᖅᓂᒥᐅᖅ, ᑭᓯᐊᓂᒥ ᐱᑕᖅᑲᖅᓴᓄ ᒥᑭᓂᑐᓂᑦ ᓄᓇᐅᕐᓴ ᐱᕐᖅᑲᖅᓴᕐᕿᓕᒫᓯᒪᓂᖕᖏᓂᑦ (ᒪᑕᓴᓕᐊᖅ ᑕᐃᓂ ᐊᑲᖕᖏᖅᑲᖅᓴᕐᕿᓕᒫᓂᐅᔪᓂᑦ) ᑕᐃᓂ (St-Onge et al, 2009). ᐅᐊᖕᓇᖕᖏᓂᑦ ᓄᓇᑕᖏᓪᓂᐅᓂᒪᕗᓪᓚᑲᓴᑦ ᐅᓇᐅᕐᓄᓪᓚᕆᓪ ᓂᑎᕆᓪᓕᑦ ᐃᖕᖏᓂᓄ Piling Group, ᑭᓇᓇᑕ ᐃᑲᓴᕿᕆᓴᖅᑯᐅᔪᓪᓚᑦ, ᐃᓴᓴᑕᓂᓄ ᐃᒪᓴᕿᕆᐅᓂᑯᓪᓚᓂᓄ ᐅᓴᕋᕆᓪᑕᐃᓪᓗ ᑲᔪᓴᓂᒪᖕᖏᓪᓚᑲᑦᑐᓂᖅᓗᑎ, ᐊᑕᑯᓗᑎᓴ ᓄᓇᐅᕐᓴ ᓱᓕᓂᑯᓂᒪᓂᑐᓂᑦ ᑭᓴᑯᐊᓗ ᐃᓪᓕᓴᕿᓴᖅᑲᖅᓗᑎᓴ ᓴᕆᕋᓴᓴᓴᖅᓯᒪᔪᓪᓚᕆᓪ. ᓂᑎᐊᓄᓪᓕ ᐱᓪᓚᕐᕆᕆᐊᓪᓚᕆᓪ ᐅᓇᐅᕐᓄᑦ ᐅᐊᖕᓇᖕᖏᓂᑦ ᓂᐱᖁᓪᓗᖅᑐᓂᖅᓂᒥᑦ Lake Harbour Group, ᑭᓇᓯᑕᐅᖅᓴ ᐅᓴᕋᐅᓴᖅᑲᐅᓪᓗᓂᓄ ᐃᓄᐊᓂᓱᓕᖅᓴ ᑕᐃᓂ, ᑭᓱᓯᓂᓕ ᐅᓴᕋᓴᖅᑲᖅᓴᕐᕿᓕᒫᓂᓄᑦᓴᖅᓴᖅᓴᖅ Lᑯᓂᖕᖏᓂᒥ ᐱᑕᖅᓴᖅᓴᖅᓴᖅ basal orthoquartzite ᐊᒻᒪ ᐃᒪᐃᓕᓂᓄ ᐱᑕᖅᖁᓕᓂᓄ iron-formation ᐊᒻᒪ metagreywacke. ᑕᒪᓇᓗ ᓄᓇ ᐅᓴᕋᓇᖅᑐᖅᑕᐅᓂᒪᕗᓪᓚᖅᓴᖅ ᐊᑕᑦᓂᓄ ᐃᓕᐅᓂᖅᓯᒪᓕᐅᓂᒪᓂᖕᖏᓂᑦ ᖁᑯᓕᓕᖅᓯᒪᓂᒪᓕᕆᓂᑦ ᐱᖓᒪᓴᖓᓂᑦ (level 3) ᓱᓄᓂᐊᓂᑦ ᓴᖅᑭᑐᐃᓐᓇ ᐅᕐᓇᕆᓂᑦ Cumberland batholith (St-Onge et al., 2007). 2015-ᒥ ᖃᑲᐅᓴᖅᓂᐅᔪᖅ ᖃᑭᖅᑕᓗᓐᓂᒥ ᐱᓕᕆᐊᓕᖅᑐᓕᕆᓂᑦ, ᐊᑕᐅᓯᖅ ᐊᖓᑎᓂᒪᖕᖏᖅᕐᕿᖅᓯᖅᑕᐅᔪᓂᓕ ᐱᓕᕆᐊᓕᕐᓴᕆᓂᒪᓕᕆᓂᑦ ᖃᑲᐅᓴᐅᓂᖅᑐᓂᒪᓗᑎ ᓄᓇᐅᕐᓴ ᖃᑲᓇᐃᓕᓂᒪᓂᑦ.

ᖁᑯᕐᓂᒪᓂᖕᖏᓂᑦ 2–3 'ᓴᓂᐸ ᑯᒃ' (Soper River) ᓄᓇᖓᓗ ᑎᑎᕋᐅᓯᓯᐅᖅᓯᒪᓕᖅᑲᖅ ᐊᖓᑎᓪᓕᕐᓂᒪᓂᖕᖏᓂᑦ ᓇᓴᓂᖅᔪᐊᑲᖅ ᐊᖁᑲᓂᔪᓚᐅᖓᓖᑦ (magmatic arc) Lᐅᖓᓗ Rae-Meta Incognita ᐃᓂᑎᑦᓚᑎᑎᓯᑦ. ᑕᒪᓇᓗ ᐋᖁᑭᕐᕿᓕᒫᓯᒪᓚᕐᓂᐅᔪᓂᖅ ᖁᑎᐊᓂᑦ 1845 Ma, ᑭᓇᓗ ᐅᑭᐅᑎᔪᑦ ᐱᑎᐊᓕᐊᓴᓯᑉᓂᓕᒫᓂᑦ ᑕᓯᐅᓂᒪᓂᑦ (Dunphy and Ludden, 1998), ᐊᒻᒪ

ca. 1842 Ma, ᒐᓐᓇᓪ ᐅᑭᐅᓚᐅᓇᓯᑎᐊᖅ ᓄᒋᐅᖏᑎᓪᒥ oldest Andean-type phase (Scott, 1997). ᐋᖅᑭᑎᐊᖅᓯᒪᖏᑎᓐᓂᐅᐸᐊᖅ ᓴᖅᑎ ᑯᖏᒥ ᐊᖏᑎᐋᕐᒪ ᐊᒻᒪ ᐃᓗᐊᓄᐊᖅᓇᖅᓱᓂ, ᐊᒻᒪᓗ ᒪᑯᓂᖏᑦ ᐅᓴᖅᑭᐅᖅᓱᓂ ᐊᓯᖓᖅᑕᓪᓕᐊᔪᓂ syn-metamorphic amphibolite-facies ᒪᐅᖏᑦ granulite-facies metamorphic foliation (St-Onge et al., 2007).

ᖁᑯᖓᓯᓂᖏᑎᑦ 1–2 ‘Bergeron’ ᓄᓇ ᐋᖅᑭᒃᑕᓪᓕᐊᓂᑯ ᑐᓗᓪᐅᖅᑎᑦᓗᒍ ᐅᓇ Superior craton ᒪᑯᓂᖏᑦ ᐃᓪᐅᖅᓯᒪᔪᓂᑦ ᐊᐃᑭᖏᑎᑐᑎᓂᑦ ᖁᑯᓴᓂᓂᕐᓂᑦ (ᑲᑎᓯᒪᓕᓗᑎᒃ Churchill plate, ᐅᕐᖓᓄᓂᓂᑦ peri-Churchill collage), ᐊᒻᒪᓗ ᐃᓯᒪᑎᐅᔪᖅ ᑕᐃᒪᐃᓂᓂᐅᑯᐊᖏᖓᓄᑦ ᐊᑯᓂᓂᖏᑦ 1820 Ma, ᐅᑭᐅᐅᓚᐅᔪᖅ ᓄᑭᔨᒧᑦ ᓴᖅᑭᑐᓂᑦ ᓴᓂᕋᓂᑦ ᖃᖅᖃᑎᐅᑦ (Scott and Wodicka, 1998), ᐊᒻᒪ 1795 Ma, ᐊᖅᕋᒍᑎᐅᔪᖅᓗᓂ ᐃᓗᐊᑐᓂᔪᑦ ᐊᖅᑯᓴᖅᓯᒪᔪᖅ ᓄᓇᒥᑦ (Wodicka and Scott, 1997). ᐅᓇ ᖃᓄᓇᑕᐅᓂᓂᐅᔪᖅ ᓴᖅᑭᑎᑦᑎᔨᑎᐅᑕᐅᖅᑐᖅ retrograde amphibolite-facies metamorphism ᒪᑯᓂᖏᑦ ᐅᓴᖅᓂᓂ granulite-facies rocks ᖁᑯᓕᐅᓂᖅᓴᐠᓂᑐᓂ ᑐᓗᖅᑕᐅᕐᕕᐃᓂᒥ ᖁᑭᖅᑕᓗᑦ ᓂᒋᐊᓂ ᒪᐅᖏᓐᓄᑦ ᐊᒻᒪᓗ ᐃᓂᖅᐅᑦ ᐃᓂᒋᔭᐅᓂᑦ (St-Onge et al., 2000b).

TECTONOSTRATIGRAPHIC ᐃᓕᓴᐘᓴᐃ

ᐅᓴᖅᐃᑦ ᓄᓇᙵᐊᓕᐅᖅᑕᐅᔪᑦ ᐅᕐᓂ Sylvia Grinnell Lake–Clearwater Fiord ᓄᓇᓕᓂ ᐱᐊᓂᓴᑕᐅᓕᐅᖅᑐᖅ ᐱᓇᓯᐊᑭᓯᓂ 8-ᓂ ᐱᓕᓚᑲᑕᓐᓂᑯᑦ, ᖁᑦᓕᒍᑦᓕᖅ ᐊᑯᑲᑕᓴᓗᑎᒃ 2015 ᐊᐅᓴᓐᓄᓂᑦ Archean crystalline ᑐᙵᓚᕕᐅᔪᑦ ᑲᓇᓐᓇᖅᑕᓯᐊᓂ ᓄᓇᓐᓇᖅᑐᓯᙵᐊᓵ ᐃᓕᖅᑲᑎᐅᖅᑐᖅ ᒪᑯᓂᖏᑦ tonalite ᐊᒻᒪ granodiorite gneiss ᑕᒫᙵᖏᑦ ᐃᓕᓴᐅᕐᓕᓕᒫᓂᓂ monzogranite, ᑕᒪᓐᓇᓗ ᑕᒫᓂ ᐱᖅᑭᓂᑯᒫᓂᑦ K-feldspar porphyritic.

Paleoproterozoic metasedimentary ᖁᑲᓱᓴᑎᓂᑦ ᐅᓴᖅᐃᑦ ᐃᓕᖅᑲᖅᓱᓂᑲᑎᒃ ᒪᑯᓂᖏᑦ quartzite, semipelite, pelite, marble, ᐊᒻᒪ greywacke ᱡᖅᑭᑲᑦᑕᖅᑐᑦ ᐊᓂᖏᑦᓴᐊᑎᑐᑦ, enclaves, screens, ᐊᒻᒪ panels ᑕᒫᓂ ᐊᒻᒪ ᖁᑎᐊᓂ ᐊᐃᑦᑭᖏᑎᑐᑎᓂ ᓄᓇᐃᑦ ᐃᓂᖏᑐᓂᑦ. Mafic-ultramafic ᑎᒥᖏᑦ ᱡᖅᑭᐅᖅᓴᑦ ᑐᖏᓕᐅᓂᔪᓕᓂᓗᑎᒃ ᒪᑯᐊ ᐃᓗᐊᓂ metasedimentary strata.

ᑕᒫᓂ ᐅᓴᖅᐅᑦ ᐃᓂᖏᑦ ᐱᑕᖅᖁᓂᖅᓴᐅᕐᑦ ᐃᒪᐃᑦᑐᓂᑦ Paleoproterozoic metaplutonic ᐊᐃᑭᖏᑎᑐᑎᐅᓕᓗᑎᒃ ᐃᒪᐃᑦᑐᓂᑦ gabbro ᐃᒪᐃᑦᑐᓄᑦ syenogranite. ᐊᖅᑯᔨᖅᓯᒪᑕᖏᓂᖅᑐᖅ ᑐᑭᖅᑲᖅᓱᖅ ᐊᐃᑭᖏᑎᑐᑎᑦ ᐋᖅᑭᒃᑕᓪᓕᐊᓯᒪᓂᖏᓐᓄᓂᑦ ᐊᖅᑯᔪᑦ ᐊᐃᑭᖏᑎᑐᑐᖅᑯᑦ, ᐊᒻᒪᓗ ᑕᒪᓐᓇ ᐃᓯᒪᓇᖅᓱᖅ ᐊᓯᖓᖅᑕᓪᓕᐊᓂᖅᑎᑦ ᐃᒪᐃᑦᑐᒥᑦ mafic-ᒥ ᐃᒪᐃᑦᑐᓂᖅᓴᐅᑕᖅᓱᓗᑎᒃ silicic compositions. ᐊᐃᑭᖏᑎᑐᑎᑦ ᐅᓴᖅᐃᑦ ᐋᖅᑭᒃᑕᓪᓕᐊᓂᖏᓐ ᓇᓗᓇᐃᔨᖅᑕᐅᓯᒪᔪᑦ ᐊᖅᑯᔭᖏᑎᑐᒧᑦ ᐊᑕᐅᒧ, ᱡᖅᑭᔨᖅᑎᑎᑦᓕᓗᑎᒃ ᓄᐊᑕᐅᔪᕕᓂᖅᓂᑦ ᐅᒧᖏᓐ U-Pb ᐅᑭᐅᖏᑎᑎᒧᑦ ᖁᑲᐅᓇᓯᓗᑎᒃ ᐱᓕᓚᕐᕕᕕᖅᑎᒥ ᐊᖅᑯᓂᓂᐅᖅᑲᖅᑕᐅᓂᑦ, ᐊᒻᒪᓗ ᑲᑎᑕᐃᓇᓚᖅᑲᖅᑕᐅᓂᑦ ᐅᒧᖏᓐ Cumberland batholith.

ᑭᖓᓕᖅᓴᖅᓕ, ᒥᑭᑎᑯᓗᐃᑦ ᐊᑯᓴᖅᓂᐅᔪᑦ ᐅᕐᓄ mafic dykes ᐊᒻᒪ ᖁᑦᓭᓂᑎᑦ ᐅᓴᖅᐃᐅ Ordovician limestone ᓄᓇᙵᐊᖅᒥ ᐋᖅᑭᒃᓯᖅᑕᐅᖓᒥᔪᑦ ᐃᓂ Sylvia Grinnell Lake–Clearwater Fiord area.

Archean crystalline basement (ᐃᓐᓴᖅᑐᒃᓯᒪᔨᐃ At–Amm)

ᑕᒪᐅᓐ ᓄᓐ ᐊᓯᖓᖅᓯᓕᓕᐊᓂᖓ ᓴᖅᑭᑎᕋᓯᒪᔪᖅ ᐅᓴᖅᓂᓂ ᖃᐅᔨᓴᖅᓂᕆᑦ ᐅᕐᓂ Hall Peninsula ᐊᒻᒪᓗ ᑲᓇᐅᖅᓯᓯᐊᓂ Sylvia Grinnell Lake–Clearwater Fiord ᓄᓇᖕᖓᐊᓕᐅᕙᖅᐸᑦ. ᐅᓴᖅᐅᓴᐃᑦ ᖃᓄᓕᒪᓕᓴᑐᑦ ᐊᔨᑎᖅᕈᑦᑐᑎᓂᑦ ᒪᐅᖓᖓ ᐅᖅᖃᐅᓴᐅᓕᖅᖃᐅᔨᓯᒪᔪᓂᑦ, ᓯᐅᖅᑕᐊᕐᕿᓗᖅᑎᑦ ᐊᖅᕈᔨᑎᐅᓂᖅᓴᓄᑦ biotite±hornblende tonalite ᒪᐅᖓᖓ granodiorite ᐃᓕᖅᑲᒍᔪᑦ ᖃᐅᓕᓱᐅᑎᓂᑦ diorite ᒪᐅᖓᖓ quartz diorite. ᐊᖅᕈᓪᓗᓂ ᐱᑭᖅᓯᓪᓕᐊᓂᐊᖅᓂᖓ, ᓯᐅᖅᐃᑦ ᐊᖅᕈᓂᖅᓴᑦ biotite±magnetite monzogranite, locally K-feldspar porphyritic, ᐊᖅᐅᔨᓴᖅᓯᒪᓂᐅᔪᑦ ᒪᐃᓂᖅ pegmatitic syenogranite veins.

Paleoproterozoic metasedimentary (ᐃᓐᓴᖅᐅᔨᓴᖅᑐᒃᓯᒪᔨᐃ PLHq–PPL)

Quartzite, semipelite ᐊᒻᒪ pelite, psammite (ᐃᓐᓴᖅᐅᔨᓴᖅᑐᒃᓯᒪᔨᐃ PLHq–PLHp)

ᖃᐅᓕᓱᓕᓂᕆᐊᖅᓯᒪᔪᑦ ᐊᒻᒪ ᖃᑲᐅᖅᑕᐃᑦ ᐅᖃᐅᓕᓯᒪᔪᑦ ᓯᓚᒧᑦ quartzite ᓴᖅᑭᖃᓕᑕᖅᐳᑦ ᐃᒪᐃᑦᑐᑎᑐᑦ panels ᐃᓱᔨᓂᖃᓕᕆᖅᐸᖅᓯᑎᓴᓐᓂᓕᑦ 100 ᒥᑕᓂᑦ ᑕᒪᖅᐅᓴᓂᑦ monzogranite (ᐊᔪᐊᖓᐊᖅ 3a, b), ᐊᒻᒪᓗ ᐃᓕᖕᒥᔪᑦ ᖃᐄᖓᓕᑐᓂᖃᕆᓚᕐᖅ ᒪᐅᓂᖓ interbedded psammite, semipelite, ᐊᒻᒪ/ᐅᕙᓚᓐᓕᑦ pelite (ᐊᔪᐊᖓᐊᖅ 3b). ᒪᐅᐊ Quartzite ᖃᐅᓕᓱᖅᑐᑎᑦ ᐃᒪᓐᓇᐃᑦᑐᑎᖃᑎᒥᕐᐳᑦ ᐃᓐᖓᑦ orthoquartzite ᒪᐅᖓᖓ feldspathic quartzite, ᖃᐄᖕᒥᔪᑦ ᐃᓕᐅᖅᑲᓂᓕᖅᓯᒪᕐᐳᑦ ᐊᒻᒪᓗ ᐃᓕᓐᓂᖅᓄᑦ ᐃᓕᖃᖅᑲᓗᑎᒃ garnet-ᒥᑦ. Pelite horizons ᐃᓕᖃᖅᑲᒋᐃᑦ assemblage biotite-garnet-sillimanite-K-feldspar-melt (ᐊᔪᐊᖓᐊᖅ 3c), ᐊᒻᒪᓗ ᓴᖅᑭᔪᓯᓕᑎᒃ ᖃᐅᓕᓱᖅᑐᑎᓂᑦ ᑭᓯᖃᖏᑭᓐᓂᖅᓴᐅᔨᓂᑦ ᐅᓄᑎᔪᓇᖅ biotite±garnet psammitic ᐅᕙᓚᓐᓂᓕᑦ biotite±garnet±sillimanite semipelitic migmatite. ᐱᑎᐊᑭᑎᐅᓯᒪᔨᑦ ᑲᑎᕋᕐᓕᕆᐅᓂᐅᔨᓂ ᐃᓕᖃᖅᑲᓯᒪᕐᐳᑦ 20 vol. % ᐊᖅᑕᔨᑎᐅᓂᖅᓴᓂ ᓯᐅᖅᓯᓂᑦ leucosome, ᐃᒪᐃᑦᑐᓂᕆᖅᑲᖅᑕᐅᔨᓂᑦ crystallised melt, ᐃᓕᖃᖅᑲᓗᓂ patch to stromatic metatexite textures, ᐊᒻᒪᓗ ᒪᐅᓂᖓ ᐱᑕᖃᖅᑎᒋᓗᑎᒃ muscovite, ᐃᓕᖃᖅᑲᓗᑎᒃ ᒪᐅᓂᖓ peak metamorphic conditions ᒪᐅᓂᖓ ᐊᒥᓯᓂᖅᐅᑦᓗᑎᒃ muscovite-dehydration (St-Onge et al., 2007; Dyck and St-Onge, 2014). Cordierite ᐱᑕᖃᓚᑦᒥᔨᖅ ᐅᔪᓚᖅᑎᑦ metasedimentary assemblages ᑲᑎᓯᒪᐅᖅᑐᓂᑦ, ᐃᒪᐃᑕᑐᖃᓂᖅᓴᖅᑲᐅᓇᑉᐳᐅᑦᓗᓂ paleopressures ᐅᖅᑕᒋᑦᓴᑕᑐᓂᑦ 6 kbar. Gossanous horizons ᐱᑕᖃᖅᑲᒍᑦ ᒪᐅᔪᓂᑦ siliciclastic units, ᒋᖅᔪᐊᓕ ᐃᓂᑎᖅᐅᓂᖓᓴᐅᕙᓚᑎᒃ ᒪᐅᓂᖓ chalcopyrite, graphite, ᐊᒻᒪ pyrite. ᑕᔪᐳᐅᓚᑐᐃᓚᐅᕐᓗᐊᖅᑎᑦᓗᒍ ᐊᑐᐃᓚᐅᖓᓕᑕᓂ ᐃᒪᒋᓂᑦ, ᒪᐅᐊ the siliciclastic ᐃᓂᖅᑎᑦ ᖃᐅᔨᓴᖅᑕᐅᕙᓪᓕᓕᐊᔨᑎᑦᑐᑦ ᐋᓴᖅᓯᒪᓂᖅᑎᑦ ᐊᔨᑎᑭᓴᖅᓴᑦ ᐅᔪᓂᖓ metasedimentary strata ᐃᓂ ᐊᖅᑐᐊᐅᖒᓂᑦ Lake Harbour Group ᐃᓂᓴᖅᖃᐅᓂᖅᑎᑦᑎᑐᑦ (St-Onge et al., 1996, 1998; Scott et al., 1997).

Marble and calc-silicate (ᐃᓕᖅᑲᒍᓴᖅ PLHc)

ᐅᖅᑕᐃᑦ ᐊᓯᖏᑐᑦ ᐊᑭᓐᓇᑎᑐᔪᓕᕆᓴᖅᑐᑦ ᐃᔨᔪᖅᑎᑭᓐᓇᖅᑲᓗᑎᒃ 100 ᒥᑕᔭᓂ ᒪᔪᓇᓂ monzogranite, ᐊᒻᒪᓗ ᐊᖅᑎᓂᖅᓴᖅᓯᒪᓕᓐᓂᑎᒃ 10 ᑭᓕᒥᑕᔭᓂᑦ ᑕᐃᓂ (ᐊᔪᐊᖓᐊᖅ 3d). ᐅᖅᑕᐃᑦ ᓯᐅᕙᐅᓂᖅᑎᑦ ᐊᖅᑎᓂᖅᓴᖅᑲᐅᔨᑦ ᐊᒻᒪ ᐊᖅᑎᓂᖅᓴᖅᑲᐅᖅᑭᓂᖅᑲᓗᑎᒃ ᐊᒻᒪ ᑕᐃᓐᑲᓗᑎᒃ ᖃᑲᓕᓱᖅᑎᓯᒪᔨᕆᑎᓂᑦ ᓇᓗᓇᖅᑎᓗᓂ ᖃᓄᐃᐃᑦᑐᕐᓕᓕᐊᓂᖅᑎᑦ ᐅᔪᓂᖓ apatite, calcite, diopside, humite, forsterite, magnetite, phlogopite, scapolite, spodumene, titanite, ᐊᒻᒪ tremolite (ᐊᔪᐊᖓᐊᖅ 3e). ᑕᒪᑭᐊ ᐊᖅᑭᑦᓯᑕᑦ ᐅᖅᑕᐃ ᐃᓯᒪᒋᐅᔨᑦ ᐃᒪᐃᑕᑦᑲᓂᓂᖅᓴᖅᑲᐅᖅᓯᐊᓚᐅᖏᖅᓂᖅᑎᓂᑦ

tectonostratigraphically ᖃᔪᑎᖑᓂᖅᓗ ᐅᕙᓂ Lake Harbour Group Lᔪᓇᖏᑐᐅᖑᕐᓄᑦᓂᑦ siliclastic units ᖃᔪᓪᒍᑦ ᓇᓗᓇᐃᖅᑕᐅᓯᒪᔪᓂᑦ.

Metagreywacke (ᐃᓪᓴᔪᖏᖅ PPL)

Metagreywacke ᑎᑎᕆᐅᓯᐅᓯᒪᔪᖅ ᐅᐊᖑᓇᖑᓂᓂ ᑲᓇᖑᓇᖅᑕᓯᐊᓂᓂ ᖃᑲᐅᓴᖅᑕᐅᕐᐳᐅᔪᒥᑦ, ᓴᖑᖑᔪᑎᑐᑦ ᐅᔪᐊ ᐃᓗᐊᒍᑦ biotite monzogranite (ᐊᓴᖓᐊᖅ 3f). ᖃᔪᓪᒍᑦ ᑎᑎᕆᖅᑕᐅᓯᒪᔪᑎᑐᑦ, greywacke ᐱᑕᖃᖑᓕᑐᖅ ᐅᕐᓂ Lake Harbour Group ᐅᓴᕆᐃᑦ ᖃᑲᓚᐃᔅᓯᑎᖑᓂᓂᑦ, ᑭᓯᐊᓂᓪ ᐱᑕᖃᓂᓴᖅᓴᐅᑦᓗᓂ ᐅᕐᓂ Longstaff Bluff ᐊᖏᑭᓯᖅᓯᒪᓂᖑᓂᓂ ᐅᕐᓂ Piling Group ᓚᓇᖓᐊᒋᑐᑦ ᐅᐊᐅᖑᓂᓂ (Wodicka et al., 2014), ᐊᓯᓴᖅᑉᑦᑕᐊᓂᓚᓴᖑᓂᓂᑦ granitoid-ᒥ ᐅᓴᕆᖑᓂᑦ.

Paleoproterozoic mafic-ultramafic sills (ᐃᓪᓴᔪᖏᖅᐃ PLHu–PLHd)

ᐅᓴᕆᐃᑦ ᓴᖑᑐᑎᐅᓪᓕᑦ Lᔪᓇᖖᑦ ᓯᐅᕆᕆᓂ ᐊᖑᑎᓂᖅᓴᖑᖑᓂ ᐊᖑᑎᓪᓕᑎᓀᖑᓂᓀᓂ ᐃLᐃᑕᖃᑦᑕᖅᑐᑦ, mafic-ᒥᑦ ᐅᕐᖑᓂ ultramafic rocks ᐅᓴᕆᖑᓀᑦ ᐅᕐᓂ ᕐᐅᐱᐱᓯ ᐃᓂᑎᓂᓂᑦ (Liikane et al., 2015) ᑕᐃLᐃᕐᐸᔪᑎᓂᓗ Lᐅᓇᑕᒪᖅ siliciclastic strata ᖃᑭᖅᑕᓄᑦ ᓂᑎᐊᓂ ᖃᑎᐸᓗᐊᓂᑦ. ᐃᓚᒃᓪᓴᔪᖏᑦ ᐃᔪᔨᓂᖃᓴᖅᑕᑦᑐᖅᑐᑦ 10-20 ᒥᑕᔭᓂᑦ, ᐃᑕᖑᑦᑕ ᐊᖑᑎᓪᑕᔨᓇᖅᓴᑎᒃ 100 ᒥᑕᔭᓂ ᐃᔪᔨᓂᖃᑕᖓᓗᑎᒃ, ᐊᓚᒪᓗ ᖃᓪᓗᒍ ᑭᓱᒥᑕᔭᓚᖑᓂ ᖃᓪᓕᑎᓀᖑᓂᓀᓇᖅᓴᑎᒃ. Lᓪᐊ mafic ᐊᓚᒪ ultramafic rocks ᐃᐱᒃᑐᑎᐅᑭᑦ ᔭᖃᑭᓴᖃᑎᖃᖅᓴᑎᒃ ᐅᓪᓂᓐᓄᑦ their host metasedimentary units, ᐊᓚᒪᓗ ᐃᓯᒪᓇᖅᓴᑎᒃ ᑐᖖᓂᓴᖅᑐᑦ. ᐊᖑᑎᓂᓴᖅᑐᑦ ᐅᓴᕆᐃᑦ ᖃᓪᓕᓱᒃᑐᑕᐅᑭᑦ, ᐊᔨᑲᖑᑕᑐᑎᐅᑦᓗᑎ ᐃLᐟᓇ ᖃᑎᓯᒪᐅᖅᑐᑦᓂᑦ clinopyroxene-orthopyroxene±hornblende metapyroxenite ᑐᖖᓴᙱᔪᖓᓂᑦ (ᐊᓯᓴᖓᐊᖅ 4a), ᑭᖓᓂᐊᒍᑦ ᐃLᑕᖑᓪᓗᑎᒃ olivine-clinopyroxene-orthopyroxene metaperidotite ᐊᓚᒪ metagabbro Lᐅᖑᓄ metaleucogabbro up section (ᐊᓯᓴᖓᐊᖅ 4b). ᐃᑕᒪᐟᐅᑦ, ᓱᖃᓂ, ᐱᑕᓓᑕᒪᓂᔪᖅ ᐃᑕᐟᓂᐊᔪᖅᑎᐅᔨᔪᖅ ᖃᖃᓴᖅᑎᓂᑦ ᐃᖃᔨᖅᑎ ᐱᑕᓓᐊᖃᖅᖅᓴᖅ ᐅᒥᖑᓄ MSc thesis ᑎᑎᕆᐅᓯᖃᖅᓴᐊᓪᓗᓂ Lᔪᓂᖑᓄ petrology, geochemistry, ᐊᓚᒪ geochronology Lᔪᓂᖑᓄ ᖃᔪᑕᓴᑦᑎᓯᒪᔪᓂᑦ ᐅᓴᕆᖑᓂᑦ ᔪᐸᐃᒃ ᑕᕆᖑᓄᓂᑦ ᐊᖃᑐᐊᓂᖃᖅᓴᑎᒃ ᐅᔪᓂᖑᓄ Raglan Ni-Cu deposit (ᐊᓯᓴᖓᐊᖅ 2). ᐅᖃᖅᐅᓯᖃᖅᖃᐟᓂᖅᓯᒪᔪᓂᑦ ᐅᒥᖑᓄ mafic-ultramafic ᐅᓴᕆᖑᓂ ᐅᕐᓂᓐᓂᑦ Liikane et al. (2015).

Paleoproterozoic metaplutonic suite (ᐃᓪᓴᔪᖏᖅᐃ Pg–Psb)

Gabbro (ᐃᓪᓴᔪᖏᖅᐃ Pg)

ᖃᑲᓯᒪᓴᐃᑦ ᓯᐅᕆᐅᓴᔪᓪᒍᑦ ᐃLᐃᑦᑐᓂ pegmatitic, kilometre-scale, layered biotite-clinopyroxene-magnetite±hornblende gabbro plutons ᐱᑕᖃᖅᖅᓂᑦ ᐱᖏᖑᓇᖅᑐᓯᒪᔪᓂ Sylvia Grinnell Lake–Clearwater Fiord ᐃᓂᒪᖑᑕ. ᐃᓪᓴᖑᓂᕆᔭᑦ, ᑕᒪᔪᔪᐊ plutons ᐃLᖃᖅᖅᑐᑦ Lᔪᓂᖑᓄ clinopyroxene-bearing anorthosite.

Quartz diorite (ᐃᓪᓴᔪᖏᖅᐃ Pd)

Quartz diorite ᓴᖅᑭᕆᖃᑕᖅᑐᑦ Lᓂᕆᑦᑐᑎᓂ, ᖃᑭᓂᖅᑐᑎᓂ, ᐊᖑᑎᔨᒪᓱᑦ ᑕᔪᓴᐅᖑᑎᑕᐅᔨᔪᑦ ᐃᓪᓴᔪᖏᖑᓂᒥᑦ ᐃᓚᓂᖃᖅᖅᑐᖅ ᑲᑎᓂᖑᓂᑦ biotite-clinopyroxene-orthopyroxene±hornblende. ᑕᔪᓴᐅᔨᑦ ᑕᔪᓴᐅᑎᐊᕐᓇᑎ ᐅᓴᖅᑲᓂᑦ plutons iᐱᖑᑭᓇᖑᓂ ᐃᓪᖑᓂᑦ ᖃᐅᔨᓴᕆᐃᐅᔨᒥᑦ, ᐊᓚᒪᓗ ᐊᔨᑎᖑᑕᖑᑎᑦ ᓴᓂᐊᓱᑦᑐᑦ ᐃᓗᐊᒍᑦ ᐃᓪᓴᔪᖏᖑᓪᓕᒪᓂᑦ ᑲᓇᑭᓗᒧᑦ (ᐊᓯᓴᖓᐊᖅ 5a).

ᓄᓇᖃᐊᖅ–ᐊᖏᑎᓂᖏᓐ ᓴᓇᓯᒪᓂᖏᓐ ᓇᓗᓇᐃᖅᓯᔪᖅ ᐃᓕᑲᑦᖏᓚᔪᖅ ᓴᖅᑭᖅᑕᕐᖅᑐᑦ ᖃᑲᓂᖏᓐᓂᖅᑐᑦ ᑭᓯᑎᖅᑐᑦ ᑐᓴᖅᑎᓂᑦ ᑐᓴᖅᑎᓂᑦ ᑐᓴᖅᑎᓂᑦ metaplutonic.

Biotite granodiorite (ᐃᓕᑲᑦᖏᓚᔪᖅ Pgo)

ᐊᖏᑎᒃᖏᑕᑐᖅ, ᐊᖏᑭᒍᐊᓗᓚᕐᑐᖅ, biotite±hornblende±magnetite granodiorite ᑎᑎᕀᖅᑕᐅᓯᒪᔪᑦ ᐅᐊᖓᓇᖏᓐ ᐱᖏᓖᓇᖏᓂᓐ ᖃᑲᐅᓴᕀᖅᐃᐅᔪᒥᑦ. ᕿᖓᓂᕆᔪᑐᑦ ᐊᓪᒪᕿᑎᐊᑦᓂᑐᓂ ᒪᓕᑦᓂᓐᓂᑦ.

K-feldspar megacrystic biotite monzogranite (ᐃᓕᑲᑦᖏᓚᔪᐃ Pmo, Pms, Pmh)

ᐊᐅᔨᒃᖏᓚᔪᖅ ᐊᐅᔨᕈᔪᑐᒍᑦ ᓯᓇᖏᓄᑲᑦ, ᕿᑎᐊᓂ ᑎᑭᑐᒍᒍ ᒪᓕᑦᓂᓐᖏᓐ, ᐊᖏᑎᔪᕆᐊᒥᑦ ᓴᑐᑏᒥᓄᑦ biotite±orthopyroxene±magnetite±garnet monzogranite ᓇᓗᓇᕎᑎᑎ K-feldspar megacrysts ᓴᖅᑭᖅᑕᕐᖅᑐᑦ ᐊᖏᑎᔪᒥᑦ ᐃᓕᓐᑭᓂᑦ ᓂᑎᐊᓂᓗ ᓯᑭᖅᑕᒃᓗᑲᑦ. K-feldspar phenocrysts ᐃᔨᑎᑐᑦ ᐊᖏᑎᓂᕐᖅᑲᖅᑐᑦ ᑎᑭᓯᒪᔪᑦ 10 cm ᓴᓂᒧᑦ, ᓄᓇᓕᒻᒥ ᑕᑯᓴᕆᑎᑕᐅᔪᑦ rapakivi ᖃᑲᓄᐃᒍᑎᓕᑦ (ovoid alkali feldspar ᑕᕐᓗᑕᐅᓯᒪᔪᑦ plagioclase feldspar; ᐊᑦᔨᵒᖓᐊᖅ 5b). ᐃᓕᑲᑦᖏᓚᔪᖅ ᐃᖅᑲᓇᐃᓱᖓᑲᓂᖅᑐᖅ ᕿᓚᒋᑎᑎᑐᑦ ᐊᖏᑎᓂᕐᖅᑲᖅᑐᓂ ᐅᐊᖓᓇᒧᖏᓚᔪ ᐊᕐᑐᖅᑲᓯᒪᔪᖅᐅᐊᖓᓇᖅᑕᓯᖏᓐᓂᑦ ᐃᓕᖏᓐᓂᑦ ᖃᑲᐅᓴᕀᖅᐃᐅᔪᒥᑦ, ᐃᓕᑎᑦᓗᓂᐅᐳᖅ σ-porphyroclasts ᐅᑯᓇᓂ ᓇᓗᓇᐃᔭᐃᔪᖅ ᖃᑯᓪᓂ ᓂᑎᐊᓂ.

Biotite monzogranite (ᐃᓕᑲᑦᖏᓚᔪᖅ Pmb)

ᐅᖃᐅᔨᖃᐅᖅᑐᖅᑐᑦ biotite±orthopyroxene±magnetite±hornblende±garnet monzogranite ᓄᓇᐅᑉ ᐊᑕᑯᓕᑐᑎᐅᐅᒃ ᖁᑭᖅᑕᒃᓗᓐᓂᑉ ᓂᑎᐊᑕ ᖁᑎᐊᓂᑦ. ᐃᓂᖏᓪᓕᓂ ᓯᐅᕆᖃᓂᖅᓴᖅᑲᖅ ᐊᖏᑎᔨᑎᐅᓂᕆᓂᑦ, ᖃᖃᓯᔪᒃᓴᑎᐳ ᐊᐅᔨᔪᑦᔪᒃᓴᑎᐳᓗ ᓯᓕᒧᑦ. ᑕᒪᑯᓯᐊ ᐃᓂᖏᑦᑐᐅᐅᖅᑐᑦ ᐊᔨᑭᖃᓕᖏᑕᖏᑐᑦ ᒪᓐᖏᓕ magnetite-rich ᐊᓗᒪ magnetite-free ᐃᓂᑎᑦᐅᔨᓂᑦ, ᐊᓗᒪ ᐃᓕᓴᖃᖅᓴᖅᑲᑎᐳ ᒪᓯᓂᖏᓐ hornblende ᐅᐊᖏᓖᖏᑕ ᐱᖏᓖᓇᖅᑕᓯᐊᓂᓂ ᑕᒧᓂ ᖃᐅᔨᔪᖅᐃᐅᔪᒥᑦ. ᐃᓕᖏᑭᓂᑦ, ᐱᑭᖅᑐᐃᑦ ᑕᑯᔨᐅᓯᒪᐅᑦ ᐃᒪᓐᓇ axial planar-ᒥᑦ ᐊᑕᐅᓯᔪᖅᑕᓕᕆᔨᓂᑦ ᐃᓂᖏᑭᓂᑦ (ᐊᔨᔪᖅᐊᖅ 5c), ᓇᓗᓇᑭᓐᓂᖅᓯᒪᔪᓗᓂᐅ ᐊᒥᓯᒪᓕᕆᐅᓂᖏᑭᓂᑦ ᒥᖅᓀᑎᐊᔪᐅᔪᒥᑦ ᑕᒧᓂ.

Garnet-biotite monzogranite (ᐃᓕᑲᑦᖏᓚᔪᖅ Pmg)

ᖃᑯᖅᓯᓯᒪᓕᖅᑐᑦ ᓯᓕᒧᑦ, ᐊᖏᑎᔪᒪᓕᑦ ᐱᑭᔪᐃᐅᔪᓇᖅᑐᑦ, ᓯᐅᔪᑎᐊᐅᓂᕈᒥ ᐊᖏᑎᓂᔪᖁᓕᖏᑦ ᐅᓴᔪᐃᑦ garnet-biotite±magnetite monzogranite ᓴᖅᑭᖅᑕᒃᓯᒪᓗᑦ ᖃᑲᐅᔨᔪᖅᐃᐅᔪᐊᑦ ᑲᓇᖏᖅᑲᓯᐊᓂᑦ. ᑕᒪᓂᓇ ᐃᓂᖅᑎᖅᐃᐅᔪᖅ ᓴᖅᑭᑦᓴᓐᓴᖅ ᐃᓗᑐᓂᖅᑎᑐᑦ ᐊᒪᒪ ᑐᖏᒪᖅᑎᑐᑦ ᒥᓂ K-feldspar megacrystic monzogranite (ᐊᔨᔪᖅᐊᖅ 3d), ᐊᒪᒪ ᐊᖏᑭᒍᑎᐅᓪᓗᓂ ᒪᓕᑦᓂᖏᓐ plutons-ᓂ ᐃᓕᓴᐅᑎᕀᑐᑦ ᒪᓕᑦᓂᖏᓐ biotite monzogranite. Garnet ᐱᑕᖅᖅᑐᐃᑦ ᐃᒪᓐᓇᐅᓕᖏᓚᓪᓗᑎᑦ 2–30 mm burgundy coloured phenocrysts, ᑕᒪᑦᑯᐊᓗ ᐱᖅᑎᖅᑲᓚᕐᓪᓗᑎᑦ ᒪᓕᑦᓂᖏᓐ (ᐃᓗᐊᓄᓐᓂᕆᖅ, ᐊᔨᔪᖅᐊᖅ 5d).

Garnet-sillimanite leucogranite (ᐃᓕᑲᑦᖏᓚᔪᖅ PLHw)

Garnet-sillimanite leucogranite ᓴᖅᑭᖅᑕᒃᑕᖅᓴᑦ ᐃᒪᓐᓇ ᐃᓗᑐᔨᓂ ᐊᑐᖅᑎᑎᖅᑲᖅᓯᒃᓗᑎᑎᑦ ᒪᓕᑦᓂᖏᓐ garnet-biotite monzogranite ᐅᕐᖓᔭᓐᓄᑦ ᓄᓇᙳᐊᑦ ᓇᓗᓇᐃᑲᑯᖏᑎᑎᑕᑦ plutons ᐊᑲᐃᐅᓂᖅᑲᓯᒪᔪᑦ ᒪᓕᑦᓂᖏᓐ garnet-biotite monzogranite ᑲᓇᖏᖅᑲᓯᐊᓂᑦ ᖃᑲᐅᔨᔪᖅᑕᐅᔪᒃ. ᐃᓂᑎᑦᐅᖓᓕᖅᑐᖅ ᓯᐅᔪᑎᐊᖓᓂᖅᓴᐅᔪᖅᑕᕐᖅᑐᑦ, ᐃᓕᓴᖅᑲᖅᑐᑎᑎᖅ 1–5 mm ᐅᔨᐅᔨᕆᔨᒥ

ᑕᖅᓴᖅᑐᖅᑐᓂ garnet phenocrysts ᐊᒻᒪ Lძᐊ sillimanite (ᐊᓱᐅᖓᐊᖅ 5e). ᐱᑕᖅᑎᓂᐅᕐᓴᖅ Lძᓂᖓ sillimanite ᐃᓗᒪᖏᓐᓇᖅᐳᖅ Lძᐊ leucogranite ᓴᖅᑭᖏᓂძᔭᑌᐊᐅᓴᖅᓯᒪᖏᖑᓂ Lძᓇᖓᓯᑦ muscovite-dehydration ᐊᐅᐦᑦᓚᐊᕐᑦᓚᐊᓂᖏᖑᓄᑦ Lძᓂᖓ metasedimentary units ᑎᑎᕆᖅᑕᐅᓗᒪᓂᖏᓕᑎᔪᑦ ᐊᓗᐊᔪᑦ ᖃᑭᖅᑕᓪᓗᓵᑦ ᓂᑭᐊᔾᔨᖏᓴᓂᕐᓂᑦ (ᓗᐢᓗᓐ, Dyck and St-Onge, 2014), ᐃᒪᖏᓇᐅᖓᓂᐱᓴᖅᑐᖅ ᐃᓕᑭᑎᑕᐅᔭᑌᐊᐅᓴᖅᓯᒪᓂᖓ ᒪᑐᒍᖓ plutonic suite.

Biotite syenogranite (ᐃᓕᓴᐅძᖏᓚᐢᖅ Psb)

ᓗᐅᕆᐃᑦ ᐊᖏᑭᓕᑎᐅᓂᖅᓴᕐᕿᑦ ᐃᒪᐃᑦᑐᙵᖅᑐᑦ pegmatitic, ᐊᐅᐸᓕᙵᖅᓗᒪᓕᑐᐃᑎᓴ ᓗᓕᒧᑦ biotite syenogranite ᐃᒪᐃᑦᑐᙵᖅᑎᑎᑌᓗᒪᓕᕐᑦ anastomosing dykes ᐃᓕᖏᑭᓂᑦ ᐃᓂᑭᔭᐅᕐᓂᑦ (ᐊᓱᐅᙵᐊᖅ 5f). ᐃᓕᖏᑭᓂᑦ ᐃᓂᑭᔭᐅᕐᓂᑦ Lძᐊ syenogranite ᐱᑭᕆᐃᐅᓗᒪᕐᑦ, ᑭᓗᐊᓂᓕ ᐃᓂᑭᔭᐅᕐᑦ ᐃᓕᓴᐅᓗᖏᑭᓵᓂᑐᓵᓂᕆᕿᖅᑐᑦ ᐊᒻᒪ ᐊᐳᕆᐃᐦᓕᖅᓴᓐᑐᖅ ᐱᑭᖅᑐᓂᑦ (ᐊᓱᐅᙵᐊᖅ 5a). ᕆᑯᑎᖅᑯᓕᓕ ᑕᒪᖅᑯᐊ ᐃᓗᑐᓂᐅᕐᓂᑦ ᐱᑕᖅᑕᖅᑕᕐᖅᐳᑦ Lძᓂᖓ phenocrysts of garnet ᐊᒻᒪ tourmaline.

ᐊᓗᖏᑦ ᐃᓕᖅძᖏᓚᐢᓂᑦ

Basaltic dykes (ᐃᓕᖅძᖏᓚᐢᐃ Mcd, Nd)

ᒪᓂᕐ ᐃᓂᑭᔭᐅᓱᑦ ᒥᑭᑐᓂᑦ 1–20 m ᓗᓕᖓᓂᕆᖅᑕᖅᑐᓂᑦ ᐅᙶᖏᓕᓕᓗᒪᖅ ᓗᐅᑎᑦᑎᐊᕙᐅᐅᓕᑦ ᐊᖏᑭᓂᐅᓂᕆᖅᑕᓕᓗᒪᖅ ᐃᓕᖏᑦ basaltic dykes containing 1–2 mm plagioclase phenocrysts ᐱᑕᖅᑲᓕᓕᑦ ᖃᑭᖅᑕᓵᓗᑦ ᓂᑭᐊᑕ ᖃᑭᑎᖅᕿᓗᐊᓂᑦ (ᐊᓱᐅᙵᐊᖅ 4c). ᑕᒪᖅძᐊ ᐃᓗᑐᔨᑎᑦ ᓂᐱᖓᓇᖅᑐᖅᑐᖅᓴᑦ ᐊᒻᒪᓗ ᑕᐃᒪᐃᓗᒪᓕᑐᐃᑎᓴ ᐄᓂ 110–120° (Tschirhart et al., 2015), ᐅᕐᓀᔭᖖᓂ ᐄᓂᐸᓗᖅ ᐅᐊᖓᓇᖓᓂᑦ ᐅᐊᖓᓇᖓᑕ ᑲᓇᖓᓇᖅᕿᓗᐊᓂᑦ. ᓗᕐᓂᓕᐅᐳᑦ ᐄᔾᖖᓂᕐᕿᓗᐅᕐᓂᑦ Neoproterozoic (ca. 720 Ma) Franklin dyke suite (Heaman et al., 1992), ᑕᒪᖅძᐊᓕ ᐊᐃᕐᐸᖏᓂ ᑲᑎᓗᒪᕆᖅᓗᒪᕐᓂ ᐱᐅᓗᐊᖓᓂᕆᓂᑦ Mesoproterozoic–Cenozoic Kekertaluk swarm of Buchan and Ernst (2013).

Limestone (ᐃᓕᖅძᖏᓚᐢᖅ Oᴀ)

ᐃᖅᑲᑐᒋᓂᑦ (<10°) limestone (Blackadar, 1967) ᐄᔾᓂᑦ ᖃᑎᐊᓂᑦ Ordovician Amadjuak Formation ᐱᑕᖅᓕᖅᑕᕐᖅᐳᑦ ᓄᓇ ᐊᐅᓕᔪᖅᐸᑦᓕᐊᓂᖏᓕᓂᑦ ᐄᓂ ᓂᑎᖅᕿᓗᐊᓂᑦ ᐱᖏᓐᓇᖏᓕᓂᑦ ᐃᓕᖏᓕᓂ ᐅᒪ Sylvia Grinnell Lake–Clearwater Fiord area (ᐊᓱᐅᙵᐊᖅ 2). ᐃᓕᖏᑭᓂᑦ ᓄᓇᓂ, Lძᐊ limestone ᓴᓂᓕᖅᑕᖅᑕᕐᖅᐳᑦ Lძᓂᖓ plutonic suite ᐃᒪᖓᓇ ᐅᐊᖓᓇᖏᑎ ᐱᖏᓐᓇᖅᕿᓗᐊᖏᑎ ᖃᓄᐅᓕᐅᑎᓕᕐᓴᖏᓐᓄᑦᓯᖏᓕᑕ, ᑕᐃᒪᐃᖓᓂᖅᓴᐅᓂძᓕᓗᑎ Paleocene rifting ᐊᑐᖅᑎᓕᓗᒍ ᐄᓂ Davis Strait (Clarke et al., 1989). Lძᐊ limestone Lძᓂᖓ ᐱᑎᐊᐹᑎᖅᑕᖅᑕᕐᖅᑐᑦ medium grey lime ᒪᕐᕿ, ᐊᒻᒪᓗ ᓂᕐᔨᑎᕆᔭᖓᓂᓄᑦ ᐃᓂᖅᑕᖅᔭᐅᓂძᓂᖓᖓᓂ ᓇᓗᓇᖕᖏᓐᓄᑦ, ᐊᓱᐅᑲᖏᑕᑐᑎᓂ ᐃᓕᐅᕐᔪᒪᓂᖓᖓᓂ ᐃᓕᖅᑕᖅᑐᑦ Lძᓂᖓ maclurites, gastropods, cephalopods, brachiopods, coral fragments, ᐊᒻᒪ crinoid stems (ᐊᓱᐅᙵᐊᖅ 4d).

EQUILIBRIUM PHASE DIAGRAMS

Phase equilibria modelling ᖃᐅᔨᔪᑎᐅᓇᓴᖅᑐᓂ Lძᓂᖓ monzogranite ᖃᑭᖅᑐᑐᓗᑦ ᓂᑭᐊᓂᑦ ᐱᓕᕆᐊᒃᓴᐅᑦᑐᖅᓴᕐᕿᑦ ᖃᐅᔨᓴᖏᑦᑕᕆᐊᒃᓴᖏᓐᓄᑦ ᐃᖏᕐᕋᓂᕐᓕᐊᔪᑦ ᓄᓇᐃᑦ, ᐅᓇᓂᖓᓕᓗ ᐊᒻᒪ ᖃᐅᔨᓄᖏᓐᓂᕐᓂ. (P, T, and X) ᐄᓂ metamorphic mineral

assemblage in felsic granitoid units (Weller et al., 2015). ᑕᒪᵇძᐊ ᖃᑲᐃᐢᑐᓂᖅᑎᒍᑦ ᐊᓱᐸᒍᑎᖅᕈ ᖃᑲᐅᓴᖃᑕᐅᓕᕆᔨᑦ İᓂᐣ P-T space, ᖃᑭᑎᐊᑉᓕᑦᓗᓂᐣ ᑎᑎᕋᐅᓕᕆᐅᓕᕆᔨᑦ ᑕİᓂᐣ metamorphic conditions of 6–8 kbar ᐊᓚᒪ 700–800°C (St-Onge et al., 2007), ᐃᓕᒪᑉᕋᖃᖅᓗᑎᒃ ᐅᖏᓪᓕᐊᑉᐸᑎᐅᓂᖏᖅᓂᑦ ᑎᑎᕋᖃᑕᐅᓕᕆᔨ ᒪᔪᓇᖏᑦ metagranitoid units, ᐃᒪᖅᓇᐅᖏᖏᓱᖃᑐᖅ ᐋᕐᑭᒋᐊᖅᓄᒃᓇᖅᖏᓪᓕᓗᓂᖅ P-T ᐃᓕᒪᑉᕋᐅᓕᕆᔨᑦ. ᑕᒪᐃᖅᓂ P-T ᐊᓚᒪ T-X phase-ᒧᑦ ᑎᑎᕋᐅᕋᖅᓄᕆᔨᑦ ᐋᕐᑭᒋᖅᑕᑕᐅᓕᕆᓂᔪᑦ ᐃᒪᐃᑦᑐᒥ ᐊᑐᖅᓗᑎᒃ THERMOCALC v3.40 ᐊᓚᒪᓗ ᓄᐊᑕᐅᕙᓪᓕᐊᖏᖅᓇᖅᑐᓄᑦ dataset tc-ds55 (Holland and Powell, 1998; ᐋᕐᑭᒋᐊᖅᑕᐅᓂᔪᑦ ᐋᑎᓕ 2004-ᒧᑦ). ᓇᓗᓇᐃᵇძᑎᖅᑭᑎᖅᑲᒪᐅᖅᑐᑦ 11-ᐅᐸᓂ ᐱᓕᕆᐊᖓᔪᓂᐣ MnO-Na_2O-CaO-K_2O-FeO-MgO-Al_2O_3-SiO_2-H_2O-TiO_2-Fe_2O_3 ᐊᑐᖅᓄᒪᓪᓗᑎᒃ ᐅᓇᒪᒪᵇᑐᓂ ᐊᑐᕐᓂᔪᑦ, ᐃᓕᒪᑉᕋᐅᓕᕆᓂᔪ ᐅᖏᓂ Weller et al. (2016). ᖃᑲᓇᑎᐣ ᓴᖏᓂᖅᑕᐊᐦᓴᖏᓪᓂᐣ ᐋᕐᑭᒋᖅᓄᒪᐅᖅᑐᐃᑦ ᐃᒪᓪᓇᐅᓕᓪᓗᐊᖅᓵᑦ ±1 kbar at the 2σ level (Powell and Holland, 2008; Palin et al., 2015). ᐊᖏᕐᓂᑦ ᐅᓴᕋᐃᑦ ᖃᑲᐅᓴᖃᑕᐅᓕᐅᖅᑐᑦ ᓄᑑᖓᒪᐊᖅᐊᕐᑎᓕᓪᓗᑎᒃ ᐅᓴᕋᖏᓐ ᐊᓱᓕᐅᓕᕆᓪᓚᓪᓕᖅᑐᓗᒥᑦ ᓄᐊᑕᐅᓕᕆᔨᓕᐅᖅᑐᑦ ᐅᒪ ᓴᕿᓪᓂᔨᖏᑦ Thériault et al. (2001) ᐅᓴᕋᐅᓴᕋᓂᐣ ᓄᐊᑕᕃᓚᓪᖏᓪᓂᐣ ᖃᑭᕐᓚᑑᓪᓗᒥᑦ (95-D078B), ᒪᓕᓕᐅᖅᑎᓪᓗᓓ ᖃᑲᐃᓕᓕᐅᕈᓯᐅᓂᔨᑦ ᐅᒪ Weller et al. (2013).

A P-T ᑎᑎᕋᐅᓴᖅᑭᒪᔨᖅ ᐋᕐᑭᒃᑕᐅᓂძ ᓴᕿᑭᓴᖅᑎᕐᑎᓴᔨᑎᐅᓇᓱᓪᓚᓂᐣ ᒪᔪᓂᖓ monzogranite sample (sample 95-D078B from Thériault et al., 2001; Figure 6a) ᓴᕿᑎᕐᑎᑭᒃᓴᕿᖅ ᖃᑲᓱᐊᕐᔨძᓗᖏᓂᐣ ᖃᑲᐃᐢᑕᒍᑎᐅᔨᓂᑦ ᒪᔪᓇᖓ high variance assemblages ᐊᖏᕈᓗᑐᓴᖅᑐᒥᑦ ᓄᓇᒥ P-T space, ᐃᒪᖏᓇ ᐅᓴᕋᐅᓂᖏᖅᓂᑦ metagranitoid rocks, ᒪᔪᐊᑐᐊᖅ magnetite (ᑐᖓᔨᖅᑐᑦ ᑐᕈᓕᐊᓚᓱᒪᔨᑦ) ᐊᓚᒪᓗ orthopyroxene (ᐅᓴᐅᓴᖅ ᑐᕈᓕᐊᓚᓱᒪᔨᑦ) ᐋᕐᑭᒃᑕᐅᓱᒪᕐ ᑕᐃᒪᖏᓇ ᐊᔨᖏᓇᓂᖅᓴᐅᓂᖓᓂᑦ ᐃᒪᖏᓇ ᐊᑐᖓᓄᓂᕐᒥᑦ sub-solidus conditions. ᑎᑎᕋᖅᑕᐅᓱᒪᔨᵇძᑦ, ᑕᒪᐃᖅᓂ orthopyroxene ᐊᓚᒪ magnetite ᐱᑕᖅᑎᑑᓂᖓᓂᐣ ᐃᓱᖅᑲᖅᓱᒪᕐ İᓂᐣ P-T range ᐊᐅᑎᖅᑲᓂᖅᓴᓂᑦ ᖃᑭᖅᑕᒍᑎᓕᑦ ᓂᒥᑦ ᖃᑭᑎᖅᐸᓱᑑᓂᑦ (ᖃᑲძᖅᑕᑦ ᑐᓱᓕᐅᓕᕆᓱᒪᔨᑦ ᓇᐃᐃᓕᓱᒪᓗᑎᒃ), ᐃᓕᓴᖅᑲᖅᓗᑎᒃ ᖃᑲᐅᓴᕿᑎᐃᓚᓂᓂᐣ ᐱᓱᑲᑕᓂᑲᑦ ᐱᓕᕆᐊᖓᔪᓂᑉᓴᓱᓕᕆᓱᓚᓂᓂᐣ ᑕᒪᐃᑎᒍᑦ ᐱᓕᕆᐊᖓᔪᓂᑉᓴᓱᓕᕆᓱᓚᓂᓂᐣ ᑕᒪᐃᐅᓗ

orthopyroxene ᐊᓚᒪ magnetite (ᑐᖓᔪᖅᑐᖅ ᑐᑭᓕᐊᖅᓯᒪᔪᖅ) ᐊᒃᑐᖅᑕᐅᑲᐅᖅᑐᕐᒃᑐᑦ ᐃᒪᐃᑦᑐᒧᑦ MH_2O. ᑕᐃᒪᐃᵒᓂᖓᓄᑦ, ᐊᓚᒡᑕᐅᖅ ᐊᒃᑐᐃᓂᐊᖅᓗᓂ ᐊᕕᒃᑐᖅᓯᒪᓂᖅᑯᑦ ᒪᑯᐊ P-T ᐊᔪᐸᖓᓂᓂᐅᔪᑦ ᐅᖅᑲᐅᓯᐅᓯᒪᔪᑦ ᖃᑯᓪᒧᑦ, ᐃᒪᐅᐸ ᐊᓯᖓᑲᖅᓪᓂᖓᖓ Ỉᓂ typical granitoid composition ᐊᑕᐅᑎᒃᑯᑦᑕᐃᵒᓇ P-T ᖁᓄᐃᑦᑐᖓᖓᓄᑦ ᐊᓚᒪ ᐊᒃᑐᐃᔪᑎᑲᓯᒪᔪᖅ ᑕᒪᐃᵒᓄᑦ ᐱᓕᕆᓂᖅ ᐱᓪᓚᐊᖓᓂᐊᓕᒃᑐᑦ.

ᑕᒪᒃᑯᐊ ᐃᓯᒪᑎᓂᐊᕐᓗᑎᑦ ᐊᒃᑐᐃᓂᑯᔪᑎᑲᐅᖅᑐᑦ ᐅᒧᖓᓪ XFe^{3+} ᑲᑎᕐᖓᐅᖅᑐᑦᓂᓂᑦ, ᐃᒪᐃᑦᑐᒥ T-XFe^{3+} ᑎᑎᕆᐅᔨᖅᓯᒪᔪᒥᑦ ᓴᓇᓪᐅᖅᓴᑦ ᑕᒪᐅᓐᑕᐃᵒᓇᖅ ᓴᖅᑭᓂᖁᖅᑎᑕᐅᖏᓪᓗᓂ (7 kbar), with XFe^{3+} varying from 0.0 to 0.5 (ᐊᔪᐃᖓᐊᖅ 6c). ᐅᓇ ᑎᑎᕆᐅᔨᖅᓯᒪᔪᖅ ᓴᖅᑭᑎᑎᓯᒪᓕᕆᖅ ᑕᒪᐃᵒᓂ magnetite (ᑐᖓᔪᖅᑐᖅ ᑐᑭᓕᐊᓐᓯᒪᔪᖅ) ᐊᓚᒪ orthopyroxene (ᐅᔨᐅᔨᕆᒥ ᑐᑭᓕᐊᓐᓯᒪᔪᖅ) ᓴᖅᑭᖅᓂᖁᖅᑖᓂ ᐅᖓᓇ XFe^{3+}, ᐃᒪᵒᓇᐅᓴᓴᖅᓱᓂᓂ ᐊᔪᐸᖅᑭᔪᑎᐅᔭᓂ ᐅᓀᓂ XFe^{3+} ᐃᓕᔪᑎᐅᓕᖅᓯᒪᑐᐃᵒᓇᓐᓂᐊᖅᑕᖁᖅᑖᓂ ᐅᓴᒪᓐᖅᑯᑦᑎᓂ ᑕᒪᐃᵒᓂ ᐱᓕᓐᓂᐊᓂ. ᐊᓐᑭᓯᖅ ᖁᓄᐃᓕᓂᓂᐅᓀᖅᑐᖅ ᐅᑯᓄᓐ magnetite- ᐊᓚᒪ orthopyroxene-bearing metagranitoid ᐅᔨᕆᓐᓂ ᑕᐃᒪᐃᑦᑐᒃᖁᖅᑐᓂᓂ ᓴᖅᑭᑎᑎᓯᒪᓕᕆᖅ ᒪᑯᐊ ᓇᓗᓇᐃᒃᑯᑯᑦ XFe^{3+} = 0.05–0.25 ᓴᓚᒪᓪᓕᖅᓱᓂᓐᓂᓂᓂ (ᓄᓇ ᐃᓕᓴᒃᑯᓯᒪᔪᖅ ᐅᒥᓐᓄ assumed value of 0.1; ᐊᐅᐸᔨᖅᑐᓂ ᑐᑭᓕᐊᓯᒪᔪᓂᑦ) ᑕᒪᐃᵒᓂ ᐱᓕᓐᓂᐊᖅᓯᒪᔪᑦ ᐁᖅᑭᑕᐅᓕᑕᐃᵒᓇᕐᓴᖅᓱᑦ ᐃᓯᒪᑎᔨᐅᔭᒥᑦ ᐅᵒᓇᖅᓂᐅᓇᔨᖅᑐᒥᑦ.

ᐊᕕᒃᑐᖅᓯᒪᓂᒃᑯᑦ ᒪᑯᐊ aeromagnetic ᑎᑎᖅᑦ ᓄᐊᑕᐅᕐᓂᓕᐊᔪᑦ ᓴᖅᑭᑎᑎᓯᒪᓕᕆᑦ ᐊᔪᐸᖓᑦᑐᑲᑎᓪᓚᓐᓂ ᓂᐱᐃᓇᖅᑐᖅᑐᖅᑐᓂᑦ ᑕᐃᓂ ᐅᔨᕐᓚᓕᓐᓂ ᐱᓕᓐᓂᕕᕐᒪᑦ (ᓯᖁᓗ, ᐊᔪᐃᖓᐊᖅ 6d; Kiss and Tschirhart, 2015a–r). ᓄᓇᒥ ᖁᒃᐅᔪᓴᑭᑎᕕᓂᑦ ᓴᖅᑭᑎᑎᓯᒪᓕᕆᑦ ᐱᔪᔾᔪᑎᒃᑯᐊᐅᓗᓴᐅᔭᓕᓐᓂᓂ ᐊᔪᐸᖓᑦᑐᑲᑎᓪᓚᓐᓂᐅᓂᕐᒥᑦ ᒪᑯᐊᓂ ᐊᔪᐸᖓᑦᑐᑲᓄᑦ ᓂᐱᐃᓇᖅᑐᖅᑐᖅᑐᓄᑦ magnetite, Ỉᓵᵒᓂᖅᓴᐅᔨᓕᑭᒃ homogeneous plutons (Tschirhart et al., 2015). ᖁᒃᐅᔪᔪᐅᔨᓕᑕᐊᔪᑦ ᑕᒪᑐᕐᖓ ᒪᓕᒃᓯᒪᑲᑕᒃᓴᑦ, ᓴᖅᑭᒋᖅᑎᑎᓂᓂᓐᓂᑯᓂᓂᑦ ᐊᓯᖏᑭᑎᐃᓂᓂᑦ ᐅᔨᓂ P, T, ᐊᓚᒪ X-ᒥ ᖁᒃᐅᔪᓚᐅᔭᔪᑎᐅᓂᐊᖅᑐᖅᓂᑦ ᐅᔪᖅᓄᓂᑦ (ᐊᓚᒪᓗ orthopyroxene) ᐃᓂᓐᓯᔪᐅᖅᓴᑎᑎᔪᑦ, ᐱᓕᓚᓂᒃᓚᐃᑦ ᓯᓕ ᓯᖅᑯᓯᓗᐊᖅᓯᒪᑎᵒᓇᒋᑦ.

ᖁᓄᐃᓕᓐᓂᓐᓯᓂᓐᓂᑦ ᐊᓯᔪᓴᑦᓕᓕᐊᓂᓐᓂᑦ ᐊᓚᒪ ᐊᓯᔪᓴᖅᓂᓐᓂᑦ ᖁᓄᐃᓕᓐᓂᓐᓯᓂᓐᓂᑦ ᐅᔨᖅᑲᐃᑦ

D_1 ᖁᓄᐃᓕᓐᓂᓐᓯᓂᓐᓂᑦ ᐊᓯᔪᖅᑴᑦᓕᓕᐊᓂᓐᓂᑦ ᐊᓚᒪ M_1 ᐊᓯᔪᖅᓂᓐᓂᑦ ᖁᓄᐃᓕᓐᓂᓐᓯᓂᓐᓂᑦ ᐅᔨᖅᑲᐃᑦ Paleoproterozoic tectonostratigraphic ᐃᓕᒃᑯᓐᓇᓴᑦ ᓇᓗᓴᐃᓄᖅᑕᐅᔪᓚᓴᑦᑐᑦ ᐱᓀᑦᓕᐊᑎᑕᐅᑐᓂᓐᓄᓂᑦ ᔪᐊᓚᒪᑴᓕᓐᓂᓐᓄᓐ ᒥᓕᒻᑕᒥᑦ ᔪᐊᐟᑕᒥᒻᓄᑦ ᐃᓗᓕᑦᑐᓂᑦ ᖁᑯᓕᓴᐟᓂᓐᓂᑦ (S_1) ᐃᒃᑲᑐᑴᓗᑐᑦ ᑯᑐᖅᑐᖅ, ᐊᓚᒪ ᓇᓕᒧᐃᵒᓇᖅᑐᑐᑦ ᐅᔨᖅᑲᐃᑦ ᑲᑎᵒᓂᖓᓂᑦ ᐊᑯᵒᑐᓂᓐᓂᑦ supracrustal ᐊᓚᒪ plutonic ᐃᓕᒃᑯᓐᓇᓴᑦ. metasedimentary strata,–ᒥᑦ S_1 ᓇᓗᓇᐃᖅᑕᐅᔪᖅ ᖁᑯᓕᓴᐟᓂᓐᓂᑦᓄᓂᑦ ᓇᓕᒧᑐᑦ M_1 biotite, sillimanite, ᐊᓚᒪ garnet, ᖁᑯᓕᓴᒃᑲᵒᓂᖁᑎᑐᖅᑐᑦ ᐱᓗᐊᖅᑐᑐᑦ plagioclase, K-feldspar ᐊᓚᒪ quartz. garnet ᐅᔨᖅᑎᑎᐊᓀᐃᐃᓂ ᒥᓕᒻᑕᓂᑲᵒᓂᓚᵒᓇᖅᑐᑦ ᐊᖓᑕᓂᖓᑦ ᐊᓚᒪ ᑕᑯᓴᐊᐅᓂᖁᑎᑲᖅᑐᑎᑦ poikiloblastic. metasedimentary ᐃᓕᒃᑯᓐᓇᓴᓂᑦ, S_1 ᓇᓗᓇᐃᖅᑕᐅᔪᖅ ᐅᔨᖅᑲᐃᐃᓄᑦ ᐊᓯᔪᓚᐊᕈᑎᓂᑦ ᐱᓗᐊᖅᑐᒥᑦ ᓄᓴᐅᔭ ᐃᑭᓐᓄᓂ (S_0). foliated mafic–ᒥᑦ ᐊᓚᒪ felsic plutonic –ᓂᑦ, S_1 ᓇᓗᓇᐃᖅᑕᐅᔪᖅ ᓇᒧᵒᓐᓄᖁᑎᑕᒃᵒᓂᓂᖁᖅᓯᒪᵒᓄᑦ ᐱᓗᐊᖅᑐᒥᑦ ferromagnesian-rich ᖁᑯᓕᔪᑎᑦ ᐃᓗᑕᓚᓗᓂᑦ granoblastic, ᒥᓕᒻᑕᓂᑦ ᐊᓐᓂᑕᓕᒃ. M_1 orthopyroxene, biotite, magnetite, clinopyroxene, hornblende, ᐊᓚᒪ/ᐅᐟᔾᔨᓗᵒᓂᑦ garnet, ᐊᓚᒪ ᖁᑯᓕᔪᑎᑦ ᐃᓗᑕᓂᖅᑐᖅᑐᑦ

ᐱᓗᐊᖅᑐᒥᑦ plagioclase ᐊᒻᒪ quartz±K-feldspar. ᓇᓕᒧᐅᓂᓴᖏᑦ orthopyroxene, biotite, clinopyroxene, ᐊᒻᒪ hornblende ᓇᓗᓇᐃᖅᓯᕐᓴ S_1 ᐃᑦᑐᓂᑦ metaplutonic ᐃᓪᒃᑯᖏᑎᔪᓂᑦ ᐱᑕᖅᖅᑎᑦᓗᒋᑦ. S_1 ᐃᑦᑐᑦ ᑕᑯᐅᓇᖅᑕᐅᔪᑦ axial-planar ᑎᑭᑦᑐᒍ ~100 m ᐊᖏᑭᓂᖏᑲ isoclinal ᐱᓚᐅᓂᖏᑦ ᐃᖅᒃᑐᑐᒥᑦ ᐅᐊᐅᓇᖏᑲᓂ ᐊᓂᑭᖏᑲᓂ ᐊᒻᒧᐊᐸᑦᓂᖏᑲᑦᐱᓚᐅᓂᖏᑦ (Dyck and St-Onge, 2014).

ᐅᔪᕿᐅᔪᑎᓪᓕᐅᑦ Lᑯᐊ granulite-facies M_1 metamorphism ᐃᓐᓂᑐᑦ ᑭᒻᒥᑭᒻᒥ ᕿᑭᓂᖅᑐᒋᓂᑦ ᒥᑕ ᐃᐅᒃᑲᓐᑕ <ᓂᐅᓯᓪᓕᐅᐸ ᐱᖏᑲᓇᖅᐸᓯᐊᓐᓂᑐᖅ ᐅᙵᓂ ca. 1.84 Ga by St-Onge et al (2007). ᓄᓇᐅᐸ ᖃᓄᐃᓪᓚᓂᖏᑲᓚᑦ ᐊᒻᒪ ᑭᓯᑕᖃᕐᓂᖏᑲᑦ ᖃᐅᐅᔪᕐᓂᑕᖅᑕᖃᕐᓂᐊᕐᑐᖅ ᑕᒪᐅᑯᓯᑕᐃᐅᓇᖅ ᐅᔪᕿᐅᔪᐃᑦ ᐱᑕᖅᖃᒪᖏᓕ ᐃᐅᓇ ᓄᓇᙱᐊᓪᓕᐅᕐᓴᖏᑦ.

D_2 ᖃᓄᐃᓪᓚᓂᖏᑦ ᐊᓯᔪᖅᐸᓪᓕᐊᓂᖏᑦ

Ptarmigan Fiord–ᒥᑦ, D_2 ᓯᓪᑎᓂᖏ ᐃᔨᔪᔪᖅ ᐱᖃᓯᐅᔪᐃᔪᖅ ᐊᖏᕐᕌᒍᓂᓵᓐᓂᑦ ᑐᐢᖏᒪᖏᑲ ᐅᔪᖅᖃᐃᑦ orthogneiss ᐊᒻᒪ Paleoproterozoic supracrustal ᐅᔪᖅᖃᐃᑦ (Chadwick et al., 2015). ᑕᒪᑲᑭᓂᑲᐃᓗᓂᐊᓂ ᐊᒻᒪ ᓯᓪᑕᑦᓂ ᐊᔪᐅᖅᓯᓂᖅ ᓴᖅᑭᖃᑦᑕᖅᑐᖅ. D_2 ᐊᔪᐅᖅᓯᓂᖏᑲ ᖃᓯᓱᖃᑦᑕᐅᑎᔪᑦ ᓇᓗᓇᐃᖅᑕᐅᔪᑦ ᖃᓯᐢᖓᓯᑦᑐᒥᑦ mylonitic ᐊᑦᑐᖅᑕᐅᔪᑦ ᐊᓯᓂᓂᖏᑲ supracrustal ᐅᔪᖅᖃᐃᑦ ᐊᒻᒪ ᐋᖅᑭᔭᓯᒪᓂᖏᑲ ᖃᓯᒋᓂᑐᑦ ᐊᑕᓂᓂ. L_2 ᐅᔪᕿᓂᐊᕆᔭᕆᐅᔪᓇᖅᑐᓂᑦ ᑐᑭᑦᓂᓂᖏᑲ, ᐊᒻᒪᓗ S_2 ᖃᐅᓪᓗᓇᖅᑕᔪᐅᔪᖅᑐᑦ ᓇᓕᒧᐅᓂᖃᖅᑐᑦ ᐊᔪᐅᖅᑕᐅᒧᒪᒥᑦ ᐊᓇᓯᒪᑎᐊᖅᑐᑦ. ᐃᔨᔪᓂᖏᑦ ᐃᓕᒋᓯᖅᑐᑦ ᐋᖅᑭᔭᓯᒪᓂᖏᑲ ᖃᓯᒋᓂᑐᑎᑦ ᐊᑎᖅᑕᐅᒧᒪᒥᑦ ᐊᒻᒪ ᑕᑭᓪᓚᕐᓇᖅᑕᖏᑲ ᐃᓕᒋᓯᖅᑐᑦ ᖃᓯᒋᓂᑐᑎᑦ ᐋᖅᑭᔭᓯᒪᓕᕆᓂᖅᑐᖅ ~25 km.

D_1 ᑭᓯᑭᓄᔪᐃᑦ (ᐃᓕᐅᑦᓗᑎᒃ ᐅᓇ S_1 foliation) ᐊᒻᒪ D_2 ᖃᓯᒋᓱᒋᔪᓯᒪᑦᓗᑎ ᐊᒻᒪ ᐋᖅᑭᑎᐊᖏᓂᓱᓯᒪᑦᓗᑎᒃ ᐅᐊᖏᓇᖅᓗ ᐅᐊᖏᓇᐅ ᐱᖏᑲᓇᖏᓄᖏᐅᐳᑦᑕᐊᓂᐅᔪᒥᑦ ᐄᒧᖏᑲ D_2 ᐃᒧᓯᒪᓂᖏᓄᑦ. ᐅᓇ D_2 ᐃᒧᓯᒪᓂᐅᔪᖅ ᓇᓗᓇᐃᖅᑕᐅᓯᒪᔪᖅ ᓄᓇᖕᖁᐊᑎᔭᑦ ᐊᒻᒪ ᓴᖅᑭᔾᖅᑎᕿᑎᑦᓗᓂᒃ ᒪᑭᑕᔪᓂ ᑲᓇᖅᓯᒪᓂᖏᑲ ᖃᓯᒋᓂᑐᑎᑦ ᐊᑐᖅᑕᐅᒧᒪᒥᑦ ᐃᒪᓕᑕᓂ mesoscopic ᐱᑕᖅᖏᑦᑕᖅ ᐊᐅᑐᐊᔪᓂᑦ ᐄᒥᖏᑲ D_2 ᖃᐅᓪᓚᓪᓯᓯᒪᓂᖏᓄᓂᑦ ᑎᑎᕿᐅᓯᐅᓯᒪᔪᑦ.

ᐅᐊᓄᓴᖏᓂ ᑯᐸᐃᒃ, ᓄᓇᐅᐸ ᖁᑲᖏᓂᓂᐊᖏᑎᓄᑦ D_2 ᐱᓚᖃᑦᑕᖅᑐᑦ ᓴᓇᓯᒪᓂᖏᑲ ᖃᓯᒋᓂᓄᖏᑲ 1 ᐊᒻᒪ 2 ᑭᑦᓪᖃᖅᑎᑕᐅᔪᖅ ca. 1.76 Ga (Lucas and St-Onge, 1992). Lucas and Byrne (1992) ᐱᔪᒪᓪᐅᖅᑐᑦ orogen-ᓇᓕᒧᐅᓂᖏᑲ ᐱᓚᕐᔪᑎᖃᖅᓯᒪᔪᖅ ᑲᔪᓯᓄᓇᖅᑐᓂᑦ ᓄᓇᒧᑦ ᓇᓕᒧᑦᑐᓂᑦ ᓄᓇᐃᑦ ᓯᓪᓚᔪᐊᒥᑦ ᐊᐳᖃᑦᑕᐅᑎᑎᓪᓗᓯᒪᔪᖅ ᐃᐃᑦᓪᒥᐊᓯᒪᔪᖅ ᐅᐊᓄᓴᖏᓕᒃ ᑲᓇᓄᖏᑲ Trans-Hudson Orogen.–ᒥᑦ.

D_3 ᖃᓄᐃᓪᓚᓂᖏᑦ ᐊᓯᔪᖅᐸᓪᓕᐊᓂᖏᑦ

ᒪᑭᑦᓗᐊᖅᑐᑦ ᐱᓚᖃᑦᑕᖅᑐᑦ ᐱᑐᖃᑦᑕᐅᓂᖅᓴᓄᑦ ᐃᓗᓪᓚᕐᓂᓄᖏᑲ ᑲᓇᓄᖏᑲ ᐅᐊᓄᓴᖏᓂ ᑲᓇᓄᖏᑲᓄᖅᐸᓪᓕᐊᔪᖅ D_3 ᐱᓚᓄᓂᖏᑦ ᐱᓚᓄᓂᖏᑲ ᐸᕐᓴᕿᐃᓯᒪᔪᖅ, ᓄᓇᖕᖁᐊᖅ ᑕᑯᕿᐅᒋᔭᖅ ᓂᑭᐊᖅ ᐊᒻᒪ ᑲᓇᓄᖏᑲ Sylvia Grinnell Lake–Clearwater Fiord–ᒧᑦ. ᐸᕐᓴᕿᐃᔪᑦ D_2 ᐊᒻᒪ D_3 ᐱᓚᔾᔪᒪᔪᑦ ᕿᓇᓯᕿᓂᖏᑲ ᖃᐅᔨᕿᐅᓇᑎᑎᑭᓯᒪᔪᖅ ᓄᓇᐅᐸ ᐃᑭᖏᑲᓂ ᓂᑭᐊᖅ ᐊᑭᑭᖅᒋᓗᐊᖅ, ᐱᖃᓯᐅᑎᓪᓗᒋᑦ ᐅᓂᒃᑳᖅᓂᒃ ᐱᖃᓯᐅᑎᑦᓗᒋᑦ ᓄᓇᓕᒻᒥᐅᑦ ᐊᒻᒪ ᐃᓚᖏᑲᓂ

ᑭᓇᐅᔨᓕᕆᓂᖏᑦ ᐃᓱᒪᒋᐅᔨᕆᕈᐊᓪᓕᐅᑦ

ᐊᒥᓱᓕᓚᐃᑦ ᐅᔨᖅᑲᐃᑦ ᖃᑲᓂᐃᓕᓕᖅᓱᓂᕐᒋᑦ ᐊᑐᐊᓂᓪᓕᐊᒪ ᐊᒻᒪ ᓴᖅᑭᖅᑕᕐᓂᓕᕐᒋᑦᑭᓇᐅᔨᓕᕆᔨᐸᑎᓴᓂᑦ ᐊᑐᐃᓂᖅᑲᓐᓇᖅᑐᑦ ᐊᓗᓇᐃᖅᑕᐅᓕᐅᖅᑐᑦ 2015–ᒥ ᐊᓗᓇᐃᖅᑕᐅᓱ ᒪᔨᓂᑦ ᑐᖁᖅᑕᐅᔨᓂᓪᓗ ᓄᓇᖓᐊᓕᐅᓕᐅᖅᑐ Sylvia Grinnel Lake–Clearwater Sound area. ᖃᐅᓕᓵᑐᑦ mafic-ultramafic sills ᐃᓗᐊᓂᑐᑦ sulphidic siliciclastic ᐅᔨᖅᑲᐃᑦ ᖃᐅᓕᑭᑐᑦ ᐅᔨᖅᑲᐃᑦ ᖃᑲᓂᐃᓕᓕᖅᓱᓂᕐᒋᑦ ᐊᓴᐸᓗᒋᔭᖏᕐᒋᑦ Ni–Cu–platinum-ᐃᓕᖏᒋᑦ ᐃᓗᓕᖏᒋᑦ ᐅᔨᕆᓂᐊᕆᔭᕐᓂᐅᔨᓕᕆᓂᖅᑐᑦ ᐊᓱᖏᓚᓂ Trans-Hudson Orogen (ᓱᓲᓕ Raglan ᐅᔨᖅᑲᐃᑦ ᑲᓇᓂᓚᓂ Cape Smith Belt oᐅᐊᓂᓇᖏᓚᓂ ᑯᐸᐃᑲ; St-Onge and Lucas, 1994; Lesher, 2007). ᖃᑲᐅᔪᕆᕕᐅᔨᒥᑦ ᖃᑲᓂᐃᓕᓕᖅᓱᓂᕐᒋᑦ ᐅᔨᖅᑲᐃᑦ ᐊᓗᓇᐃᔨᖅᑎᕆᕐᑎᐊᓂᖅᑳᓕᐃᑦ ᓄᑲᐃᓂ Liikane et al. (2015). ᐅᑲᑯᓱᕆᖅᓱᒪᔨᑦ ᐅᔨᖅᑲᐃᑦ ᐊᓗᓇᐃᖅᑕᐅᓱᒪᔨᑦ ᐊᒥᓱᓕᓂᓐᓂᑦ ᐊᒋᓐᓂᓕᕐᒋ ᓄᓇᖓᐊᒥᑦ, ᐃᓕᓐᒋᑦ ᕿᓇᖓᐊᑕᕿᕆᔭᐅᓐᓇᐃᓂᓇᓚᐊᓕᓵᑐᑦ ᐊᓱᓐᒋᑦ ᕿᑐᖅᑕᕐᓂᖅᑐᑦ ᐱᔨᒥᓇᖅᑐᑦ sulphide-bearing gossans; ᐊᒻᒪ magnetite ᐊᒻᒪ ᐱᐅᔨᑦ ᐅᔨᕆᓂᐊᕆᔭᕐᓂᐅᔨᓕᕆᓂᖅᑐᑦᓂᓐᓄᔨᐃᑦ, ᐱᕆᓱᐅᑎᑦᓗᑎᐅᔨᕆᕐᓂᐅᔨᓕᕆᓂᖅᑐᑦ apatite ᐊᒻᒪ diopside.

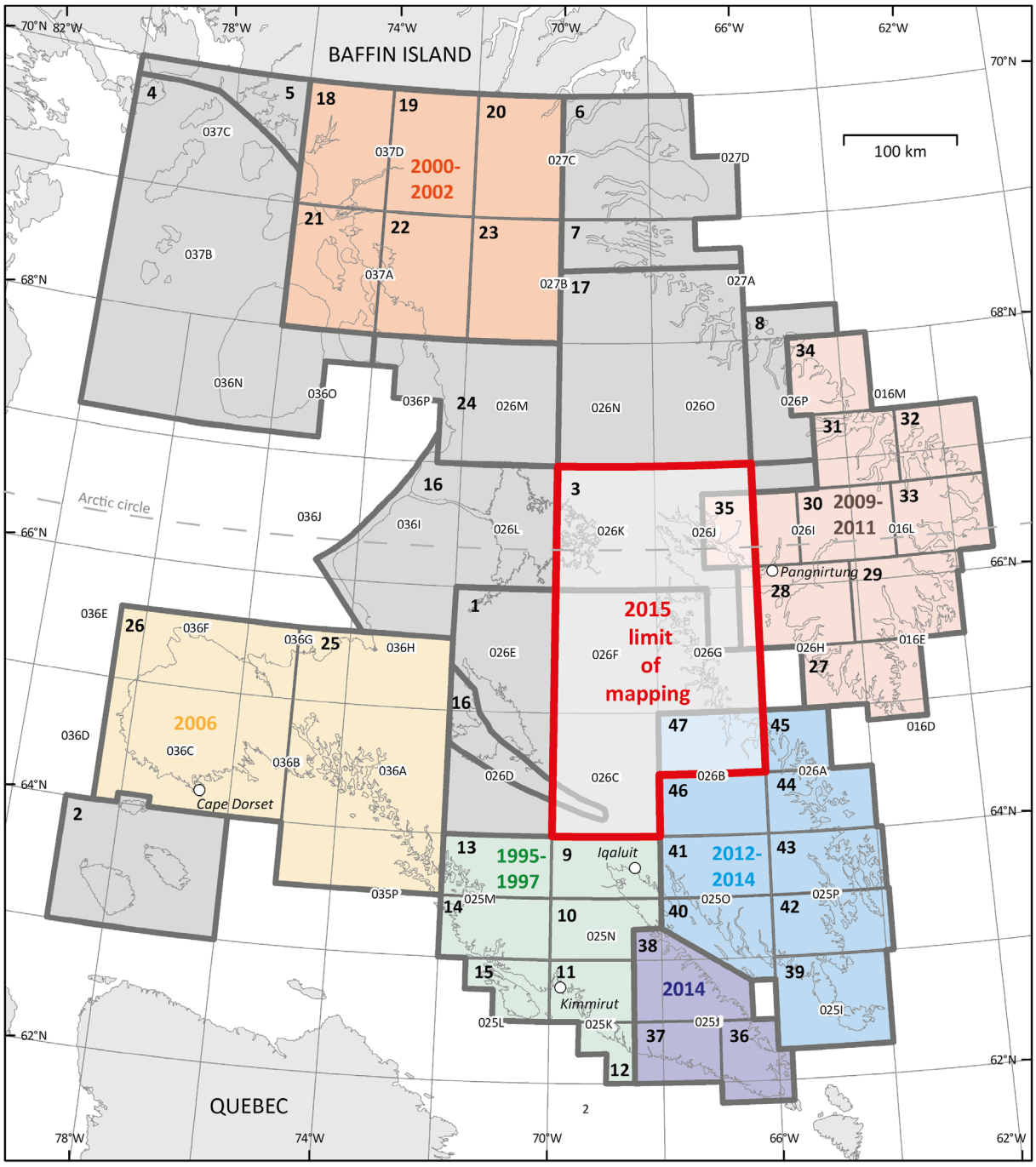

ᐊᕐᓂᖅᓱᐊᖅ 1. ᓇᓗᓇᐃᔾᔨᓕᓂᖅᓯᒋᐊᓂ ᖃᐅᖅᐱᐃᓐᓇᖅᑐᒥᓂ ᓄᓇᖅᐱᐊᓕᐅᔭᕐᓂᖅᐱᓕᕆᐊᖅᐱᓱᒋᔭᐅ ᖁᑭᖅᑕᓗᓐᓄᑦ, ᓄᓇᕗᑦ. ᓇᒋᓐᓂᖅᓱᒃ 2015–ᒥ ᓂᒋᐊᓂ–ᖁᑎᐊᓂ ᖁᑭᖅᑕᓗᓚᒥ ᑕᐅᔪᐃᐅᑕᐅᔭᕐᔨᖅ ᐊᐅᓚᖅᑐᖅ ᑐᑭᓕᐊᖅᑐᑦ ᓚᓂᕐᖏᑦ, ᐱᔨᓴᖅᑕᐅᔭᑦᓗᓂᓗ ᐅᑦᓗᒥᒋᖅᓱᓂᑦ ᓄᓇᖅᐱᐊᓂᑦ ᓂᒋᐊᓂ 70 °N. ᖁᕐᓂᓂᓂᖅᓚᐃᑦ ᓵᔪᐅᑎᑦ ᓇᓗᓇᐃᖅᑭᔨᓪᓚᑦ ᓄᓇᖅᐱᐊᒪᑦ ᖃᐅᐅᔨᒋᐊᕈᑎᑦ ᐊᑦᖢᖅᑭᓕᓚᑦᑎᓪᓗᑦ ᐊᒪᒪ ᑎᑎᕐᖁᖅᑭᔨᓪᓚᑦ ᐊᒃᓱ. ᐊᒥᐊᓵᓪᓚ ᓇᓗᓇᐃᖅᑭᔨᓪᓚᑦ ᓇᒋᓐᓂᖅᓯᒋᐊᓂ ᐊᒪᒪ ᐊᕐᕌᒍ(ᐃᑦ) ᖃᐅᔨᔪᖅᑕᐅᕐᕕᖅᑭᔨᓪᓚᑦ. ᓵᔪᐅᑎᓵᓪᓚ ᑎᑎᖅᑲᖅᑲᖅᑐᑎᓂ ᓇᓗᓇᐃᖅᑭᔨᓪᓚᑦ ᑲᓇᑕᒥ ᓄᓇᖅᐱᐊᓕᐅᔭᓂᒪᑦ ᓄᓇᖅᐱᐊᑦ.

1. Blackadar, R.G., 1967. Geology, Cumberland Sound, District of Franklin; Geological Survey of Canada, Preliminary Map 17-1966, scale 1:506 880. doi:10.4095/108490

2. Blackadar, R.G., 1970. Nottingham, Salisbury, and Mill Islands, District of Franklin; Geological Survey of Canada, Map 1205A, scale 1:250 000. doi:10.4095/109212

3. Jackson, G.D., 1971. Operation Penny Highlands, south-central Baffin Island; *in* Report of Activities, Part A: April to October 1970, Geological Survey of Canada, Paper 71-1, Part A, p. 138–140.

4. Trettin, H.P., 1975. Geology, Lower Paleozoic geology, central and eastern parts of Foxe Basin and Baird Peninsula, Baffin Island, District of Franklin; Geological Survey of Canada, Map 1406A, scale 1:500 000. doi:10.4095/109081

5. Morgan, W.C., 1982. Geology, Koch Island, District of Franklin; Geological Survey of Canada, Map 1535A, scale 1:250 000. doi:10.4095/127056

6. Henderson, J.R., 1985a. Geology, McBeth Fiord-Cape Henry Kater, District of Franklin, Northwest Territories; Geological Survey of Canada, Map 1605A, scale 1:250 000. doi:10.4095/120467

7. Henderson, J.R., 1985b. Geology, Ekalugad Fiord-Home Bay, District of Franklin, Northwest Territories; Geological Survey of Canada, Map 1606A, scale 1:250 000. doi:10.4095/120468

8. Jackson, G.D., 1998. Geology, Okoa Bay-Padloping Island area, District of Franklin, Northwest Territories; Geological Survey of Canada, Open File 3532, scale 1:250 000. doi:10.4095/209911

9. St-Onge, M.R., Scott, D.J., and Wodicka, N., 1999a. Geology, Frobisher Bay, Nunavut; Geological Survey of Canada, Map 1979A, scale 1:100 000. doi:10.4095/210833

10. St-Onge, M.R., Scott, D.J., and Wodicka, N., 1999b. Geology, Hidden Bay, Nunavut; Geological Survey of Canada, Map 1980A, scale 1:100 000. doi:10.4095/210835

11. St-Onge, M.R., Scott, D.J., and Wodicka, N., 1999c. Geology, McKellar Bay, Nunavut; Geological Survey of Canada, Map 1981A, scale 1:100 000. doi:10.4095/210836

12. St-Onge, M.R., Scott, D.J., and Wodicka, N., 1999d. Geology, Wright Inlet, Nunavut; Geological Survey of Canada, Map 1982A, scale 1:100 000. doi:10.4095/210840

13. St-Onge, M.R., Scott, D.J., and Wodicka, N., 1999e. Geology, Blandford Bay, Nunavut; Geological Survey of Canada, Map 1983A, scale 1:100 000. doi:10.4095/210837

14. St-Onge, M.R., Scott, D.J., and Wodicka, N., 1999f. Geology, Crooks Inlet, Nunavut; Geological Survey of Canada, Map 1984A, 1:100 000 scale. doi:10.4095/210838

15. St-Onge, M.R., Scott, D.J., and Wodicka, N., 1999g. Geology, White Strait, Nunavut; Geological Survey of Canada, Map 1985A, scale 1:100 000. doi:10.4095/210839

16. Sanford, B.V. and Grant, A.C., 2000. Geological framework of the Ordovician system in the southeast Arctic platform, Nunavut; *in* Geology and Paleontology of the southeast Arctic Platform and southern Baffin Island, Nunavut; Geological Survey of Canada, Bulletin 557, p. 13–38.

17. Jackson, G.D., 2002. Geology, Isurtuq River-Nedlukseak Fiord, Nunavut; Geological Survey of Canada, Open File 4259, scale 1:250 000. doi:10.4095/213304

18. St-Onge, M.R., Scott, D.J., Corrigan, D., and Wodicka, N., 2005a. Geology, Ikpik Bay, Baffin Island, Nunavut; Geological Survey of Canada, Map 2077A, scale 1:100 000. doi:10.4095/221054

19. St-Onge, M.R., Scott, D.J., Corrigan, D., and Wodicka, N., 2005b. Geology, Flyway Lake, Baffin Island, Nunavut; Geological Survey of Canada, Map 2078A, scale 1:100 000. doi:10.4095/221091

20. St-Onge, M.R., Scott, D.J., Corrigan, D., and Wodicka, N., 2005c. Geology, Clyde River, Baffin Island, Nunavut; Geological Survey of Canada, Map 2079A, scale 1:100 000. doi:10.4095/221092

21. St-Onge, M.R., Scott, D.J., Corrigan, D., and Wodicka, N., 2005d. Geology, Piling Bay, Baffin Island, Nunavut; Geological Survey of Canada, Map 2080A, scale 1:100 000. doi:10.4095/221093

22. St-Onge, M.R., Scott, D.J., Corrigan, D., and Wodicka, N., 2005e. Geology, Straits Bay, Baffin Island, Nunavut; Geological Survey of Canada, Map 2081A, scale 1:100 000. doi:10.4095/221094

23. St-Onge, M.R., Scott, D.J., Corrigan, D., and Wodicka, N., 2005f. Geology, Dewar Lakes, Baffin Island, Nunavut; Geological Survey of Canada, Map 2082A, scale 1:100 000. doi:10.4095/221095

24. Jackson, G.D., 2006. Geology, Hantzsch River area, Baffin Island, Nunavut; Geological Survey of Canada, Open File 4202, scale 1:250 000. doi:10.4095/221809

25. St-Onge, M.R., Sanborn-Barrie, M., and Young, M.D., 2007a. Geology, Mingo Lake, Baffin Island, Nunavut; Geological Survey of Canada, Open File 5433, scale 1:250 000. doi:10.4095/224163

26. St-Onge, M.R., Sanborn-Barrie, M., and Young, M.D., 2007b. Geology, Foxe Peninsula, Baffin Island, Nunavut; Geological Survey of Canada, Open File 5434, scale 1:250 000. doi:10.4095/224222

27. Sanborn-Barrie, M., Young, M., Whalen, J., and James, D., 2011a. Geology, Ujuktuk Fiord, Nunavut; Geological Survey of Canada, Canadian Geoscience Map 1 (2nd edition, preliminary), scale 1:100 000. doi:10.4095/289237

28. Sanborn-Barrie, M., Young, M., and Whalen, J., 2011b. Geology, Kingnait Fiord, Nunavut; Geological Survey of Canada, Canadian Geoscience Map 2 (2nd edition, preliminary), scale 1:100 000. doi:10.4095/289238

29. Sanborn-Barrie, M., Young, M., Whalen, J., James, D., and St-Onge, M.R., 2011c. Geology, Touak Fiord, Nunavut; Geological Survey of Canada, Canadian Geoscience Map 3 (2nd edition, preliminary), scale 1:100 000. doi:10.4095/289239

30. Sanborn-Barrie, M. and Young, M., 2013a. Geology, Circle Lake, Nunavut; Geological Survey of Canada, Canadian Geoscience Map 5 (preliminary), scale 1:100 000. doi:10.4095/288929

31. Sanborn-Barrie, M., Young, M., Keim, R., and Hamilton, B., 2013. Geology, Sunneshine Fiord, Nunavut; Geological Survey of Canada, Canadian Geoscience Map 6 (preliminary), scale 1:100 000. doi:10.4095/288931

32. Sanborn-Barrie, M. and Young, M., 2013b. Geology, Padle Fiord, Nunavut; Geological Survey of Canada, Canadian Geoscience Map 37 (preliminary), scale 1:100 000. doi:10.4095/292014

33. Sanborn-Barrie, M. and Young, M., 2013c. Geology, Durban Harbour, Nunavut; Geological Survey of Canada, Canadian Geoscience Map 38 (preliminary), scale 1:100 000. doi:10.4095/292015

34. Sanborn-Barrie, M. and Young, M., 2013d. Geology, Qikiqtarjuaq, Nunavut; Geological Survey of Canada, Canadian Geoscience Map 39 (preliminary), scale 1:100 000. doi:10.4095/292016

35. Jackson, G.D. and Sanborn-Barrie, M., 2014. Geology, Pangnirtung Fiord, Nunavut; Geological Survey of Canada, Canadian Geoscience Map 4 (preliminary), scale 1:100 000. doi:10.4095/288928

36. St-Onge, M.R., Rayner, N.M., Steenkamp, H.M., and Gilbert, C., 2015a. Geology, Terra Nivea, Baffin Island, Nunavut; Geological Survey of Canada, Canadian Geoscience Map 215E (preliminary); Canada-Nunavut Geoscience Office, Open File Map 2015-02E, scale 1:100 000. doi:10.4095/296104

37. St-Onge, M.R., Rayner, N.M., Steenkamp, H.M., and Gilbert, C., 2015b. Geology, Pritzler Harbour, Baffin Island, Nunavut; Geological Survey of Canada, Canadian Geoscience Map 216E (preliminary); Canada-Nunavut Geoscience Office, Open File Map 2015-03E, scale 1:100 000. doi:10.4095/296109

38. St-Onge, M.R., Rayner, N.M., Steenkamp, H.M., and Gilbert, C., 2015c. Geology, Grinnell Glacier, Baffin Island, Nunavut; Geological Survey of Canada, Canadian Geoscience Map 217E (preliminary); Canada-Nunavut Geoscience Office, Open File Map 2015-04E, scale 1:100 000. doi:10.4095/296111

39. Steenkamp, H., Gilbert, C., and St-Onge, M.R., 2016a. Geology, Loks Land, Baffin Island, Nunavut, NTS 25-I (part); Geological Survey of Canada, Canadian Geoscience Map 264 (preliminary); Canada-Nunavut Geoscience Office, Open File Map 2016-01, scale 1:100 000. doi:10.4095/297344

40. Steenkamp, H., Gilbert, C., and St-Onge, M.R., 2016b. Geology, Ward Inlet (south), Baffin Island, Nunavut, NTS 25-O (south) and NTS 25-J (part); Geological Survey of Canada, Canadian Geoscience Map 266 (preliminary); Canada-Nunavut Geoscience Office, Open File Map 2016-02, scale 1:100 000. doi:10.4095/297349

41. Steenkamp, H., Gilbert, C. and St-Onge, M.R., 2016c. Geology, Ward Inlet (north), Baffin Island, Nunavut, NTS 25-O (north); Geological Survey of Canada, Canadian Geoscience Map 265 (preliminary); Canada-Nunavut Geoscience Office, Open File Map 2016-03, scale 1:100 000. doi:10.4095/297348

42. Steenkamp, H., Gilbert, C., and St-Onge, M.R., in press a. Geology, Beekman Peninsula (south), Baffin Island, Nunavut, NTS 25-P (south) and NTS 15-M (part); Geological Survey of Canada, Canadian Geoscience Map 267 (preliminary); Canada-Nunavut Geoscience Office, Open File Map 2016-04, scale 1:100 000. doi:10.4095/297351

43. Steenkamp, H., Gilbert, C., and St-Onge, M.R., in press b. Geology, Beekman Peninsula (north), Baffin Island, Nunavut, NTS 25-P (north) and NTS 15-M (part); Geological Survey of Canada, Canadian Geoscience Map 268 (preliminary); Canada-Nunavut Geoscience Office, Open File Map 2016-05, scale 1:100 000. doi:10.4095/297352

44. Steenkamp, H., Gilbert, C., and St-Onge, M.R., 2016d Geology, Leybourne Islands (south), Baffin Island, Nunavut, NTS 26-A (south); Geological Survey of Canada, Canadian Geoscience Map 269 (preliminary); Canada-Nunavut Geoscience Office, Open File Map 2016-06, scale 1:100 000. doi:10.4095/297353

45. Steenkamp, H., Gilbert, C., and St-Onge, M.R., 2016e. Geology, Leybourne Islands (north), Baffin Island, Nunavut, NTS 26-A (north); Geological Survey of Canada, Canadian Geoscience Map 271 (preliminary); Canada-Nunavut Geoscience Office, Open File Map 2016-07, scale 1:100 000. doi:10.4095/297355

46. Steenkamp, H., Gilbert, C., and St-Onge, M.R., in press c. Geology, Chidliak Bay (south), Baffin Island, Nunavut, NTS 26-B (south); Geological Survey of Canada, Canadian Geoscience Map 272 (preliminary); Canada-Nunavut Geoscience Office, Open File Map 2016-08, scale 1:100 000. doi:10.4095/297357

47. Steenkamp, H., Gilbert, C., and St-Onge, M.R., in press d. Geology, Chidliak Bay (north), Baffin Island, Nunavut, NTS 26-B (north); Geological Survey of Canada, Canadian Geoscience Map 270 (preliminary); Canada-Nunavut Geoscience Office, Open File Map 2016-09, scale 1:100 000. doi:10.4095/297354

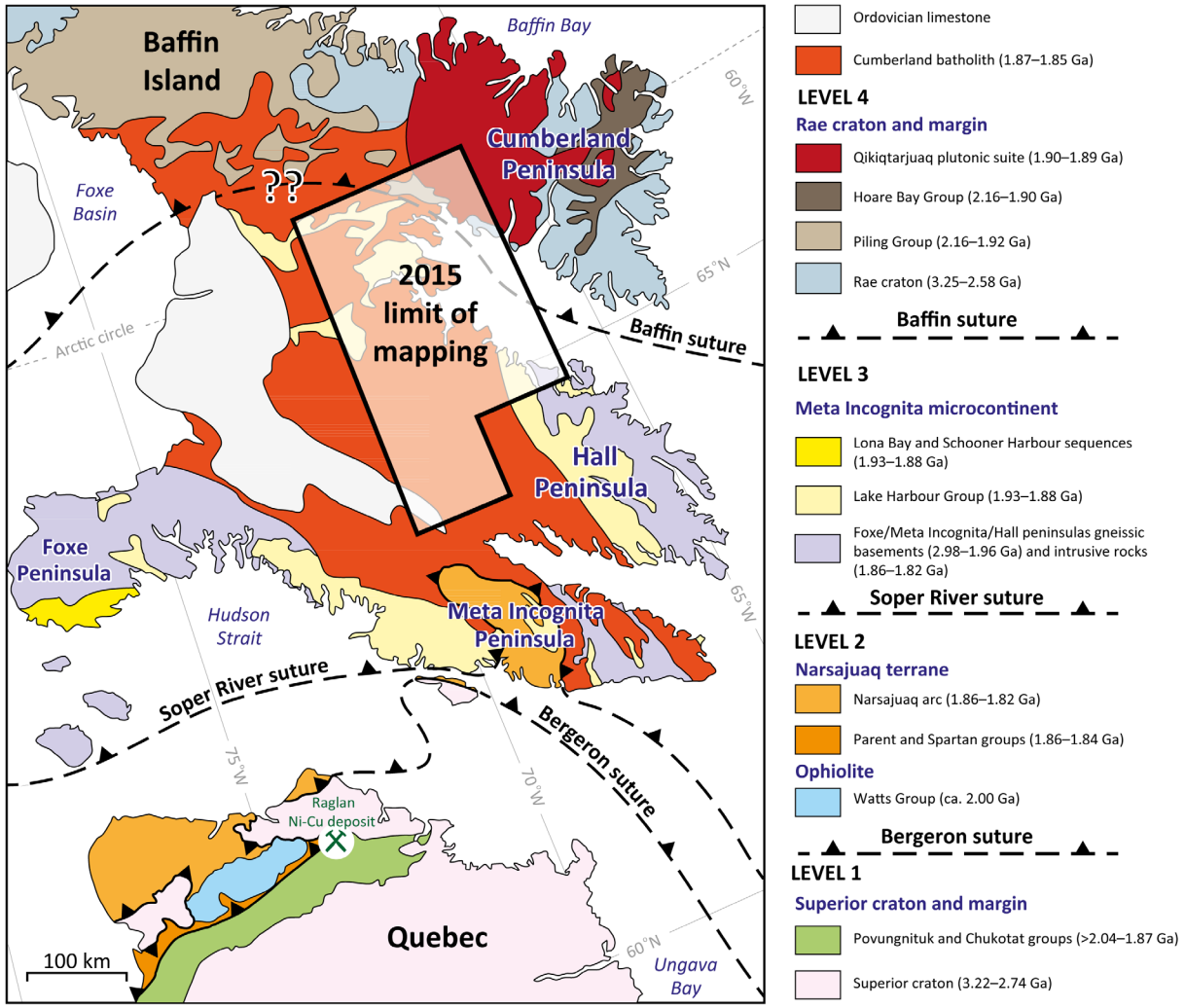

ᐊᖏᓐᓇᐃᐊᖅ 2. ᑐᑭᓯᓇᖅᓯᑎᑕᐅᕆᑎᐊᖅᓯᒪᔨᖅ ᓄᓇᐅᖓᓗ ᓄᓇᖓᓂᓂ ᓄᓇᖓᐃᐊᖅ ᑯᐸᐃᒃᓯᑭᐸᐅᖅ ᐃᓕᑎᕐᖓᖓ Trans-Hudson Orogen (ᐊᑲᖅᑭᒋᐊᖅᑕᐅᓯᒪᔨᖅ ᑭᖓᓂᐊᔪᓂ St-Onge ᐱᓕᓀᖅᑎᖓᓕᓪᓗ., 2007), ᑕᑯᐊᐅᑎᕆᑎᔨᖅᑎᕆᒪᒐᑦ ᐊᑲᖅᑭᓯᒪᓂᖓᓕᒃᑯᓕ ᐊᑯᓀᓐᓂᖓᓕᒃᑯᓕ ᐱᖓᓕᓯᑦ ᓄᓇᐃᑦ ᑲᑎᓂᖓᓕᒃᑯᓕ, ᐊᑐᓄᐃᖅᑕᐅᓯᒪᔨᑦ ᖃᐅᔨᐊᐅᓪᓗᑎ.

ᐊᓕᓐᖓᐊᖅ 3. ᐊᓕᓐᖓᐊᖅ ᑕᑯᓴᐅᑎᑕᑎᓵᖅ ᐃᖅᑲᖏᑦᑐᓂᑦ Sylvia Grinnell Lake–Clearwater Fiord. ᑎᑎᖅᑲᑲᖅᑐᑎᑦ ᓱᓴᐅᑎᓪᓗᑦ ᑕᓪᖅᐱᐊᓂ ᑎᑭᖅᑯᐊᓂ ᐊᑐᓂ ᐊᓕᓐᖓᐊᓂᑦ ᓇᓗᓇᐃᖅᓯᒪᑎᐅᓵᑦ 15SAB-ᖅᑲᐅᓴᖏᓐᓄᑦ. a) 10 m ᑕᑯᓴᖅ ᓯᓚᒋᓐᓂᑯ quartzite ᐅᓴᖅᑲᑦ biotite–ᒋᑦᑐᓂ ᐅᓴᖅᑲᐃᑦ. b) ᖃᑯᓗᓴᑎᐊᖅᑐᑦ quartzite ᐃᓗᐊᓂᑐᑦ ᐃᖅᑲᖏᑕ ᒪᖅᓂ ᐃᓗᐊᓂᓗᓐᓂᑦ. c) ᑕᑯᓴᐅᑎᑕᓵᕆ 1–2 cm ᐊᐅᕐᖅᑐᑦ ᐅᓴᖅᑎᑐᐊᖏᐃᓕᐊᓯᓴᕐᓂᓕᕆᓂᑦ ᐅᓴᖅᑲᓂᑦ ᐃᒍᓯᒪᓕᑐᓂ ᓴᖅᑐᓗᓂ ᐊᓄᔪᖅᓯᒪᓵᑦ ᐃᓗᓕᖅᑲᖅᑐᑦ biotite ᐊᓯᒪ sillimanite. d) ᖃᐅᔨᑐᖅᓯᒪᓵᒥᑦ ᓇᓗᓇᖏᑦᓂᖏᓐ ᑐᓴᓄᐃᐃᑦ ᐅᓴᖅᑲᐃᑦ ᐃᓗᐊᓂ biotite-orthopyroxene monzogranite. e) ᓴᐅᒥᓕ: ᓂᐱᖅᑲᖃᓕᓂᑦ ᑐᓴᓄᐃᐃᑦ ᐅᓴᖅᑲᐃᑦ ᓄᓇᐅᕐᓵ ᖃᑲᒪᑦ ᑐᓴᓄᐃᖅ, ᑕᓪᖅᐱᐊᓂ: ᑲᑎᓴᓂᖅᑐᑦ ᒧᐸᓐᓂᑦ ᐊᓕᓐᖏᓐᓄᑦᑎᓐᖓᖏᓐᓄᑦ ᖃᑲᐅᓂᓴᑎᓄᑦ, diopside ᐊᓯᒪ phlogopite. f) ᖃᓗᓇᐃᖅᓯᒪᓴᖏᑦ metagreywacke ᐃᓗᐊᓂ biotite monzogranite.

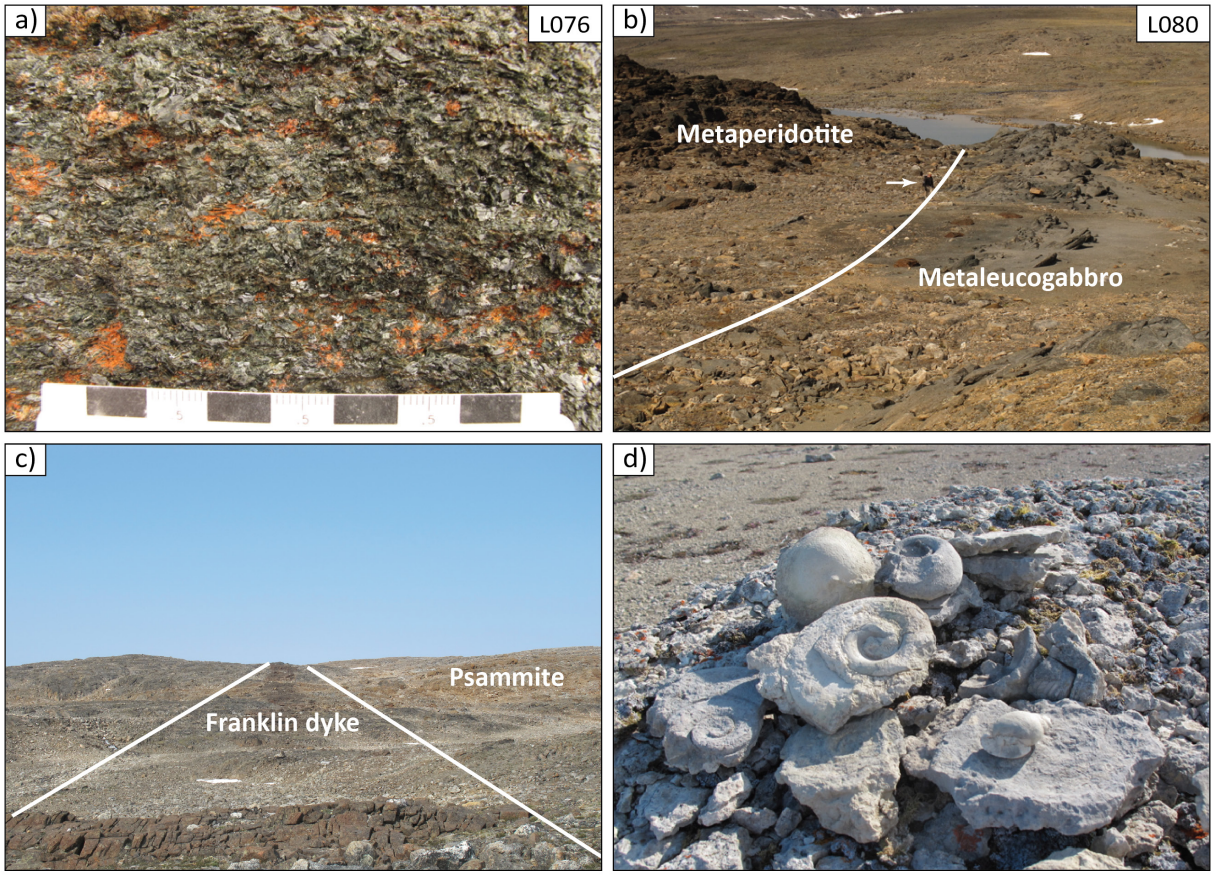

ᐊᓴᓂᖅᐳᐊᖅ 4. ᐊᓴᓂᖅᐳᐊᑦ ᐊᓯᖏᓐᓂᑦ ᐊᐃᓕᑐᖅᓯᒪᔪᓂᑦ Sylvia Grinnel Lake–Clearwater Fiord-ᒥᑦ. ᐊᑐᐊᓂᖅᑲᖅᑎᑦᓗᒍ, ᑎᑎᖅᑲᐃᑦ ᓴᓴᐅᑎᖅᑲᖅᑐᑦ ᑕᓕᖅᐱᒻᒥ ᖃᓄᐃᑦ ᑎᑭᖅᑯᖏᓐᓂ ᐊᑐᓂ ᐊᓴᓂᖅᐳᐊᑦ ᓇᓗᓇᐃᖅᓯᔪᑦ 15SAB- ᖃᑲᓴᓴᖃᐱᒻᒪᑦ. a) ᖃᓂᓴᖅᓯᒪᔪᖅ metaclinopyroxenite ᐊᑦᓕᓂᖅᕿᖏᓂᑦ ᖃᓄᓵᕐᑐᓂᑦ mafic sill. ᕿᐅᓂᓂᖅᐱᐃᑦ ᓇᓗᓇᐃᖅᓯᔪᑦ ᒥᑭᔪᒥᑦ ᖃᓇᓄᓕᓂᖏᓕᓵᓕᐅᖅᑕᖏᓐᓇᓄᑦ ᐅᑎᖅᑎᑕᐅᓂᖏᓐᖓ hornblende-ᒧᑦᖅ. b) ᕿᑎᐊᓂ –ᖃᓄᐃᓕᓂ ᖃᓄᓵᕐᑐᓂᑦ mafic sill, ᑕᓄᐃᓴᐅᑎᑎᔪᖅ ᑲᔪᕈᔪᒥᑦ metaperidotite ᖃᓄᕐᑲᖅᑐᓂ ᑲᔪᕈᔪᒥᑦ metaleucogabbro. ᖃᑲᓴᓴᖅᑲᐢᑦ ᐊᖏᕐᓂᖏᓐᓇᓄᑦ (ᖃᑲᓴᓂᖅᐳᐊᓕᓗ) 1.8 m ᑕᕈᓂᖏᓐᖓ. c) ᕿᒥᕈᒥᒥ ᐱᓕᓵᔪᑦ psammite ᖃᓄᓕᓵᖃᑕᐅᑎᔪᑦ ᐊᐃᓴᔪᒪᓂᖏᑦ Franklin dyke, ᓄᓄᑐᑦ ᑲᔪᕈᔪᖃᓂᕿᖃᖅᑐᖅ ᐊᓱᒪᓗ ᐃᓕᖏᓐᖓ ᑲᑎᑎᑎᑎᔪᑦ ᐅᐊᓂᑎᐊᑉᓂᖅᓴᐅᔪᓂᑦ. ᔪᒥᓴᔪᒪᓂ ᖃᓂᑎᕐᓯᓗᐊᓂ 10m ᓴᓂᒧᑦ. d) ᕿᑭᐱᒻᒪᔪᓂᑦ ᓴᖏᖏᓐᓇᓗᑎ ᓄᓇᐅᕐᓴᓄᓕᓂ0 limestone, ᑕᓄᐃᓴᐅᑎᑎᔪᖅ ᐅᐊᓂᑎᐊᑭᓂᓴᓂᑦ ᔪᐊᓱᒪᖅᓯᒪᓂᖅᓴᒥᑦ ᓄᓇᒥᑦ. ᖃᑲᓴᓴᖅᑲᐃᐅᔪᖅ ᑕᓄᐃᓴᐅᖏᓐᖓ ᔪᑭᓂᐊᓂ 50 cm.

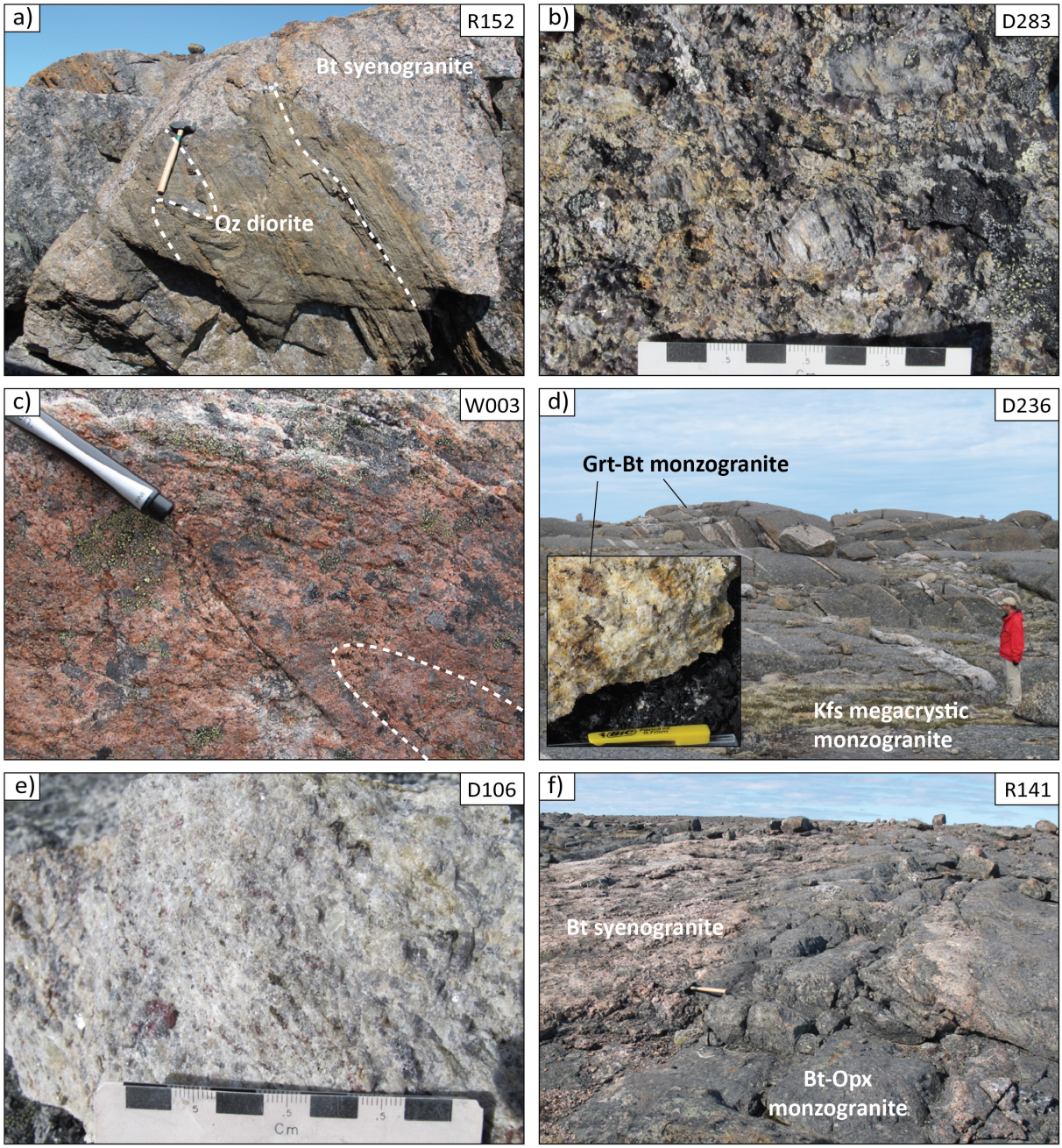

ᐊᓴᓂᖏᐊᖅ 5. ᓇᓗᓇᐃᖅᓯᒪᔪᑦ ᐊᓴᓂᖏᐊᑦ metagranitoid-ᓂᑦ Sylvia Grinnell Lake–Clearwater Fiord-ᒥᑦ. ᑎᑎᖅᑲᑲᖅᑐᑎᑦ ᓱᓴᐅᑎᓕᑦ ᖁᔨᓂᐅᔪᓂᒃ ᑐᓴᖅᐱᐊᓂ ᑎᑭᖅᑕᐊᓂ ᐊᑐᓂ ᐊᓴᓂᖏᐊᓂᑦ ᓇᓗᓇᐃᖅᑕᐅᔪᑦ 15SAB- ᖁᐅᓴᓴᕐᐱᖅ. a) ᓇᓗᓇᐃᓴᖅᓯᒪᔪᑦ ᐱᓚᓴᓯᒪᔪᑦ ᐊᓴᒪ ᐅᓴᒪᑕᐃᑦ quartz diorite ᐊᖏᕐᔪᒪᓚᐅᑦᓗᑎ grained biotite syenogranite. b) ᖁᑲᒧᖅᑐᑦ K-feldspar megacrystic monzogranite ᑕᑯᔭᐅᑎᕐᑎᔪᖅ 3–6 ᓯᐊᓂᑕᒫᑕᐃᑦ ᑕᑯᔭᐅᑎᕐᑎᓴᑲ rapakivi ᖁᓄᐃᑕᖏᓂᖏᓐᖓ. c) ᐊᓴᐲᑎᓂᓚᓂ ᓂᐱᖅᑲᖏᓪᓗᑦ ᐱᓚᓯᒪᔪᑦ biotite-orthopyroxene monzogranite. d) ᐊᖏᕐᔪᒪᓚᒃ K-feldspar megacrystic monzogranite ᑲᑎᔭᒪᔪᑦ ᐊᒥᓯᒪᓕᕆᓂᖅᓴᓕᓂᑦ biotite-garnet monzogranite ᓯᒥᑦᑕᐅᓯᒪᔪᓂᑦ. ᖁᑲᐅᔭᕐᑲᑎᒧᑦ ᐊᖏᕐᓂᖏᓐ ᐅᓇᐅᔪᖅ 1.8 m ᑕᑭᓂᖏᓐ. ᐊᓴᓂᖏᐊᖅ: ᖁᓂᓇᖅᑲᓯᒪᔪᖅ biotite-garnet monzogranite ᖁᑲᐅᔭᕐᑕᕆᖅ, ᑕᑯᔭᐅᑎᕐᑎᔪᖅ 1–3 ᓯᐊᓂᑕᒫᑕᐃᐅᐸᕈᔪᑐᑦ ᐊᒥᐊᖏᓐ garnet phenocrysts ᐊᓕᒪ ᓴᑦᑐᓂᑦ ᐊᓄᔪᕐᓴᐅᓇᓂ ᓇᓗᓇᐃᖅᑕᐅᔪᖅ ᐅᒧᖏᓐ sub-parallel biotite flakes. e) ᖁᓂᓇᖅᑲᓯᒪᔪᖅ garnet-sillimanite leucogranite, ᑕᑯᔭᐅᔪᑦ ᐊᒥᓯᑦ ᒥᖅᑯᑎᐅᐸ ᓄᐊᖏᓚᑎᑐᑦ ᐊᖏᓂᓂᖅᑲᑐᑦᓯᒃ ᐊᒥᐊᓕᑦ ᐅᔪᖅᑕᐃᑦ. f) ᐊᖏᕐᔪᒪᓚᒃ biotite-orthopyroxene monzogranite ᑲᑎᓄᖏᓚᔪᑦ ᐊᒥᓯᒪᓕᓄᓕ ᑲᑎᓄᓂᖅᑲᓇᖏᑦ biotite syenogranite ᓯᒥᑦᑕᐅᓯᒪᔪᑦ. ᐊᖏᑎᓂᖓᔭᖏᓐ ᐅᓇᐅᔪᖅ 35 cm ᑕᑭᓂᖏᓐ.

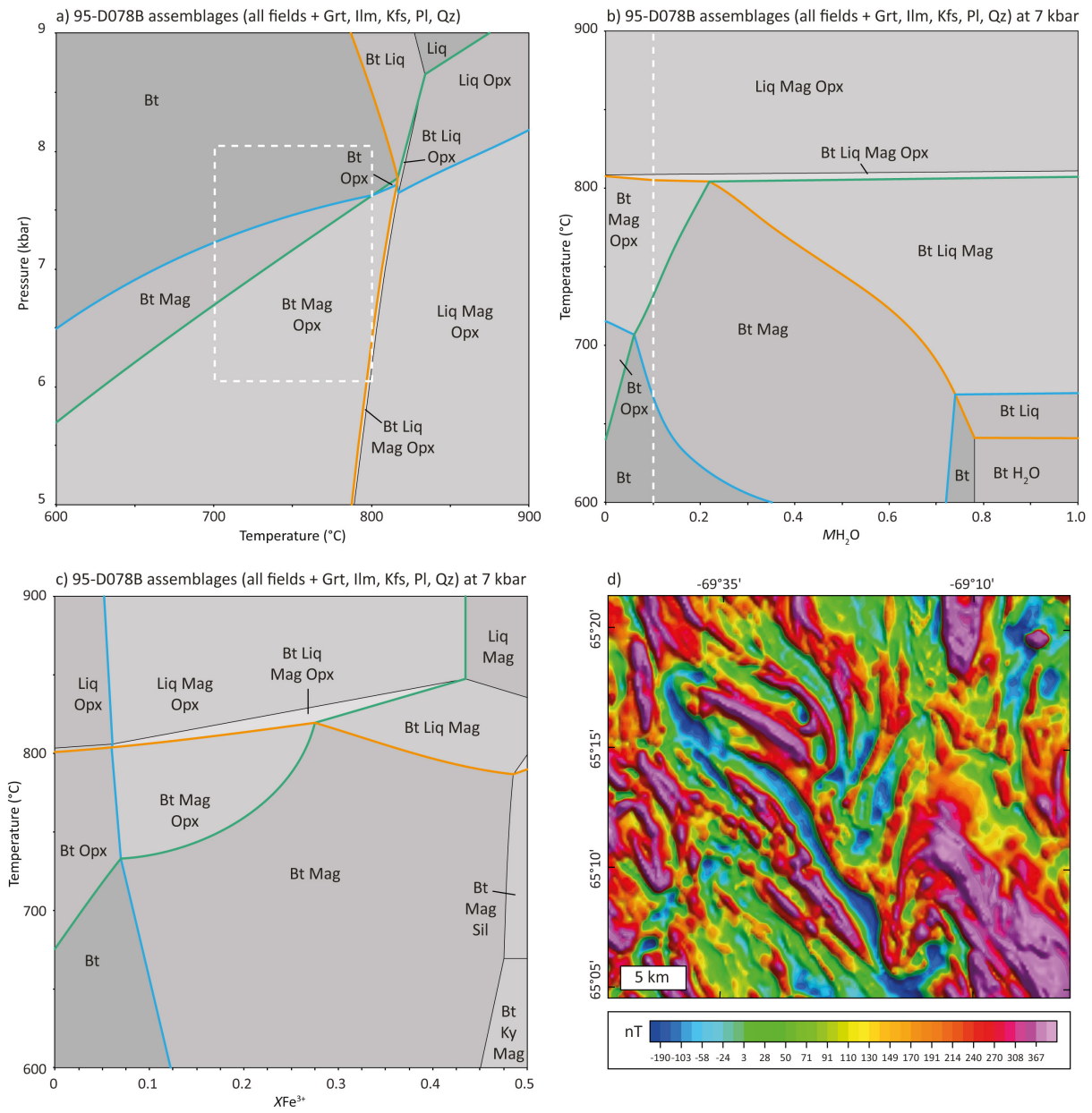

ᐊᕆᔨᖏᔪᐊᖅ 6. ᓇᓕᒧᑎᑎᑎᓂᕐᒥᑦ ᐊᕆᔨᖏᔪᐊᑦ ᑕᑯᓴᐅᑎᑎᐅᓵᑦ ᖃᐅᐅᔨᕋᓴᓴᓂᒃ monzogranite, ᖃᑭᓂᖅᑐᑎᑦ metagranitoid amphibolite-granulite ᓇᒡᒐᓂᖏᑲ ᐊᑦᑐᐊᓂᓕᑦ: a) P-T ᐊᕆᔨᖏᔪᐊᖅ; b) T-MH_2O ᐊᕆᔨᖏᔪᐊᖅ; c) T-XFe^{3+} ᐊᕆᔨᖏᔪᐊᖅ; d) ᑲᑎᑦᑐᒥᑦ ᖃᐅᐅᔨᕋᕐᕕᐅᔪᓂᒃ biotite±magnetite±orthopyroxene monzogranite ᖃᐅᐅᔨᕋᕐᕕᐅᔪᒥᑦ.

ᖃᐅᔨᓴᓂᐊᖅᑕᓂ

Blackadar, R.G., 1967. Geological Reconnaissance, southern Baffin Island, District of Franklin; Geological Survey of Canada, Paper 66-47, 32 p. doi:10.4095/100926

Buchan, K.L. and Ernst, R.E., 2013. Diabase dyke swarms of Nunavut, Northwest Territories and Yukon, Canada; Geological Survey of Canada, Open File 7464. doi:10.4095/293149

Chadwick, T.C., St-Onge, M.R., Weller, O.M., Carr, S.D., and Dyck, B.J., 2015. Ptarmigan Fiord basement–cover thrust imbricates, Baffin Island, Nunavut: summary of fieldwork; *in* Summary of Activities 2015, Canada-Nunavut Geoscience Office, p. 61–72.

Clarke, D.B., Cameron, B.I., Muecke, G.K., and Bates, J.L., 1989. Early Tertiary basalts from the Labrador Sea and Davis Strait region; Canadian Journal of Earth Sciences, v. 26, p. 956–968.

Corrigan, D., Pehrsson, S., Wodicka, N., and de Kemp, E., 2009. The Palaeoproterozoic Trans-Hudson Orogen: a prototype of modern accretionary processes; *in* Ancient Orogens and Modern Analogues, J.B. Murphy, J.D. Keppie, and A.J. Hynes (ed.), The Geological Society, London, Special Publications, v. 327, p. 457–479. doi:10.1144/SP327.19

Dunphy, J.M. and Ludden, J.N., 1998. Petrological and geochemical characteristics of a Paleoproterozoic magmatic arc (Narsajuaq Terrane, Ungava Orogen, Canada) and comparisons to Superior Province granitoids; Precambrian Research, v. 91, p. 109–142.

Dyck, B.J. and St-Onge, M.R., 2014. Dehydration-melting reactions, leucogranite emplacement and the Paleoproterozoic structural evolution of Hall Peninsula, Baffin Island, Nunavut; *in* Summary of Activities 2013, Canada-Nunavut Geoscience Office, p. 73–84.

Heaman, L.M., LeCheminant, A.N., and Rainbird, R.H., 1992. Nature and timing of Franklin igneous events, Canada: implications for a Late Proterozoic mantle plume and the break-up of Laurentia; Earth and Planetary Science Letters, v. 109, p. 117–131.

Henderson, J.R., 1985. Geology, McBeth Fiord-Cape Henry Kater, District of Franklin, Northwest Territories; Geological Survey of Canada, Map 1605A, scale 1:250 000. doi:10.4095/120467

Hoffman, P.F., 1988. United Plates of America, the birth of a craton: Early Proterozoic assembly and growth of Laurentia; Annual Reviews of Earth and Planetary Sciences, v. 16, p. 543–603.

Holland, T.J.B. and Powell, R., 1998. An internally consistent thermodynamic dataset for phases of petrological interest; Journal of Metamorphic Geology, v. 16, p. 309–343.

Kiss, F. and Tschirhart, V., 2015a. Residual total magnetic field, aeromagnetic survey of the Amittok Lake area, Baffin Island, Nunavut, NTS 26-J south; Geological Survey of Canada, Open File 7888, scale 1:100 000. doi:10.4095/296504

Kiss, F. and Tschirhart, V., 2015b. First vertical derivative of the magnetic field, aeromagnetic survey of the Amittok Lake area, Baffin Island, Nunavut, NTS 26-J south; Geological Survey of Canada, Open File 7889, scale 1:100 000. doi:10.4095/296505

Kiss, F. and Tschirhart, V., 2015c. Residual total magnetic field, aeromagnetic survey of the Amittok Lake area, Baffin Island, Nunavut, NTS 26-K south; Geological Survey of Canada, Open File 7890, scale 1:100 000. doi:10.4095/296506

Kiss, F. and Tschirhart, V., 2015d. First vertical derivative of the magnetic field, aeromagnetic survey of the Amittok Lake area, Baffin Island, Nunavut, NTS 26-K south; Geological Survey of Canada, Open File 7891, scale 1:100 000. doi:10.4095/296507

Kiss, F. and Tschirhart, V., 2015e. Residual total magnetic field, aeromagnetic survey of the McKeand River area, part of NTS 26-B/North, Nunavut; Geological Survey of Canada, Open File 7819, scale 1:100 000. doi:10.4095/296382

Kiss, F. and Tschirhart, V., 2015f. First vertical derivative of the magnetic field, aeromagnetic survey of the McKeand River area, part of NTS 26-B/North, Nunavut; Geological Survey of Canada, Open File 7820, scale 1:100 000. doi:10.4095/296383

Kiss, F. and Tschirhart, V., 2015g. Residual total magnetic field, aeromagnetic survey of the McKeand River area, part of NTS 26-C/South, Nunavut; Geological Survey of Canada, Open File 7821, scale 1:100 000. doi:10.4095/296384

Kiss, F. and Tschirhart, V., 2015h. First vertical derivative of the magnetic field, aeromagnetic survey of the McKeand River area, part of NTS 26-C/South, Nunavut; Geological Survey of Canada, Open File 7822, scale 1:100 000. doi:10.4095/296385

Kiss, F. and Tschirhart, V., 2015i. Residual total magnetic field, aeromagnetic survey of the McKeand River area, part of NTS 26-C/North, Nunavut; Geological Survey of Canada, Open File 7823, scale 1:100 000. doi:10.4095/296386

Kiss, F. and Tschirhart, V., 2015j. First vertical derivative of the magnetic field, aeromagnetic survey of the McKeand River area, part of NTS 26-C/North, Nunavut; Geological Survey of Canada, Open File 7824, scale 1:100 000. doi:10.4095/296387

Kiss, F. and Tschirhart, V., 2015k. Residual total magnetic field, aeromagnetic survey of the McKeand River area, part of NTS 26-F/South, Nunavut; Geological Survey of Canada, Open File 7825, scale 1:100 000. doi:10.4095/296388

Kiss, F. and Tschirhart, V., 2015l. First vertical derivative of the magnetic field, aeromagnetic survey of the McKeand River area, part of NTS 26-F/South, Nunavut; Geological Survey of Canada, Open File 7826, scale 1:100 000. doi:10.4095/296389

Kiss, F. and Tschirhart, V., 2015m. Residual total magnetic field, aeromagnetic survey of the McKeand River area, part of NTS 26-F/North, Nunavut; Geological Survey of Canada, Open File 7827, scale 1:100 000. doi:10.4095/296390

Kiss, F. and Tschirhart, V., 2015n. First vertical derivative of the magnetic field, aeromagnetic survey of the McKeand River area, part of NTS 26-F/North, Nunavut; Geological Survey of Canada, Open File 7828, scale 1:100 000. doi:10.4095/296391

Kiss, F. and Tschirhart, V., 2015o. Residual total magnetic field, aeromagnetic survey of the McKeand River area, part of NTS 26-G/South, Nunavut; Geological Survey of Canada, Open File 7829, scale 1:100 000. doi:10.4095/296392

Kiss, F. and Tschirhart, V., 2015p. First vertical derivative of the magnetic field, aeromagnetic survey of the McKeand River area, part of NTS 26-G/South, Nunavut; Geological Survey of Canada, Open File 7830, scale 1:100 000. doi:10.4095/296393

Kiss, F. and Tschirhart, V., 2015q. Residual total magnetic field, aeromagnetic survey of the McKeand River area, part of NTS 26-G/North, Nunavut; Geological Survey of Canada, Open File 7831, scale 1:100 000. doi:10.4095/296394

Kiss, F. and Tschirhart, V., 2015r. First vertical derivative of the magnetic field, aeromagnetic survey of the McKeand River area, part of NTS 26-G/North, Nunavut; Geological Survey of Canada, Open File 7832, scale 1:100 000. doi:10.4095/296395

Lesher, C.M., 2007. Ni-Cu-(PGE) deposits in the Raglan area, Cape Smith Belt, New Quebec; *in* Mineral Deposits of Canada: a Synthesis of Major Deposit Types, District Metallogeny, the Evolution of Geological Provinces and Exploration Methods, W.D. Goodfellow (ed.), Geological Association of Canada, Special Publication, v. 5, p. 351–386.

Liikane, D.A., St-Onge, M.R., Kjarsgaard, B.A., Rayner, N.M., Ernst, R.E., and Kastek, N., 2015. Frobisher suite mafic, ultramafic and layered mafic-ultramfic sills, southern Baffin Island; *in* Summary of Activities 2015, Canada-Nunavut Geoscience Office, p. 21–32.

Lucas, S.B. and Byrne, T., 1992. Footwall involvement during arc-continent collision, Ungava orogen, northern Canada; Journal of the Geological Society of London, v. 149, p. 237–248.

Lucas, S.B. and St-Onge, M.R., 1992. Terrane accretion in the internal zone of the Ungava orogen, northern Quebec. Part 2: Structural and metamorphic history; Canadian Journal of Earth Sciences, v. 29, p. 765–782.

Nekvasil, H., 1991. Ascent of felsic magmas and formation of rapakivi; American Mineralogist, v. 76, p. 1279–1290.

Palin, RM., Weller, O.M., Waters, D.J., and Dyck, B., 2015. Quantifying geological uncertainty in metamorphic phase equilibria modelling; a Monte Carlo assessment and implications for tectonic interpretations; Geoscience Frontiers. doi:10.1016/j.gsf.2015.08.005

Powell, R. and Holland, T.J.B., 2008. On thermobarometry; Journal of Metamorphic Geology, v. 26, p. 155–179.

Scott, D.J., 1997. Geology, U-Pb, and Pb-Pb geochronology of the Lake Harbour area, southern Baffin Island: implications for the Paleoproterozoic tectonic evolution of north-eastern Laurentia; Canadian Journal of Earth Sciences, v. 34, p. 140–155.

Scott, D.J. and Wodicka, N., 1998. A second report on the U-Pb geochronology of southern Baffin Island; Geological Survey of Canada, Current Research 1998-F, p. 47–57.

Scott, D.J., St-Onge, M.R., Wodicka, N., and Hanmer, S., 1997. Geology of the Markham Bay – Crooks Inlet area, southern Baffin Island, Northwest Territories; Geological Survey of Canada, Current Research 1997-C, p. 157–166.

St-Onge, M.R. and Lucas, S.B., 1994. Controls on the regional distribution of iron-nickel-copper-platinum group element sulfide mineralization in the eastern Cape Smith Belt, Quebec; Canadian Journal of Earth Sciences, v. 31, p. 206–218.

St-Onge, M.R., Hanmer, S., and Scott, D.J., 1996. Geology of the Meta Incognita Peninsula, south Baffin Island: tectonostratigraphic units and regional correlations; Geological Survey of Canada, Current Research 1996-C, p. 63–72.

St-Onge, M.R., Scott, D.J. and Lucas, S.B., 2000a. Early partitioning of Quebec: Microcontinent formation in the Paleoproterozoic; Geology, v. 28, p. 323–326.

St-Onge, M.R., Scott, D.J., Wodicka, N., and Lucas, S.B., 1998. Geology of the McKellar Bay – Wight Inlet – Frobisher Bay area, southern Baffin Island, Northwest Territories; Geological Survey of Canada, Current Research 1998-C, p. 43–53.

St-Onge, M.R., Searle, M.P., and Wodicka, N., 2006. Trans-Hudson Orogen of North America and Himalaya-Karakoram-Tibetan Orogen of Asia: Structural and thermal characteristics of the lower and upper plates; Tectonics, v. 25, TC4006, 22p. doi:10.1029/2005TC001907

St-Onge, M.R., Wodicka, N., and Ijewliw, O., 2007. Polymetamorphic evolution of the Trans-Hudson Orogen, Baffin Island, Canada: Integration of petrological, structural and geochronological data; Journal of Petrology, v. 48, p. 271–302. doi:10.1093/petrology/eg1060

St-Onge, M.R., Wodicka, N., and Lucas, S.B., 2000b. Granulite- and amphibolite-facies metamorphism in a convergent plate-margin setting: Synthesis of the Quebec-Baffin segment of Trans-Hudson Orogen. Canadian Mineralogist, v. 38, p. 379–398.

St-Onge, M.R., Van Gool, J.A.M., Garde, A.A., and Scott, D.J., 2009. Correlation of Archaean and Palaeoproterozoic units between northeastern Canada and western Greenland: constraining the pre-collisional upper plate accretionary history of the Trans-Hudson orogen; *in* Earth Accretionary Systems in Space and Time, P.A. Cawood and A. Kroner, The Geological Society, London, Special Publications, v. 318, p. 193–235. doi:10.1144/SP318.7

Thériault, R.J., St-Onge, M.R., and Scott, D.J., 2001. Nd isotopic and geochemical signature of the Paleoproterozoic Trans-Hudson Orogen, southern Baffin Island, Canada: implications for the evolution of eastern Laurentia; Precambrian Research, v. 108, p. 113–138.

Tschirhart, V., St-Onge, M.R., and Weller, O.M., 2015. Preliminary geophysical interpretation of the McKeand River area, Baffin Island, Nunavut: insights from gravity, magnetic and geological data; *in* Summary of Activities 2015, Canada-Nunavut Geoscience Office, p. 49–60.

Weller, O.M., Dyck, B.J., St-Onge, M.R., Rayner, N.M, and Tschirhart, V., 2015. Completing the bedrock mapping of southern Baffin Island, Nunavut: plutonic suites and regional stratigraphy; *in* Summary of Activities 2015, Canada-Nunavut Geoscience Office, p. 33–48.

Weller, O.M., St-Onge, M.R., Rayner, N., Searle, M.P., and Waters, D.J., 2016. Miocene magmatism in the Western Nyainqentanglha mountains of southern Tibet: an exhumed bright spot?; Lithos, doi:10.1016/j.lithos.2015.06.024

Weller, O.M., St-Onge, M.R., Searle, M.P., Rayner, N., Waters, D.J., Chung, S.L., Palin, R.M., Lee, Y.H., and Xu, X.W., 2013. Quantifying Barrovian metamorphism in the Danba Structural Culmination of eastern Tibet; Journal of Metamorphic Geology, v. 31, p. 909–935. doi: 10.1111/jmg.12050

Whalen, J.B., Wodicka, N., Taylor, B.E., and Jackson, G.D., 2010. Cumberland batholith, Trans-Hudson Orogen, Canada: Petrogenesis and implications for Paleoproterozoic crustal and orogenic processes; Lithos, v. 117, p. 99–118. doi:10.1016/j.lithos.2010.02.008

Wodicka, N. and Scott, D.J., 1997. A preliminary report on the U-Pb geochronology of the Meta Incognita Peninsula, southern Baffin Island, Northwest Territories; Geological Survey of Canada, Current Research 1997-C, p. 167–178.

Wodicka, N, St-Onge, M.R., Corrigan, D., Scott, D.J., and Whalen, J.B., 2014. Did a proto-ocean basin form along the southeastern Rae cratonic margin? Evidence from U-Pb geochronology, geochemistry (Sm-Nd and whole rock), and stratigraphy of the Paleoproteorozoic Piling Group, northern Canada; GSA Bulletin, v. 126, p. 1625–1653. doi: 10.1130/B31028.1

ᐊᓯᖏᑦ ᑐᓴᐅᒪᔨᐅᔨᓗᐊᖅᑐᑦ

ᑐᓴᒃᓴᒃᑲᓂᐅᑎᑕᐅᔪᑦ ᐅᖓᓂ ᖃᑦᕿᓴᐅᔨᒃᑯᖏᓚᔪᑦ ᓄᓇᐅᔪᓐ ᖃᐅᓄᐃᒪᓕᖏᓚᖏᓂᑦ ᓇᓗᓇᐃᔨᐃᒃᑲᓂᕐᓂᔪᓕᔪ ᓴᖅᑭᔨᖏᑦᑐᑦ PDF-ᒥ ᓄᓇᖕᖓᐊᖅᓯᑦ, ᐃᓕᐅᑎᑕᐅᖏᑦᑐᑦ ᐅᖓᓂ ᓄᓇᖕᖓᐊᖅᓯᑦ ᑎᑎᕐᖃᑕᐅᓯᒪᔪᓂᑦ, ᐅᕙᖓᓵᓂᓂᑦ ᐃᓕᐅᑎᑕᐅᓯᒪᖏᑦᑐᑦ ᓄᓇᖕᖓᐊᓕᓇᓂᑯᑦ ᓄᐊᕐᑎᕐᖓᓐᓂᑦ. ᑐᓴᒃᓴᒃᑲᓂᐅᑎᑕᐅᔪᖅ ᑎᑎᕐᓯᒪᓂᖅᓱᓄᑦ Excel® ᑎᑎᕐᓕᕆᔨᖏᑦᑐᓂᑦ ᓄᓇᖕᖓᐊᔪ ᖃᑦᓗᐃᓕᓴᖅᓱᓂᑦ.

ᑎᑎᕐᖃᑐᖅ ᖃᐅᓕᑕᒪᐊᕐᓇᖅᓱᒃ

ᐊᐱᖅᑯᑎᒃᓴᒪ ᐅᖃᑦᖃᑕᐅᔪᑦ, ᐊᓪᓚ ᐅᖃᑦᐅᓯᓴᐃᓕᑦ ᐱᔪᓕᑎᖃᖅᑐᑦᓄᓇᓕᑦ ᖃᐅᔨᓴᓂᕐᓗᑦ ᑐᓴᐅᒪᔨᐃᒃᑲᓂᕐᓂᑦ ᐃᓗᓕᓕᒫᓂᑦ ᑐᖕᖏᓐᓂᑎᑕᐅᔨᓴᒪᓕᓕᒫᓂᑦ ᐅᖓᓃᓕᓐᓂᑦ.

M.R. St-Onge
Geological Survey of Canada
601 Booth Street
Ottawa ON
K1A 0E8
marc.st-onge@canada.ca

ᓇᒫᔨᓂᕐᒥᓄᑦ ᐊᑐᖅᑕᐅᔪᑦ

ᑕᑯᓴᐅᑎᑦᑎᔪᑦ: Universal Transverse Mercator
ᐊᑐᖅᑕᐅᔪᑦ: ᒫᑕᐃᑦ
ᐊᖏᑦᑐᖅᓯᒪᓂᖏᓐᓄ: 19
ᓴᓂᒧᑦ ᐱᒋᐊᖕᖓᓐᓄ: NAD83
ᑐᑭᒧᑦ ᐱᒋᐊᖕᖓᓐᓄ: ᑐᑭᖃᖅᑐᖅ ᐃᒪᖕᒧᑦ ᓇᓕᒧᓐᓂᓐᓄ

ᓯᕗᒧᐊᒋᐊᖅᑐᑦ ᓇᒫᔨᓂᕐᒥᑦ

ᐱᓕᕐᓇᓕᓐᓂ ᑐᑭᒧᑦ: 70°00’00”W
ᖃᓇᓐᓇᓕᓐᓂ ᑐᑭᒧᑦ: 68°00’00”W
ᐅᐊᓐᓇᓕᓐᓂ ᓴᓂᒧᑦ: 67°00’00”N
ᓂᒋᓕᓂ ᓴᓂᒧᑦ: 66°30’00”N

ᖃᖅᑎᖅᑐᒧᑦ ᐃᓕᓴᖅᑯᓯᒪᔪᖅ

ᓄᐊᑕᐅᓯᒪᔪᑦ ᐊᖅᑭᓯᖅᓯᒪᓕᐅᖅᑯᓯᒪᔪᑦ ᐊᑐᖅᑕᐅᔪᓐᓇᕆᔨᖅᑕᐅᒃ ᐃᒪᐃᑦᑐᑉᑯᑦ ArcGIS™ ᑭᐳᒥᐅᑕᓂᖕᖏᓚᔪᓄ 10.1 ᐊᖅᑭᑉᑕᐅᓂᑯᑦ ESRI®.

ᑐᑭᓯᐊᕈᑎᑦ ᐊᑐᖅᑕᐅᔪᑦ ᑐᑭᓯᐊᕈᑎᓄᑦ

ᓄᓇᓂᑦ ᖃᐅᔨᓴᓂᓕᒫᓂᑦ ᑐᑭᓯᐊᕈᑎᑦ ᐊᔪᔨᖕᖏᑦᑐᑦ ᐃᓗᓕᖅᑐᖅᑕᐅᒃ ᐱᖃᓯᐅᑎᓯᒪᔪᑦ ᑕᕐᖓᓂ ᓴᖅᑭᑎᑕᐅᔪᓂᑦ ᒪᑕᓐᓂᖅᑐᖅᑕᐅᒃ GSC–ᑯᑦᐱᑕᓚᐊᖅ ᖃᐅᐊᖓᐃᓐᓇᖅᑐᒥᑦ <ᖃᓇᑕᐅᓯᒪᔪᑦ (ᓴᖅᑭᖅᑎᑕᐅᑕᐅᖅᑎᓐᓇᑕᑦ 2.6). ᑎᑎᕐᖃᓯᒪᔪᖅ ᓇᓗᓇᐃᔨᐃᓕᑐᓂ ᖃᓇᓴᐅᔭᓂᖓᓂᒪᑦ ᐊᖅᑭᑉᑕᐅᓯᒪᓂᒪᓕᒫᑦ ᐃᓕᖓᑦᓂᓐᓂᑦ ᐃᓕᓐᓂᐅᓂᒃᑲ ᐊᑐᐃᓐᓇᐅᓕᖓᓂᒃᑯᓂ ᐅᖓᓃ…\Data\DataModelInfo.

ᓴᓇᓯᒪᓂᖅ XML ᐃᖃᑲᓇᐃᔨᕐᓴᑦ ᐊᑕᖅᑭᓇᓂ ᒪᑕᓂᓂᑲᖅᑭᑕᖃᖅ ᑕᐃᑦᑯᓂᖅ ᖃᓄᐃᑕᖅᓯᓂᖅᑭᓂᓂ. ᐊᑐᐊᓇᕐᓂᐊᖅᑭᑦᓯᓂ, ᖃᓄᐃᑦᑐᓂᖅᑭᑦ ᑎᑎᕋᖃᓯᒪᔪᑦ ᐱᓕᕆᖃᑕᖃᖅᑐᑦ ᕿᑐᐊᖅᓯᓇᖅᑐᓂ ᑐᑭᓯᒪᓕᓇᖅᑭᑦᓯᓂ ᖃᓄᐃᑦᑐᓂᖅᑭᑎᒍᑦ.

ᓕᐃᓴᓯ ᐊᑐᐃᓂᓇᕆᔨᖅ ᖃᓄᑦᓯᓄᑐᑦ ᑕᑯᓚᑦᓂᓂᑦ ᑕᐃᒪᓕᖅᑐᑦ.

LICENCE AGREEMENT

View the licence agreement at
http://open.canada.ca/en/open-government-licence-canada

ACCORD DE LICENCE

Voir l'accord de licence à
http://ouvert.canada.ca/fr/licence-du-gouvernement-ouvert-canada